GEORG SPEYER HAUS

TECHNISCHE UNIVERSITÄT DARMSTADT

Graduiertenkolleg Biologicals 1172

Functional analysis of the APAF-1 binding protein FAM96A

Vom Fachbereich Biologie der Technischen Universität Darmstadt

zur

Erlangung des akademischen Grades

eines Doctor rerum naturalium

genehmigte Dissertation von

Dipl.-Biol. Bettina Schwamb

aus Worms

1. Referent/ Referentin: Prof. Dr. B. Süß

2. Referent/Referentin: Prof. Dr. M. Zörnig

3. Referent/Referentin: Prof. Dr. B. Laube

Tag der Einreichung: 6.3.2013

Tag der mündlichen Prüfung: 17.5.2013

Darmstadt, 2013

(D 17)

Ehrenwörtliche Erklärung:

Ich erkläre hiermit ehrenwörtlich, dass ich die vorliegende Arbeit entsprechend den Regeln guter wissenschaftlicher Praxis selbstständig und ohne unzulässige Hilfe Dritter angefertigt habe.

Sämtliche aus fremden Quellen direkt oder indirekt übernommenen Gedanken sowie sämtliche von Anderen direkt oder indirekt übernommenen Daten, Techniken und Materialien sind als solche kenntlich gemacht. Die Arbeit wurde bisher bei keiner anderen Hochschule zu Prüfungszwecken eingereicht.

Darmstadt, den ……

.....

Table of contents

Summary

Apoptosis, as a special form of programmed cell death (PCD) is an essential developmental process that is involved in tissue homeostasis and, whose deregulation has severe pathological implications for an organism. Thus, the evasion of the apoptotic program is one hallmark capability of cancer cells. Tumor suppressor genes (TSG) under normal conditions fulfill functions like sensing DNA-damage or regulating gene expression and they may contribute to the induction of apoptosis. In most cancer cells, TSG are mutated, inactivated or their expression level is reduced to enable neoplastic outgrowth and tumor cell proliferation. Furthermore, inactivation or blockage of TSG function may contribute to activation and upregulation of anti-apoptotic oncogenes. The identification and functional characterization of novel pro-apoptotic proteins, which can act as tumor suppressors themselves, is important in cancer research.

In this study, the novel APAF-1 binding protein FAM96A, which was discovered in a yeast two hybrid screen, was functionally characterized, and its involvement in tumorigenesis and Fe-S cluster biogenesis was elucidated. Importantly, the endogenous interaction with monomeric APAF-1 was confirmed.

Furthermore, FAM96A has recently been described to interact with the cytosolic iron sulfur assembly protein Ciao1. A combined functional contribution of Ciao1 and FAM96A to intrinsic apoptosis was excluded by overexpression and knockdown experiments during this study. Ciao1 exhibits a rather anti-apoptotic function, which is independent of FAM96A and, most probably, connected to its role in cytosolic Fe-S biogenesis. However, a scaffolding function of FAM96A during cytosolic iron-sulfur assembly might reflect a conserved function of the protein.

Ciao1 was described to regulate the transcriptional activity of WT1, a tumor suppressor in childhood nephroblastoma. Here, a reduction of *WT1* mRNA expression upon simultaneous Ciao1 overexpression was observed, whereas the contribution of FAM96A to the regulation of the WT1 transcription factor was only minor.

The role of FAM96A in intrinsic apoptosis was investigated by stable lentiviral protein overexpression in cancer cells. Human colon carcinoma and murine renal cancer cells were transduced to upregulate their FAM96A levels. These stable cell lines were compared to control vector transduced cells in apoptosis assays investigating the effects of FAM96A overexpression on the intrinsic pathway. Upon induction of PCD by the chemotherapeutic agents mitomycin C and the second-generation platinum derivative oxaliplatin, cell killing was enhanced when FAM96A

was simultaneously upregulated. Accordingly, when protein levels were diminished as a consequence of lentiviral short hairpin RNA (shRNA)-mediated knockdown, a significant desensitization of murine fibroblast and RKO cells to the induction of the intrinsic apoptosis pathway was observed. Furthermore, the influence of increased FAM96A expression levels was investigated *in vivo* in subcutaneous tumor xenograft experiments in NOD/SCID mice. The engraftment potential of colon cancer cells was drastically impaired in FAM96A groups compared to controls, and tumor growth was reduced in RKO as well as Renca-lacZ tumors. While a regulatory influence of FAM96A on intrinsic apoptosis could be observed, the cell cycle distribution of Renca-lacZ was not affected by FAM96A upregulation.

Although several approaches were taken to elucidate the molecular mechanism of the pro-apoptotic contribution of FAM96A to intrinsic apoptosis and its putative function during apoptosome assembly, it remains unresolved until now. A potential scaffolding function of FAM96A during apoptosome assembly or an involvement as a nucleotide exchange factor on APAF-1 cannot be excluded. As a pro-apoptotic protein, FAM96A resembles a putative tumor-suppressor gene, and losses within the *FAM96A* locus were detected by comparative genomic hybridization. Here, copy number aberrations were observed most prominently in gastrointestinal stromal tumors (GIST) where 48.8% of tumors analyzed indicated deletions. This was further addressed by immunohistochemistry of 53 GIST patient samples, and independent of cancer origin, no positive staining for FAM96A could be observed. A second patient cohort of GISTs of distinct grading was analyzed for *FAM96A* mRNA expression, which was reduced in 29 out of 31 samples. Upon re-introduction of FAM96A in established GIST cell lines, susceptibility towards apoptotic treatment with the state-of-the-art tyrosine kinase inhibitor Imatinib Mesylate and, in the case of imatinib-resistant GIST, staurosporine was increased compared to controls. Tumorigenicity of GIST882 cells re-expressing FAM96A was significantly reduced in a tumor xenograft experiment, and the engraftment potential was diminished. Quantitative real time PCR analysis on the time point of FAM96A loss in the course of tumorigenesis indicate that reduction of FAM96A mRNA levels may occur as an oncogenic event during malignant transformation of interstitial cells of Cajal, the suspected cell of origin of GIST. FAM96A therefore represents a marker for GIST and a novel tumor suppressor protein in this cancer entity. Nonetheless, FAM96A exhibits its tumor-suppressive potential not only in GIST, but also in further tumor entities as suggested by multi-tumor tissue arrays. Protein levels were reduced in renal and transitional cell carcinoma compared to normal kidney and bladder tissue.

The physiological function of the protein was further investigated by the establishment and preliminary analysis of a conditional *FAM96A* knockout mouse model. Here, *FAM96A/lacZ* reporter mice were generated in which Exon 3 of the *FAM96A* gene was deleted following breeding of mice with *CMV-Cre* mice. Strong endogenous *FAM96A* promoter activity was observed in tissues of the immune system such as spleen and thymus, and in the gastrointestinal tract of the *FAM96A*$^{-/-}$ mice. Surprisingly, and in contrast to observations from yeast, drosophila and zebrafish model systems, where knockout of the gene was lethal, *FAM96A*$^{-/-}$ mice were born and vital and displayed no obvious phenotype under non-stressed conditions.

Zusammenfassung

Apoptose als eine Sonderform des programmierten Zelltods ist ein konservierter, entwicklungsphysiologisch relevanter Prozess, der zur Gewährleistung der Gewebshomöostase wesentlich beiträgt. Eine Fehlregulation des apoptotischen Zelltods hat schwerwiegende pathologische Implikationen und ist zum Beispiel wesentlich für die Krebsentstehung und neurodegenerative Erkrankungen mit verantwortlich. Sowohl inaktivierende Mutationen in pro-apoptotischen Genen als auch die Aktivierung anti-apoptotischer Onkogene tragen zur Ausbildung von Neoplasien bei. In nicht-kanzerogenen Zellen regulieren Sensorproteine, sogenannte Tumorsuppressoren, physiologische Abläufe wie den Zellzyklus, die Apoptose oder sind für die Zelldifferenzierung verantwortlich. Die Identifizierung und Charakterisierung neuer, potentieller Tumorsuppressorgene (TSG) stellt darum einen wichtigen Inhalt der aktuellen Krebsforschung dar.

In dieser Arbeit wurde das in einem Hefe-2-Hybridsystem isolierte APAF-1-bindende Protein FAM96A als Tumorsuppressor charakterisiert und seine pro-apoptotische Rolle im intrinsischen Apoptoseweg näher definiert. Zunächst wurde die Interaktion der im Hefe-2-Hybridsystem isolierten Partner APAF-1 und FAM96A mit den endogenen Bindungspartnern in HEK293T Zellen verifiziert. Preliminäre Daten von transienten Überexpressionsexperimenten und zur APAF-1-Interaktion des Proteins lieferten einen Hinweis auf eine pro-apoptotische Funktion und sollten bestätigt werden. Um eine weitere, funktionelle Charakterisierung des Proteins zu ermöglichen, wurden stabile Zelllinien zur FAM96A-Überexpression generiert und auf ihr Apoptoseverhalten hin mit Kontrollvektor-transduzierten Zellen verglichen. Diese Überexpressionsstudien wurden sowohl in humanen Kolonkarzinomzellen (RKO) als auch in einer murinen Nierenkrebszelllinie (Renca-lacZ) durchgeführt, und der intrinsische Zelltod wurde mit Hilfe von Chemotherapeutika wie Mitomycin C oder Oxaliplatin induziert. Hierbei konnte die pro-apoptotische Funktion des Proteins bestätigt werden. Dieser stimulatorische Einfluss des Proteins auf den mitochondrialen Apoptoseweg wurde durch FAM96A-Deletionsanalysen mit Hilfe von „short hairpin“ RNAs in murinen Fibroblasten und RKO-Zellen verifiziert. Ein signifikanter Desensitisierungseffekt gegenüber UV-induzierter Apoptose als Resultat der verringerten FAM96A-Proteinexpression konnte hier im Vergleich zu Kontrollvektor-transduzierten Zellen festgestellt werden.

Mit Hilfe subkutaner Tumorxenograftexperimente in immunkompromittierten NOD/SCID Mäusen wurde die *in vivo* Relevanz dieser Beobachtungen näher

eruiert. Ein stark verringertes Tumorwachstum gegenüber der Kontrollgruppe konnte in den Gruppen mit gesteigerter FAM96A-Expression nachgewiesen werden. Desweitern ließ sich ein signifikant inhibitorischer Einfluss der Überexpression auf das Anwachsen der RKO-Tumoren feststellen. Insgesamt konnte eine suppressive Rolle von FAM96A auf das Wachstum und Anwachsen von Tumoren im Tiermodell nachgewiesen werden. Ein Einfluss der Überexpression von FAM96A auf die Zellzyklusverteilung von Renca-lacZ Zellen konnte nicht beobachtet werden. Um die potentielle Tumorsuppressorfunktion des pro-apoptotischen Zelltodregulators FAM96A näher zu charakterisieren wurde *in silico* in einer CGH (comparative genomic hybridization) Datenbank nach chromosomalen Aberrationen des Genlokus in einer Vielzahl von Tumorentitäten recherchiert. Deletionen im *FAM96A* Lokus konnten in 48,8% der Fälle für gastrointestinale Stromatumoren (GIST) nachgewiesen werden. Diese Beobachtung wurde mit Biopsien von zwei unabhängigen Patientenkohorten bestätigt. Zunächst wurden 31 Tumorproben mit Hilfe quantitativer real time PCR auf ihre *FAM96A* mRNA-Mengen analysiert, und in 29 von 31 untersuchten Tumoren konnte ein verringertes FAM96A-Expressionsniveau im Vergleich zu normalem Ileum beobachtet werden. Die deutlich reduzierte FAM96A-Expression verhielt sich unabhängig von der Tumorklassifizierung (Grading). In einer zweiten Patientenanalyse wurden 53 GIST-Proben immunhistochemisch auf ihre FAM96A-Proteinexpression hin untersucht. Hier ließ sich für keine der 53 Proben aus verschiedenen Regionen des humanen Verdauungsapparates eine positive FAM96A-Färbung im Vergleich zur Positivkontrolle Lebergewebe nachweisen. Der Verlust der FAM96A-Expression im Laufe der Entstehung von GIST aus Cajalzellen stellt somit einen molekularen Marker für diese Tumorentität dar. Möglicherweise wird die Reduktion der *FAM96A* mRNA-Expression bereits während der malignen Transformation im Laufe der GIST Onkongenese initiiert. Mittels real time PCR-Analysen wurde in transformierten GIST-Vorläuferzellen ein geringeres *FAM96A*-Level als bei wildtyp-Cajalzellen festgestellt. Desweiteren wurde der Einfluss einer FAM96A Re-expression in etablierten GIST-Zelllinien untersucht. Hierfür wurden sowohl Imatinib-resistente GIST48, als auch Imatinib-sensitive GIST882 Zellen lentiviral transduziert und der Einfluss von Kinaseinhibitor-vermittelter Apoptose in FAM96A re-exprimierenden Zellen ermittelt. Eine erhöhte FAM96A-Expression in beiden Zelllinien führte zu einer gesteigerten Suszeptibilität gegenüber der Kinaseinhibition durch Imatinib. Auch im Tumorxenograftmodell konnte in GIST sowohl ein statistisch signifikant reduziertes Tumorwachstum als auch eine verringerte Anzahl angewachsener Tumoren nach FAM96A Re-expression beobachtet werden. Die potentielle

Tumorsuppressor Funktion des pro-apoptotischen Proteins konnte somit in GIST bestätigt werden. FAM96A wirkt aller Wahrscheinlichkeit nach nicht nur in GIST als Tumorsuppressor, denn es konnte ein signifikant verringertes Proteinexpressionslevel immunhistochemisch in Nierenzellkarzinomen und Urothelzellkarzinomen nachgewiesen werden. Die Charakterisierung der tumorsuppressiven Funktion von FAM96A in diesen Entitäten stellt einen Fokus aktueller Untersuchungen dar.

Desweiteren wird eine Funktion des Proteins bei der Eisen-Schwefelclusterbiosynthese angenommen, die durch die beschriebene Interaktion von FAM96A mit Ciao1 nahegelegt wird. Ciao1 wiederum stellt einen essentiellen Regulator der zytosolischen Eisen-Schwefelclusterbiosynthese (CIA) dar und ist für die Beladung von Fe-S-Apoproteinen maßgeblich verantwortlich. Zunächst wurde die Interaktion von überexprimiertem FAM96A mit endogenem Ciao1 in HEK293T Zellen verifiziert und ein potentieller gemeinsamer Einfluss der beiden Interaktionspartner auf die Apoptoseregulation untersucht. Nach Überexpressions- und Deletionsanalysen von Ciao1 konnte ein antagonistischer, anti-apoptotischer Effekt des CIA-Proteins nachgewiesen werden. Dieser ist voraussichtlich auf die Beteiligung des Proteins bei der Fe-S-Biosynthese zurückzuführen. Viele Fe-S-Proteine sind in wichtige Stoffwechselprozesse und DNA-Reparaturmechanismen involviert. So wirkt sich ein gesteigertes Ciao1-Expressionslevel vermutlich positiv auf die Beladung zytosolischer Fe-S-Apoproteine mit ihrer prosthetischen Gruppe aus.

Eine weitere interessante und publizierte Funktion von Ciao1 ist die Regulation der Transkriptionsfaktoraktivität von WT1. Die beschriebene inhibitorische Wirkung von Ciao1 auf die Aktivität von WT1 wurde in Luciferase-Reporteranalysen in der AG Zörnig nicht bestätigt. Ciao1 trug zu einer signifikanten Steigerung der Fireflyluciferase-Expression durch WT1-vermittelte Aktivität des Amphiregulin-promoters bei. Daraufhin sollte der gemeinsame Einfluss von Ciao1 und FAM96A auf WT1-Zielgene analysiert werden. Da das WT1-Protein seine eigene Promoteraktivität reguliert, wurde die *WT1* mRNA-Expression mit Hilfe von quantitativer real time PCR nach Transfektion von *Ciao1* und *FAM96A* untersucht. Hier konnte eine deutliche Reduktion der *WT1* mRNA nach simultaner Überexpression von Ciao1 nachgewiesen werden. Die Rolle von FAM96A bei der Regulation der *WT1*-mRNA-Expression kann, den durchgeführten Experimenten zufolge, als vernachlässigbar eingestuft werden. Ciao1 fungiert möglicherweise zur Feinjustierung der WT1-Aktivität, indem es den Transkriptionsfaktor bindet und dieser seine autosuppressive Funktion am eigenen Promoter nicht mehr effizient ausüben kann und somit die Aktivität von WT1 über Ciao1 gesteigert wird.

Zur weiteren Analyse der physiologischen Funktion von *FAM96A* wurde in dieser Arbeit ein konditionales *FAM96A* Knockout-Mausmodell etabliert und preliminär analysiert. Durch Cre-vermittelte Rekombination wurde Exon 3 des *FAM96A* Gens deletiert. Das verbleibende Transkript unterliegt der Genfallenmutagenese und wird durch das Vorkommen eines Splice-Akzeptors in der Selektionskassette hinter Exon 2 posttranskriptional trunkiert. Die inserierte Genkassette enthält neben einem Polyadenylierungssignal am 3´ Ende ein lacZ-Reporterelement. Die lacZ-Expression spiegelt die Promoteraktivität des *FAM96A* Promoters wider und kann durch X-Gal-Färbung in murinen Organen nachgewiesen werden. Eine starke Aktivität des *FAM96A* Promoters konnte in Organen des Immunsystems wie etwa Thymus und Milz beobachtet werden. Weiterhin war eine signifikante Färbung im Ileum der homozygoten *FAM96A*$^{-/-}$-Tiere nachzuweisen. In vorangehenden Analysen wirkte sich das Ausschalten von FAM96A im Zebrafisch, der Fruchtfliege und der Hefe embryonal lethal auf die Organismen aus. Überraschenderweise scheint die Deletion von *FAM96A* in der Maus jedoch nicht zu einem embryonal-lethalen Phänotyp zu führen und die Tiere zeigen kein auffälliges Erscheinungsbild im ungestressten Zustand. Dies könnte auf eine mögliche funktionelle Redundanz zwischen FAM96A und seinem Homolog FAM96B hinweisen.

1. Introduction

1.1 Mechanisms of cell death

Cell death is initiated in a genetically controlled or uncontrolled fashion and plays a major role in organismal development, homeostasis and pathology. Two major classes of cell death exist. While necrosis was initially described as a non-programmed alternative, apoptosis is an evolutionary conserved mechanism of programmed cell death (PCD) that was first described in 1842 by Carl Vogt (Vogt, 1842). During apoptosis cells shrink, chromatin condenses, nuclear DNA is fragmented, phosphatidylserine is translocated from the inner to the outer membrane leaflet and plasma-membrane blebs containing cytosolic material form. The generation of apoptotic bodies which are engulfed by phagocytes (Kerr et al., 1972) is a major feature of this cell death mechanism. Apoptosis can be induced via two intensively studied signaling pathways: the intrinsic and the extrinsic pathway. While the intrinsic pathway is triggered by DNA damage, nutrient depletion, oxidative stress or chemotherapeutic treatment, extrinsic cell death is induced by extracellular ligands that interact with so-called death receptor molecules. Both apoptosis pathways are mediated by sequential activation of cysteine aspartases (caspases) that reside as inactive zymogens in the cytosol. Caspases that are involved in the regulation of apoptosis can be divided into two major classes: initiator or apical caspases (Caspase-2,-8,-9 and -10) and effector or executioner caspases (Caspase-3, -6 and -7) (Olsson and Zhivotovsky, 2011; Shi, 2002). Two initiator caspase molecules autoactivate each other due to their close proximity following their recruitment to protein platform complexes, and they activate effector caspases by proteolytic cleavage (Salvesen and Dixit, 1999; Shi, 2004).

Deregulated apoptosis has many clinical implications such as cancer, autoimmune diseases, neuronal disorders, hepatitis, cardiovascular diseases and sepsis (Hotchkiss et al, 2009).

Necrosis was initially described as an unregulated mechanism of death resulting from injury of a cell. The characteristic morphological features of necrosis are distinct from apoptosis. Among them are swelling of the cell, rapid mitochondrial dysfunction and plasma membrane rupture (Degterev and Yuan, 2008). More and more evidence for a structured regulation of necrosis emerged within the last decade, and the term “necroptosis” for one particular type of programmed necrosis attained acceptance (Galluzzi and Kroemer, 2008; Proskuryakov et al., 2003).

In contrast to apoptosis, necrosis is attributed with an inflammatory immune reaction that plays a role in acute hypoxic or ischemic injury (Hotchkiss et al., 2009). A tight regulation of both major cell death pathways and their interconnection is important in many evolutionary and pathological processes of a cell (Hotchkiss et al., 2009).
Several other genetically controlled, but non-apoptotic cell death pathways exist of which type II or autophagic cell death, mitotic catastrophe and poly (-ADP-ribose) polymerase-1 (PARP-1)-mediated necrotic killing, also termed Parthanatos, are only three examples (Degterev and Yuan, 2008; Galluzzi et al., 2012). The mitochondrial inner-membrane protein AIF (apoptosis inducing factor) or the endonuclease EndoG can, in a Cytochrome c-like manner, once released into the cytosol also trigger caspase-independent cell death. AIF as well as EndoG, can translocate to the nucleus and are responsible for chromatin condensation and DNA fragmentation (Broker et al., 2005; Li et al., 2001). A more functional and biochemical characterization of cell death subroutines is emerging, in contrast to the former morphological definitions and is subject to current controversial discussions (Galluzzi et al., 2012).

1.1.1 The intrinsic apoptosis pathway

Mitochondrial apoptosis is triggered by cellular stress signals such as growth factor deprivation, ER (endoplasmatic reticulum) stress, hypoxia, viral infections or DNA damage induced by irradiation or chemotherapy. Upon receipt of such a signal, p53 is activated and can initiate transcription of its pro-apoptotic target genes *Puma, Noxa* and *BAX* (Nakano and Vousden, 2001; Oda et al., 2000; Thornborrow et al., 2002; Yu et al., 2003). Puma and Noxa are members of the BH3-only subset of BCL-2-family proteins that can induce oligomerization of mitochondrial membrane proteins of the BCL-2 protein family: the pro-apoptotic members BAX, BAK or, in reproductive tissues, BOK (Kirkin et al., 2004; Portt et al., 2011). These proteins regulate the mitochondrial membrane potential and can form pores within the mitochondrial outer membrane, enabling Cytochrome c to escape from the inner membrane space. Mitochondrial membrane integrity is normally preserved by inhibition of BAX and BAK due to their interaction with anti-apoptotic members of the BCL-2 family (BCL-2, BCL-W, A1, MCL1 or BCL-x_L) (Borner, 2003; Kirkin et al., 2004; Skulachev, 1998). Anti-apoptotic BCL-2 family members can be antagonized by BH3-only proteins. In the cytosol, Cytochrome c can bind, together with dATP, to the WD40 repeat region of the key adaptor protein of intrinsic apoptosis: apoptotic peptidase activating factor-1 (APAF-1) (Li et al., 1997; Zou et al., 1997). APAF-1

then unfolds from its autoinhibited conformation and can oligomerize and form a heptameric multi-protein complex that serves as a platform for pro-Caspase-9 recruitment and activation (Cain et al., 1999; Yuan et al., 2010). Caspase-9, as an initiator caspase, cleaves and activates downstream effector caspases such as Caspase-3, -6 or -7 that promote apoptosis of the affected cell. Caspases are, in addition, regulated by members of the inhibitor of apoptosis (IAP) family (XIAP, cIAP1/2, Survivin, NIAP, ML-IAP and BRUCE) that are themselves inactivated by the mitochondrial proteins Smac/DIABLO (Second mitochondria-derived activator of caspases/Direct IAP-binding protein with Low Pi) and Omi/HtrA2. IAPs are characterized by their baculoviral IAP repeat (BIR) domain responsible for inhibitory protein-interactions with already activated Caspase-3, -7 or -9 (Gyrd-Hansen and Meier, 2010). Upon activation of effector caspases, a wide variety of target proteins involved in many physiological processes such as macromolecular synthesis or signal transduction are cleaved, ultimately leading to cell death (Fischer et al., 2003).

1.1.2 The extrinsic pathway of cell death

The extrinsic pathway of apoptosis is triggered by extracellular ligands that bind to death receptors such as tumor necrosis factor receptor 1 (TNFR1), TNF-related apoptosis-inducing ligand receptor 1/2 (TRAILR1/2), CD95/FAS/APO1, Death receptor (DR) 3, DR6, ectodysplasin A receptor and nerve growth factor receptor (NGFR) (Lavrik et al., 2005; Wajant, 2003). Death receptors belong to the TNF receptor superfamily and are characterized by their cytoplasmatic death domain (DD). A so-called death inducing signaling complex (DISC) is generated by CD95 and TRAILR1/2 following recruitment of FADD (Fas associated protein with death domain), a cytosolic protein that interacts with the death domains of the receptors via its own DD. FADD can itself recruit death effector domain (DED)-containing proteins such as pro-Caspase-8 or-10 to the DISC. When two molecules of pro-Caspase-8 are translocated to the DISC, induction is achieved *via* autocatalytic cleavage and the fully active initiator caspase can further activate downstream caspases like Caspase-3 (Dickens et al., 2012).

A cross-talk between the extrinsic and the intrinsic pathway of apoptosis in type II cells is mediated by the pro-apoptotic BCL-2 familiy member BID. Active Caspase-8 can cleave and activate BID, and the truncated tBID form then translocates to mitochondria and initiates Cytochrome c release upon binding to BAK or BAX (Korsmeyer et al., 2000; Scaffidi et al., 1998; Wei et al., 2000). The intrinsic pathway

in these cells serves as an additional amplification loop, which is needed due to the low levels of CD95 DISC formation and Caspase-8 activation in type II cells upon death receptor activation (Scaffidi, 1998). Type I cells, on the other hand, strongly activate Caspase-3 directly *via* the death receptor pathway. A detailed overview of the two pathways mediating apoptotic cell death is presented by Figure 1.1.

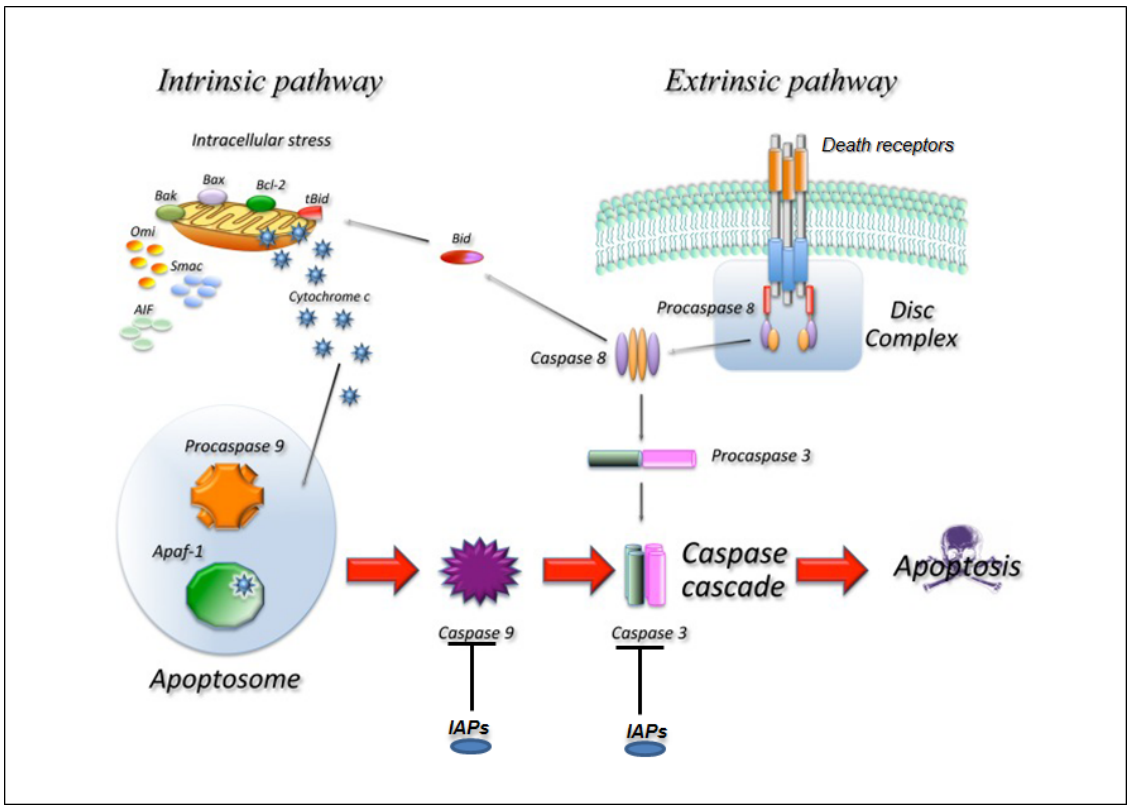

Figure 1.1: Schematic overview of apoptotic pathways
Apoptosis is mediated via two different pathways, the intrinsic and the extrinsic pathway. The two signaling pathways are crosslinked in type II cells through truncation of BID as an amplification loop of the extrinsic pathway due to low levels of Caspase-8 activation. Adapted from Favaloro et al., 2012.

1.1.3 The apoptosome as a key complex formed during intrinsic apoptosis

The apoptosome is a huge complex between 700 kDa and 1 MDa whose assembly can be induced *in vitro* by the addition of Cytochrome c and dATP to cytosolic fractions of cells (Lauber et al., 2001; Twiddy et al., 2006). Its molecular weight and stoichiometry is until now a matter of debate. APAF-1 represents a key component within the complex, generating a platform for protein interactions (Yuan et al., 2010). The large cytosolic molecule of 130 kDa resides within the cytosol in an autoinhibited conformation and can unfold and oligomerize upon Cytochrome c binding and ADP exchange (Reubold et al., 2009; Reubold et al., 2011; Riedl et al.,

2005; Yu et al., 2005; Yuan et al., 2010). APAF-1 contains 3 major sequence motifs: at the N-terminus, a caspase activation and recruitment domain (CARD), followed by a nucleotide binding and oligomerization domain (NOD), and a C-terminal series of 12-13 WD40 repeats. The interaction with pro-Caspase-9 is mediated by the CARD domains of both proteins (Qin et al., 1999; Reubold et al., 2011), while the interaction with Cytochrome c occurs within the regulatory WD40 region (**Fig. 1.2**). A platform for caspase activation is formed by 7 oligomerized APAF-1 molecules, and the loosely tethered CARD domain forms a tilted disk-like structure above the activation hub where pro-Caspase-9 molecules can dock and become activated (Yuan et al., 2011; Yuan et al., 2010). A model for the activation of pro-Caspases-9 and -3 is depicted in Figure 1.2 C. *APAF-1* exists in 5 major isoforms generated by alternative splicing that differ in size and amino acid composition (Benedict et al., 2000). APAF-1_S is the smallest protein isoform that was originally described by Zou et al. (Zou et al., 1997). Whether this isoform is able to bind Cytochrome c or activate pro-Caspase-9 is discussed controversially (Benedict et al., 2000; Zou et al., 1997). APAF-1_{XL} is the most abundant and physiologically relevant isoform, consisting of an additional N-terminal 11 amino acid insert and an extra WD40 repeat, designating it as the longest APAF-1 protein isoform. APAF-1_{LN} contains only the N-terminal insert but lacks the additional WD40 repeat. APAF-1_{LC} contains the extra WD40 repeat, while the 11 amino acids at the N-terminus are missing. APAF-1-ALT is a fifth isoform devoid of WD40 repeats and represents an inhibitory opponent of APAF-1_{XL} (Ogawa et al., 2003). Many models of caspase activation have been proposed, but the exact stoichiometry of molecules within the apoptosome complex still remains unresolved. Proteins observed within the apoptosome complex are: XIAP, Caspase-3, pro-Caspase-9, Cytochrome c, Smac/DIABLO and Omi/HtrA2 (Twiddy et al., 2006) .

Active Caspase-3 is suggested to share the same binding site within the activation hub as pro-Caspase-9 and therewith serve as an inhibitor for initiator caspase induction (Yuan et al., 2011). Another level of intrinsic apoptosome regulation is based on the intracellular pro-Caspase-9 concentration, which regulates the duration of the molecular timer for Caspase-3 activation. Caspase-9 activation is suggested to follow a CARD-displacement mechanism where one molecule of activated caspase is subsequently replaced by pro-Caspase-9 due to its higher affinity for APAF-1 (Malladi et al., 2009)

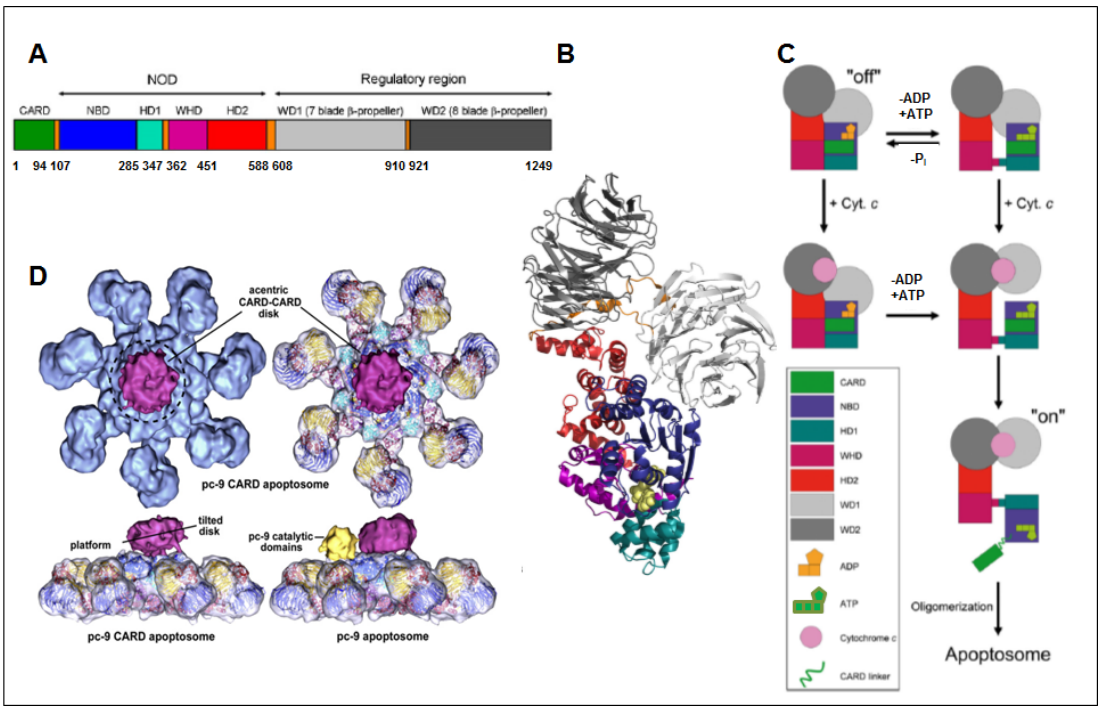

Figure 1.2: APAF-1_{XL} structure and the formation of the apoptosome complex
During apoptosome formation, APAF-1 serves as a platform for caspase binding and activation. The domain structure of the full length APAF-1 protein and the structure lacking the CARD domain are presented by A and B (color code for different domains based on A). A model for APAF-1 activation that occurs upon Cytochrome c binding, replacement of the bound nucleotide and opening of the molecule is depicted by C. The structure of the apoptosome complex with its central hub and tilted disc formed by the CARD domains of Caspase-9 (pc-9: proCaspase-9) and APAF-1 is represented in D. Figure adapted from Reubold, Yuan *et al.*, 2012.

Apoptosome formation is regulated by a further multitude of events and involved signaling proteins (**Fig. 1.3**). Intracellular nucleotide, calcium or potassium ion concentrations can serve as potential pro-survival factors by direct binding to Cytochrome c, preventing nucleotide exchange or APAF-1 oligomerization (Bao et al., 2007; Cain et al., 2001; Chandra et al., 2006). The oncoprotein Prothymosin-α (ProT) can also prevent apoptosome formation by binding to APAF-1 (Qi et al., 2010).

Heat shock proteins -27, -70 and -90 also serve to rescue the cell from apoptosis induction at several levels of apoptosome formation, whereas Hsp70 can also promote apoptosome formation together with cellular apoptosis susceptibility protein (CAS) and putative HLA (human leukocyte antigen)-DR associated protein I (PHAPI) (Kim et al., 2008). These proteins serve to facilitate nucleotide exchange on APAF-1 or assist heptamerization. Hepatocellular carcinoma antigen HCA66 is a positive regulator of apoptosome formation and influences Caspase-9 recruitment (Piddubnyak et al., 2007). The different published stages of apoptosome regulation are displayed by Figure 1.3.

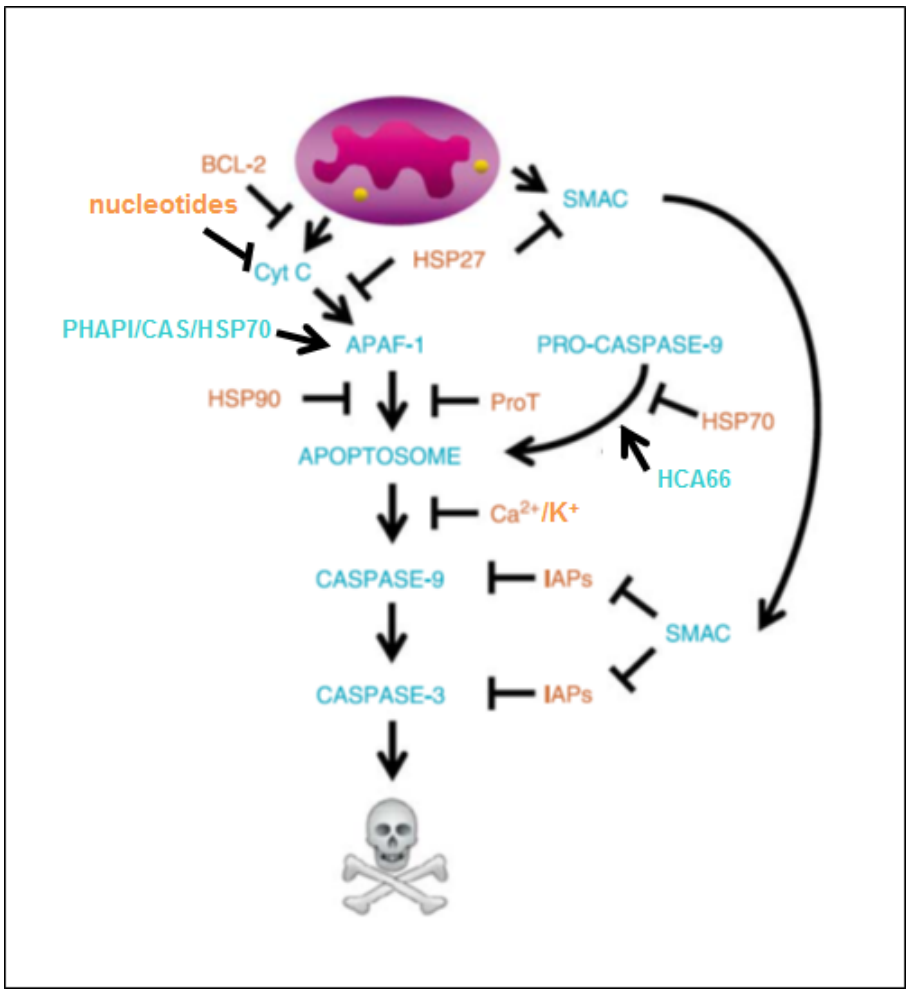

Figure 1.3: Regulation of apoptosome formation and apoptosis induction
Formation of the apoptosome and apoptosis are inhibited and positively regulated at various checkpoints, where the concentration and abundance of physiological factors defines whether signaling is blocked or cell death proceeds. Adapted from Fadeel *et al*., 2007.

1.1.4 Deregulation of apoptosis in cancer and recent therapeutic interventions

An important hallmark of cancer is the evasion of tumor cells from the apoptotic program. This process confers resistance to chemotherapy or other therapeutic interventions, enables metastasis formation and limits overall patient survival. Apoptosis resistance is enabled in 50% of cancers due to mutations in the p53 tumor suppressor protein, the “guardian of the genome” (Hanahan and Weinberg, 2000; Hanahan and Weinberg, 2011). A lot of p53-based therapy trials for cancer treatment are ongoing, including gene, drug and immunotherapy (Lane et al., 2010). As p53 is responsible for the upregulation of BAX, apoptosis is inhibited when p53 wildtype activity is lost (Zornig et al., 2001). Diminishing p53 function implicates deregulation of BCL-2 and BCL-x_L, anti-apoptotic BCL-2 family members that are

subjected to downregulation by the transcription factor p53 in normal cells (Miyashita et al., 1994). Consequently, BCL-2 and BCL-x_L are described to be overexpressed in a wide range of human cancers (Kirkin et al., 2004). The disrupted homeostasis of BCL-2 family proteins largely contributes to dysregulated apoptosis in cancer and is targeted by several approaches. Upregulation of BCL-2 in cancer can be antagonized by the BCL-2 antisense oligonucleotide oblimersen, or BCL-2 family members can be targeted by BH3-mimetic small molecule inhibitors such as ABT-737 or ABT-263, HA-14-1, gossypol, epigallocatechin-3-gallate or obatoclax (Flack et al., 1993; Kessel and Reiners, 2007; Lock et al., 2008; O'Brien et al., 2009; Oltersdorf et al., 2005; Qin et al., 2007). Pro-apoptotic family members of the BCL-2 family normally function as tumor suppressors, and loss-of-function mutations of *BAX* and *BAK* have been reported in several tumor entities (Kondo et al., 2000; Rampino et al., 1997). *APAF-1* also resembles a direct target of p53, and its expression has been reported to be frequently reduced or inactivated in cancer (Soengas et al., 2001). Due to alternative gene use, closely-related oncogenic members of the same gene family are expressed, while expression of the tumor suppressor gene *PHAP* is eliminated in prostate adenocarcinoma (Bai et al., 2001). Overexpression of HSPs, ProT and the kinase AKT, which is known to inhibit Cytochrome c release, upregulate XIAP and Survivin, or phosphorylate the pro-apoptotic BH3-only protein BAD and Caspase-9, have been reported in correlation with several malignancies and poorer clinical outcomes (Cardone et al., 1998; Datta et al., 1997; Kennedy et al., 1999; Qi et al., 2010; Tran et al., 1999). Increased expression of IAP proteins (XIAP, Survivin) has been reported in a variety of cancer entities, while nonmalignant tissue expressed normal levels of IAPs. Upregulation of IAPs is common in cancer, making them attractive targets for chemotherapy. Several antisense oligonucleotides and small molecule inhibitors (Smac mimetics) for IAPs -in monotherapy and in combinatorial treatments- have been tested in Phase I/II clinical trials (http://www.clinicaltrials.gov/; (D'Amelio et al., 2008; Fischer and Schulze-Osthoff, 2005; Fulda et al., 2002). A reduction of caspase expression is common in many cancer entities and therefore, molecules that re-establish increased caspase-activation such as RGD-peptides or derivatives of the small molecule MX-2060 (Buckley et al., 1999; Fischer and Schulze-Osthoff, 2005; Zhang et al., 2004) are under therapeutic investigation. Direct Caspase-3 introduction into cancer cells is another approach followed by fusion to a Her-2-antibody or adenoviral infection (D'Amelio et al., 2008).

The cell death response induced *via* the extrinsic apoptosis pathway is also within the focus of current therapeutic investigations. TRAILR1 and 2 signaling is activated

by agonistic human monoclonal antibodies such as conatumumab, tigatuzumab, lexatumumab, mapazumumab and drotizumumab. Dulanermin is a recombinant TRAIL-ligand agonist that triggers death receptor signaling and is currently in clinical trials (Ocker and Hopfner, 2012). Proteasome inhibitors, heat shock protein inhibitors and histone deacetylase inhibitors can activate ER stress-mediated cell death and restore APAF-1 and Caspase-9 levels (Ocker and Hopfner, 2012).

1.2 Tumor suppressor genes and their downregulation in cancer

Apart from the most commonly mutated tumor suppressor gene (TSG) described, *p53*, many other genes can act as tumor suppressors. Most often, these genes are associated with cell cycle regulation (*RB*) or are involved in differentiation, apoptosis and proliferation (*WT1, NF1, PTEN*) (Vogelstein and Kinzler, 2004). Normal cells tightly control these processes by a balanced homeostastis between proto-oncogenes and TSGs (Evans and Prosser, 1992; Lai et al., 2012). In tumorigenesis, loss of heterozygosity (LOH) of a TSG is involved in the spontaneous formation of neoplasms. Point mutations within the remaining functional allele often lead to LOH and tumor formation as a consequence of inherited predisposition. Hereditary as well as non-hereditary cancers are thought to derive from at least four or more mutation events in important cellular signaling pathways (Berger et al., 2011). Haploinsufficiency occurs when a diploid cell has only one functional copy of one allele that is incapable of retaining the wild type condition. Haploinsufficiency and dose- and activity-dependency have been controversially discussed, but are common for important TSGs such as *p53* or *PTEN* in many tumors. Obligate haploinsufficiency of a TSG is explained by an essential function of the TSG in cellular processes, so that its homozygous deletion would trigger cell death or senescence (Berger et al., 2011). Therefore, the expression or activity of such a tumor suppressor is only lowered, but not entirely lost in tumors.

The discovery of novel tumor suppressor genes that are affected by mutational events triggering oncogenesis is highly important for the interference with initiation and progression of malignant disease. High-throughput screenings for genome-wide genetic aberrations or copy number profiling serve to identify mutated or deleted regions in tumors.

1.3 FAM96A

FAM96A was discovered in a yeast two-hybrid screen of a mouse thymoma cDNA library with the *C. elegans* homologue of *APAF-1*: *CED-4*, as well as several *APAF-1*$_S$ deletion constructs as baits (K. Völp, unpublished). The human *FAM96A* gene locus is located on chromosome 15 (q22.31), is 21.4 kb long and consists of 5 exons. The mRNA is processed into two alternative splice isoforms (NM_032221.4 = isoform A, NM_001014812.1= isoform B) of which isoform A is the predicted "canonical" sequence (http://www.expasy.org/). While isoform A (*FAM96A* for further reading) codes for 160 amino acids with a predicted molecular weight of 18.355 kDa, isoform B is smaller with a size of 102 amino acids and 11.634 kDa. The small protein appears with a molecular weight of around 20 kDa in Western Blot analysis and contains a DUF59 domain (domain of unknown function, aa 39-156) shared by a family of ATPases (Lezhneva et al., 2004) as well as iron-sulfur cluster proteins (Almeida et al., 2005; Lezhneva et al., 2004). Only two proteins exist in mammals that contain this sequence motif: FAM96A and its homolog FAM96B/MIP18. Both proteins share a 50% sequence similarity and bind to the cytosolic iron sulfur cluster protein Ciao1 (Chen et al., 2012). Interestingly, FAM96B is suggested to be involved in chromosome segregation as a member of the MMXD protein complex (Ito et al., 2010). In contrast to the observed contribution of FAM96B to DNA maintenance processes, Stehling et al. rather suggest this to be related to Fe-S protein biogenesis (described in **1.5.1**) (Stehling et al., 2012). A further function for FAM96B was published recently by Yang et al. The protein, and especially the DUF59 domain, were observed to be involved in regulating the expression of the transcription factor E2-2 and therewith proliferation and migration of endothelial cells (Yang et al., 2011).

In silico predictions suggest ER-targeting of the longer isoform due to an N-terminal 27 amino acid signal sequence with a cleavage site between aa 27 and 28 (SignalP 4.1 Server (www.cbs.dtu.dk/services/SignalP), **Fig. 1.4 A**, yellow). Investigations on the subcellular localization of the protein, however, revealed FAM96A to occur within the cytoplasmic and partly within the nuclear compartment. In spite of the *in silico* predicted N-terminal signal peptide, no targeting to the lumenal compartment could be observed (Chen et al., 2012; Jung, 2012; Pick, 2006).

Chen et al. reported recombinant, bacterially expressed FAM96A (aa 39-156), lacking the signal peptide, to form stable monomers and two different domain swapped dimers that are controlled by two hinge loop regions within the molecule (84-TPTVPH-89 and 121-GTHSTEE-127). The two DUF59-dimers are suggested to

have distinct functions *in vivo* (Chen et al., 2012). Furthermore, FAM96A was observed to dimerize when Flag-tagged, overexpressed proteins extracted from cellular lysates were separated under non-reducing conditions *via* SDS-PAGE (Pick, 2006). Dimerization is suspected to be achieved by one of the 5 cysteine residues (Pick, 2006) located within the DUF59 domain of which at least one was *in silico* predicted to be highly reactive (J. Heering, Frankfurt University, unpublished). The domain structure and structures of the crystallized monomer and the two distinct domain-swapped dimers are presented in Figure 1.4.

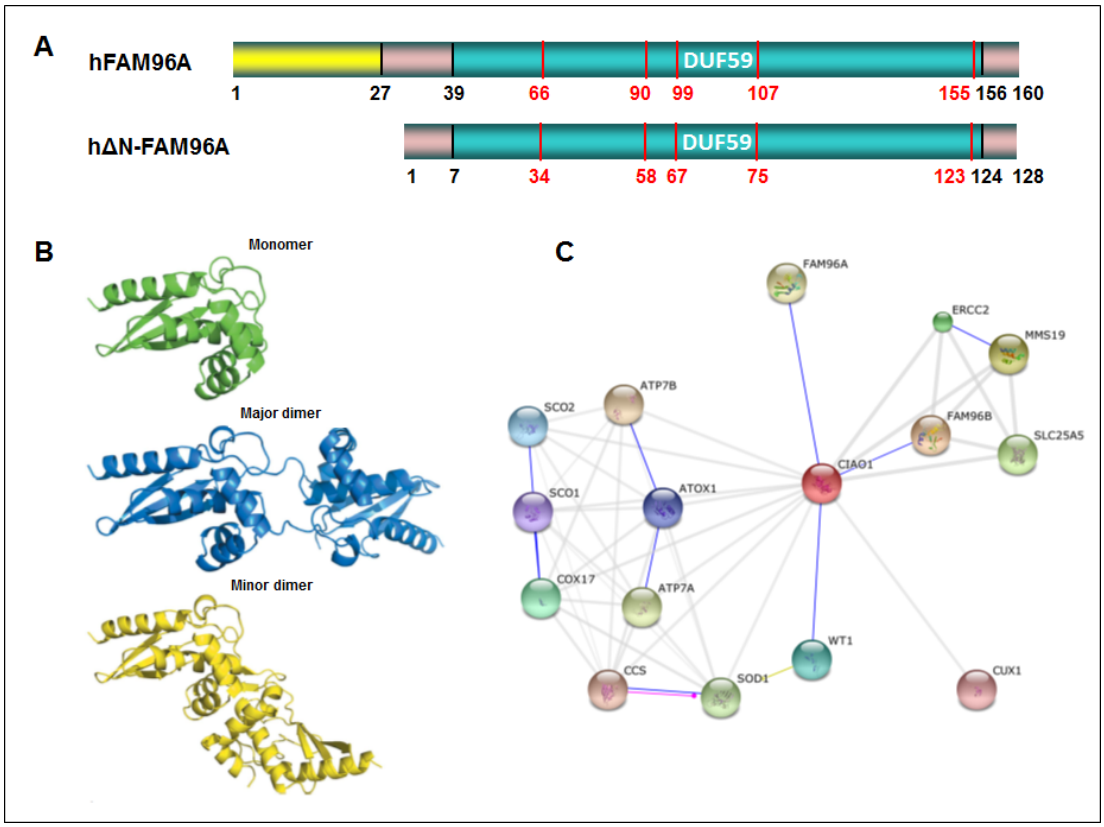

Figure 1.4: Domain and dimeric structure of FAM96A and its involvement in the Ciao1-interaction network
From an alternative translation initiation site, two separate FAM96A proteins are generated, of which the longer isoform contains an N-terminal signal sequence in addition to the C-terminal DUF59 (domain of unknown function). The 5 cysteine residues in FAM96A and the smaller isoform ΔN-FAM96A are highlighted in red (A). FAM96A forms stable monomeric and dimeric structures *in vitro* (taken from Chen et al., 2012) (B). FAM96A binds to Ciao1 and is included in the Ciao1-interaction network (http://string-db.org/) (C). Blue lines indicate published, experimentally verified binding of proteins.

The protein is highly conserved among species (Pick, 2006) and ubiquitously expressed in murine and human tissues and cell lines (AG Zörnig, unpublished data). *FAM96A* mRNA can be detected in the interdigital web of developing mouse limbs during embryogenesis (AG Zörnig, unpublished data). The integration of

FAM96A within the Ciao1-interaction network according to the string database is depicted in Figure 1C (verified interactions are indicated by blue lines). Preliminary data from transient *FAM96A* upregulation revealed the protein to sensitize cells to apoptotic stimuli employing the mitochondrial pathway (Pick, 2006). Due to an alternative start codon 32 amino acids downstream of the first ATG, a smaller isoform of around 17 kDa, ΔN-FAM96A, is generated (Pick, 2006). This isoform is assumed to play an antagonistic role, referring to earlier investigations (AG Zörnig, unpublished), functionally comparable to the smaller isoform of BCL-$_X$L, BCL-$_X$S.

1.4 Gastrointestinal stromal tumors

Gastrointestinal stromal tumors (GIST) are of mesenchymal origin and derive from malignant transformation of the interstitial cells of Cajal (ICC). These cells are pacemaker cells of the intestine that are responsible for contractile activity (peristalsis) of smooth muscle cells (Bardsley et al., 2010; Sanders, 1996; Sanders et al., 1999). An important therapeutic and prognostic marker of GIST is the expression of the KIT tyrosine kinase receptor at the tumor cell surface. In normal cells, survival and proliferation are induced *via* the type III receptor tyrosine kinases such as KIT- or platelet-derived growth factor receptor alpha (PDGFRA/B) pathways. Ligand binding of stem cell factor (SCF or PDGF) induces activation of the MAPK- (mitogen-activated protein kinase) and the PI3K/AKT-pathways, which are continuously triggered without ligand stimulation in transformed cells. 70-80% of GISTs are described to harbor *c-kit* mutations. The most common primary oncogenic *c-kit* mutations have been reported for the juxtamembrane domain of the receptor that is encoded by Exon 11. The extracellular domain of the KIT protein, encoded by Exon 9 is less frequently mutated than the juxtamembrane domain and mutations in the activation loop, encoded by Exon 17 and the ATP-binding domain (Exon 13) are uncommon (Corless et al., 2011). GISTs are usually heterozygous for the receptor tyrosine kinase (RTK) mutations, however, in approximately 15% of tumors, the second allele is lost as a result of non-disjunction and only the mutant allele is expressed (Chen et al., 2008). Another RTK that can be mutated in GIST is *PDGFRA*. Mutations can occur in the juxtamembrane (Exon 12), the ATP-binding (Exon 14) or the activation loop (Exon 18) and the same downstream signaling pathways as of KIT are constitutively activated (Corless et al., 2011). Mutant KIT and PDFRA can both be stabilized by HSP90 (Bauer et al., 2006; Matei et al., 2007), however, *PDGFRA*-activated GIST show distinct expression profiles and lower malignancy compared to *KIT*-mutated tumors. Other driver mutations in genes such as *BRAF*, *HRAS*, *NRAS* can lead to activation of the MAPK signaling and oncogenic growth independent of *KIT* or *PDGFRA* mutations. These malignancies resemble so-called “wild-type” GISTs, in which defects in SDH (succinate dehydrogenase) or mutations in *NF1* (neurofibromin1) have also been reported. Apart from the constitutively activating RTK mutations, tumor suppressor genes such as *CDKNA*, *p27* and *TP53* are commonly downregulated in malignant GIST (Corless et al., 2011).

Since 2000, the kinase inhibitor Imatinib Mesylate (IM) that was originally developed for therapeutic intervention in chronic myelogenous leukemia (CML) is also used for treatment of gastrointestinal stromal tumors (Heinrich et al., 2000). Imatinib can directly bind to the ATP-binding site of KIT and thereby stabilize the kinase in its inactive conformation and inhibit substrate phosphorylation and activation. Imatinib treatment is an important option for the chemo- and radiotherapy resistant GIST, achieving a median survival of 5 years in 70-85% of patients with advanced disease. While overall patient survival is increased, TKI therapy using IM has some drawbacks of which the most important ones are disease persistence and resistance towards treatment. Most of the wild-type and PDGFRA mutant GISTs are resistant to IM treatment, and only few patients (3-5%) suffering from *c-kit* mutated, IM-sensitive cancers are effectively cured (Corless et al., 2011). This is due to persistence and survival of transformed ICC stem cells (ICC-SC), the precursor cells of ICC and GIST. These cells are characterized by the expression of CD44, CD34 and receptors for insulin (Insr) and insulin-like growth factor (Igfr) on their surface. Most importantly, they are independent of SCF/KIT- signaling for survival, as they express only minor amounts of KIT ($KIT^{low}CD44^{+}CD34^{+}Insr^{+}$ $Igf1r^{+}$), rendering them resistant towards IM therapy. To overcome this problem of IM resistance, combinatorial treatments for selective targeting of KIT^{low} cancer stem cells need to be established (Bardsley et al., 2010).

Primary and secondary resistance towards imatinib treatment resembles the second major drawback of GIST therapy and is addressed by a variety of next-generation tyrosine kinase inhibitors such as sunitinib, nilotinib, sorafenib, dasatinib etc (Demetri, 2011). Secondary resistance most often occurs in the same gene and allele as the initial, primary driver mutation and confers resistance to imatinib treatment. These mutations are predominantly located within the ATP-binding pocket (Exon 13 or 14) and directly interfere with IM interaction. The second most common secondary mutations are within the activation loop (Exon 17 or 18) of the KIT kinase and stabilize the protein in its active conformation (Corless et al., 2011). Additionally, there is heterogeneity of resistance among multiple GIST lesions, resulting in up to seven independent secondary mutations within one patient (Liegl et al., 2008). Future approaches for GIST therapy would combine small molecules (such as RTK inhibitors) for suppression of tumor growth and apoptosis induction of all GIST cell subsets in order to eradicate the entire malignant tissue and truly cure the disease (Corless et al., 2011). The PI3K/AKT-pathway, for example, is important for GIST survival, and consequently, AKT presents a relevant therapeutic target in imatinib-resistant tumors (Bauer et al., 2007). Targeting of Hsp90 in cell culture

experiments by 17-AAG revealed promising results in imatinib-resistant GIST (Bauer et al., 2006). Furthermore, when the BCL-2 inhibitor ABT-737 was used on imatinib-resistant GIST cell lines, significant pro-apoptotic effects could be observed, providing another rationale for combinatorial targeting of RTK and other independent but complementary mechanisms (Reynoso et al., 2011).

1.5 Iron sulfur cluster biosynthesis

Iron sulfur clusters are evolutionarily highly conserved. Their participation in the origin of life is widely discussed, and they were discovered in the 1960s in mitochondrial membranes and ferredoxin (Mortenson et al., 1962; Sieker et al., 1972; Wachtershauser, 1988). They are essential for enzymatic reactions involved in fundamental biological processes such as respiration, photosynthesis or DNA repair. Two proteins of the citric acid cycle, aconitase and succinate dehydrogenase, as well as respiratory chain complexes I-III, carry Fe-S clusters. Fe-S clusters are co-factors that organize as [2Fe-2S] or [4Fe-4S] in eukaryotes and serve to transfer electrons from one protein to another, thereby catalyzing and regulating enzymatic reactions. The process of iron sulfur cluster biogenesis is therefore highly conserved from bacteria to humans, and so are the proteins involved (Rouault, 2012). Human mitochondrial Fe-S cluster biogenesis is initiated by complex formation of the dimeric cysteine desulfurase NFS1 to which two ISCU molecules bind and, together with the scaffold protein ISD11, this core complex provides an interaction platform for Frataxin. Upon Frataxin binding, the Fe-S cluster is assembled and can be transported to the recipient proteins. Together with two chaperone proteins of the heat shock protein family (HSC20 and most likely HSC70) that bind to ISCU, conformational changes in ISCU are induced that facilitate transfer of the Fe-S cluster onto target apoproteins or secondary scaffold proteins. The assembled Fe-S cluster can be transported across the mitochondrial membrane, a procedure assisted by the integral membrane protein ABCB7, and can then be loaded onto cytosolic apoproteins. *De novo* iron sulfur cluster assembly within the cytosolic and nuclear compartments has been reported (Tong et al., 2003; Tong and Rouault, 2006). While still under debate whether this is also the case in yeast, cytosolic iron-sulfur cluster assembly (CIA) is important for a wide variety of processes in humans. The first protein discovered to be involved in CIA was Cfd1/NUBP2 (cytosolic Fe-S cluster-deficient1) that forms a scaffold complex for Fe-S clusters with NBP35/NUBP1. Together with Ciao1 and IOP1/NARFL, clusters are then

transferred to apoproteins. Proteins that are involved in mammalian CIA and mitochondrial iron sulfur cluster assembly are depicted in Figure 1.5.

Several human pathologies such as Friedreich´s ataxia, mitochondrial encephalomyopathy, ISCU myopathy, sideroblastic anaemia and multiple mitochondrial dysfunction syndrome have recently been associated with defects in iron-sulfur cluster biogenesis (Rouault, 2012).

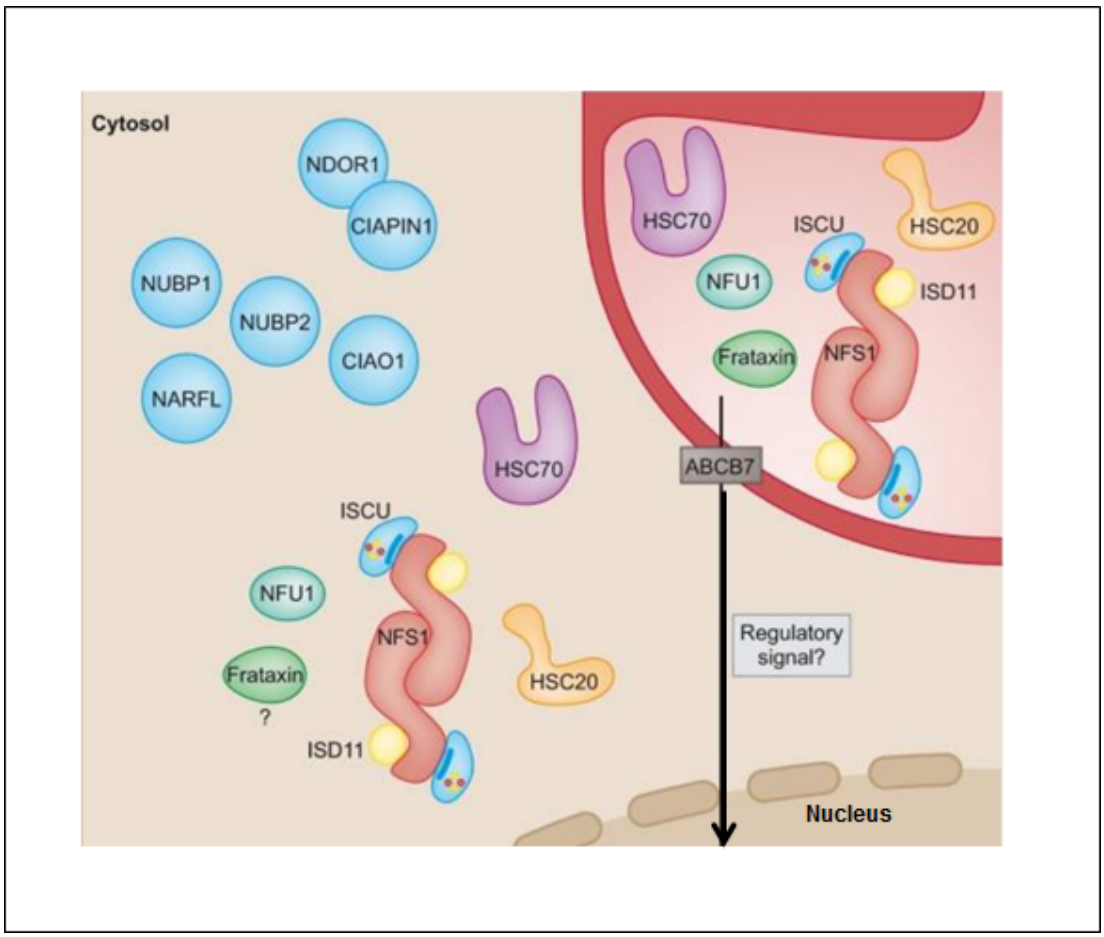

Figure 1.5: Mammalian iron sulfur cluster assembly
In humans, the assembly of Fe-S is not exclusively restricted to mitochondria, but can occur *de novo* within the cytoplasm (CIA). Alternatively, Fe-S clusters are generated in the mitochondria and transported into the cytoplasm where target apoproteins are loaded. A potential regulatory signal is transmitted to the nucleus to secure mitochondrial iron homeostasis. The Figure was adapted from Rouault et al., 2012.

1.5.1 Physiological functions of Ciao1

Ciao1 is an essential, highly conserved protein (Johnstone et al., 1999) of human cytosolic iron sulfur cluster assembly, and its depletion is lethal in yeast and *Drosophila melanogaster.* Yeast Cia1 can be functionally replaced by its human

homologue, indicating the importance of CIA conservation in eukaryotes. The doughnut-shaped structure of the *S. cerevisiae* Cia1 is defined by a central axis around which 7 blades (WD40 repeats) of a β-sheet propeller fold (Srinivasan et al., 2007). Ciao1 also contains seven WD40 domains and, as many other WD40 repeat-containing proteins, it is suggested to coordinate multi-protein complex assemblies (Li and Roberts, 2001). The 38 kDa protein is located in the nuclear and cytosolic compartment (Johnstone et al., 1998) and is described to play a role in DNA maintenance as an integral protein of the MMXD complex together with MMS19, MIP18 (MMS19-interacting protein; FAM96B), XPD and adenine nucleotide translocase ANT2 (Ito et al., 2010). The complex is assumed to play a role in chromosome segregation, whereas other groups suggested that the effects on DNA repair of MMS19-depleted cells result from impaired Fe-S protein biogenesis, and that MMS19 links CIA to DNA metabolism *via* maturation of Fe-S apoproteins. The described late-acting CIA targeting complex contains MMS19, Ciao1, ANT2, and FAM96B, and can load various target proteins. The complex is suggested to be involved in Fe-S loading of many nuclear genome stability factors apart from XPD: RTEL1, FANCJ, DNA Pol delta, DNA primase (Pri2) and DNA2 (Gari et al., 2012; Stehling et al., 2012; van Wietmarschen et al., 2012).

Ciao1 has been found in a YTH screen to interact with the transcription factor WT1. The interaction of FAM96A with Ciao1 was first observed in a YTH screen for disease-associated genes (Rual et al., 2005) and confirmed by Chen et al. (Chen et al., 2012).

Apart from its essential function which is conserved from lower to higher eukaryotes, mammalian Ciao1 seems to be involved in transcriptional regulation of the zinc-finger transcription factor Wilms Tumor 1 (WT1) (Johnstone et al., 1998).

1.6 The transcription factor WT1

The human *WT1* gene is located on chromosome 11p13 and is functionally inactivated by mutations in approximately 20% of Wilms' tumors, a childhood nephroblastoma. Other known genetic alterations in this cancer entity include inactivation of the tumor suppressors *WTX* (Wilms tumor gene on the X chromosome) and *TP53,* and stabilizing mutations of the oncogene *CTNNB1* (β-catenin). In leukemia, however, and in some types of solid tumors, *WT1* has been described as an oncogene. In undifferentiated hematopoietic cells, WT1 is important for viability, whereas in committed cells WT1 is essential for differentiation. Due to

this functional dependence on the cellular developmental status, WT1 cannot ambiguously be classified to function as a TSG or an oncogene (Huff, 2011).

The human *WT1* gene contains 10 Exons, which encode a transcription factor with four zinc-finger motives at the carboxy- and a proline glutamine rich protein interaction domain at the amino-terminus. Two different alternative splice sites in Exons 5 and 9 give rise to 4 major protein isoforms: WT1 A (-/-, lacking Exon 5 and 9), B (+/-, containing Exon 5, lacking Exon 9), C (-/+) and D (+/+). Together with alternative translational start sites and RNA editing, in total 24 different isoforms are generated in humans that give rise to the four predominant WT1 proteins. The isoforms that differ in alternative splicing of Exon 9 are functionally distinct from each other (Hastie, 2001; Yang et al., 2007). Here, the omission or insertion of three amino acids (lysine, threonine and serine (KTS)) determines if the protein is involved in transcriptional regulation (-KTS) or RNA processing (+KTS) (Hastie, 2001). The four zinc-finger motifs mediate binding to GC-rich consensus Egr1 binding sites (5'-GNGNGGGNG-3'), WTE (WT1 binding site) sites (5'-GCGTGGGAGT-3') or $(TCC)_n$ regions (Han et al., 2004).

WT1 expression is tissue-specific and the 52-54 kDa protein is predominantly localized in the nuclear compartment but can shuttle between the cytoplasma and nucleus (Niksic et al., 2004). The transcription factor was described to regulate a wide range of supposed target genes which include growth factor genes (*Amphiregulin, IGF-II, PDGF-A, CSF-1, TGF-β1*); growth factor receptors (*insulin receptor, IGF-1R, EGFR*) and other genes associated with proliferation or apoptosis (*N-myc, c-myc, BCL-2, BAK, Bag3, WID, PAX2, Cyclin E, E-cadherin, CSF-1*) (Cesaro et al., 2010; Han et al., 2004; Morrison et al., 2005). Furthermore, human and murine WT1 proteins inhibit the transcription of their own promoter upon overexpression, establishing a negative feedback-loop for autoinhibition (Malik et al., 1994; Rupprecht et al., 1994). These findings are in line with the transient expression pattern of WT1 during kidney development. *WT1*$^{-/-}$ mice display severe developmental defects in the genitourinary system and heart and die *in utero* at day E 13.5 (Moore et al., 1999).

Ciao1 has been reported to bind to the zinc-finger domains of all 4 WT1 protein isoforms, and can decrease transcriptional activity of WT1 (Johnstone et al., 1998).

1.7 Aims of the study

Decreased or lost expression of pro-apoptotic TSGs, together with an increased expression of proto-oncogenes induces malignant outgrowth, and re-establishment of these natural anti-cancer genes is important in tumor therapy. Because there are various, yet unknown mutational events contributing to malignant transformation, the identification and characterization of novel TSGs is an important topic in current cancer research. As an interaction partner of APAF-1 and a potential regulator of the intrinsic apoptosis pathway, FAM96A represents a putative new tumor-suppressor.

Objectives addressed in this study were the following:

(I) A profound functional characterization of FAM96A was one major focus of this study. Importantly, the endogenous interaction of FAM96A and APAF-1 was confirmed. Next, a detailed functional analysis of the cytosolic protein and the elucidation of its potential tumor-suppressor activity *in vitro* and *in vivo* was addressed by modulation of gene expression in normal and cancer cell lines and tumor xenograft experiments.

(II) As the *FAM96A* gene encodes a putative TSG, its differential expression pattern in several primary tumor tissues and the correlation of FAM96A expression with malignancy in certain cancer entities was investigated. Gastrointestinal stromal tumors are the most common mesenchymal tumor of the gastrointestinal (GI) tract and harbor deletions of the *FAM96A* locus with a high incidence, as revealed by CGH analyses. The deletion of the *FAM96A* gene in GISTs might contribute to recurrence of the tumor after resection and imatinib therapy, and re-establishment of FAM96A protein expression in GIST tumor cell lines was one focus of this work. Furthermore, this study aimed to identify other tumor entities that display decreased or lost protein levels of FAM96A.

(III) Apart from its potential contribution to the regulation of the intrinsic apoptosis pathway, FAM96A can bind to a mediator of cytosolic iron sulfur cluster assembly, Ciao1. The interaction with Ciao1 and a potential interplay of the two interaction partners in the regulation of intrinsic apoptosis and the activity of the transcription factor WT1 was analyzed in the course of this work.

(IV) Another aim of this study was to investigate the physiological function of FAM96A, and therefore, a conditional knockout mouse model was established and preliminarily analyzed.

2 Materials and Methods

2.1 Materials

2.1.1 Laboratory equipment

Autoclave Tuttnauer Systec 2540 EL	*Systec*, Wettenberg
BioRad Power PAC 300	*BIO-RAD Laboratories*, Munich
Branson Sonifier 250	*Heinemann,* Schwäbisch Gmünd
CASY® Cell Counter	*Schärfe Systems*, Reutlingen
Centrifuge Megafuge 1.0R	*Heraeus*, Hanau
Centrifuge Micro 220R	*Hettich Zentrifugen*, Tuttlingen
Centrifuge Minifuge GL	*Heraeus*, Hanau
DNA sub cellTM, for agarose gels	*BIO-RAD Laboratories*, Munich
Electrophoresis power supply EPS 301	*GE Healthcare*, Freiburg
FACSCalibur	*Becton Dickinson*, Heidelberg
FACScan	*Becton Dickinson*, Heidelberg
Fluorescence stereomicroscope MZ16FA	*Leica Microsystems*, Wetzlar
Fluorescence microscope Eclipse TE300	*Nikon Instruments*, Düsseldorf
Freezer CFC free (-80°C)	*Sanyo*, Wiesloch
Freezing container *Cryo1°C "Mr. Frosty"*	*Nalgene*, Roskilde, Denmark
Fridge (4°C) and freezer (-20°C)	*Liebherr Int*., Ochsenhausen
Hypercassettte ™	*GE Healthcare*, Freiburg
Gene Amp PCR System 9700	*Applied Biosystems*, Darmstadt
Incubator IR-sensor (37°C, 5% CO 2)	*Sanyo*, Wiesbaden
Laminar air flow cabinet	*Clean Air*, Woerden
LightCycler® 480	*Roche*, Mannheim
Microwave oven	*Baxter Scientific*,Unterschleißheim
Optimax Typ TR film developer	*MS Laborgeräte*, Wiesloch
pH meter FE20 Five Easy	*Mettler Toledo*, Schwerzenbach
Pipettes	*Brand*, Wertheim
Pipetus-accu	*Hirschmann*, Neckartenlingen
Roller RM5 Assistant 348	*Karl Hecht GmbH*, Sondenheim
Sequencer AB1377	*Perkin Elmer*, Rodgau
SemiPhor, Semi dry blotting device	*Pharmacia*, Freiburg
Shaker Rocky NG	*Frögel Labortechnik*, Lindau
SmartSpecTM3000 Spectrophotometer	*BIO-RAD Laboratories*, Munich
Table top centrifuge, Biofuge pico	*Heraeus*, Hanau
Thermocylcer GeneAmp PCR 9700	*Applied Biosystems*, Darmstadt
Thermomixer compact, heating block	*Eppendorf*, Hamburg
Ultracentrifuge L8M (swinging buckets)	*Beckmann Coulter*, Krefeld
UV-table GelDoc 2000	*BIO-RAD Laboratories*, Munich
UV-Stratalinker 1800	*Stratagene*, Heidelberg
Ultra-Turrax Homogenizer	*IKA*, Staufen
Vortex Genie2	*Bender & Hobein*, Zurich
Water bath	*GFL*, Burgwedel

2.1.2 Consumables

Cell culture well plates	*Corning*, Amsterdam, Netherlands
Cell culture dishes (10mm, 145mm)	*Greiner*, Frickenhausen
Cell culture flasks	*Sarstedt*, Nümbrecht
Cell strainer (100 µm pores)	*Becton Dickinson*, Heidelberg
Cryo tubes	*Nunc*, Denmark
Cuevettes	*Sarstedt*, Nümbrecht
FACS Tubes	*Greiner*, Frickenhausen
Fujifilm Medical XRAY Film Super RX	*Fujifilm*, Düsseldorf
Gloves	*Rösner-Mautby*, Kiefersfelden
Nitrocellulose membrane 45µm	*Whatman*, Dassel
Parafilm	*Pechiney Plastic Packaging*,USA
PCR plates (96-well)	*Abgene*, Schwerte
Pipette tips	*Sarstedt*, Nümbrecht
Pipette tips with filters	*BioZym*, Oldendorf
Polyallomer tubes (open-top thinwall)	*Beckman Coulter*, Krefeld
Polystyrene tubes	*Becton Dickinson*, Heidelberg
QIAshredder columns	*Qiagen*, Hilden
Reaction tubes (0.2 ml - 2 ml)	*Eppendorf*, Hamburg
Reagent reservoirs	*Corning*, Amsterdam, NL
Scalpel (diposable)	*Servoprax*, Wesel
Sterile filter units (0.45 µm, 0.22 µm)	*Corning*, Amsterdam, NL
Syringe, 0.5 ml	*Becton Dickinson*, Heidelberg
Syringe (2ml, 5ml, 10 ml)	*Codan Medical*, Rodby,Denmark
Ultra-Turrax Tubes (12,0/75mm)	*Greiner*, Frickenhausen
µMacs columns	*Miltenyi Biotec,Bergisch Gladbach*
Whatman Chromatography paper 3MM	*Whatman*, Dassel

2.1.3 Reagents

Agarose Ultra Pure™	*Invitrogen, Darmstadt*
Ampicillin	*AppliChem GmbH*, Darmstadt
ANNEXIN V-FITC	*Beckton Dickinson*, Heidelberg
Aprotinin	*Sigma-Aldrich*, Steinheim
APS (Ammonium Persulfate)	*Sigma-Aldrich*, Steinheim
Benchmark™ Prestained Protein ladder	*Invitrogen,* Darmstadt
Bovine Pituitary Extract (BPE)	*Beckton Dickinson*, Heidelberg
Bovine Serum Albumin	*Thermo Fisher Scientific,* Dreieich
Bradford Reagent (Roti®-Quant)	*Carl Roth*, Karlsruhe
Bromophenol Blue	*Carl Roth*, Karlsruhe
BSA (Bovine Serum Albumin)	*PAA Laboratories*, Pasching
CHAPS (3- ((3-cholamidopropyl) dimethylammonio)-1-propanesulfonic acid)	*Sigma-Aldrich*, Steinheim
Complete Mini Protease Inhibitor Cocktail	*Roche*, Mannheim
Cytochrome C from Bovine heart	*Sigma-Aldrich,* Steinheim

dATP	*Sigma-Aldrich,* Steinheim
Deoxy nucleotide triphosphate	*Ge Healthcare,* Munich
Digitonin	*Sigma-Aldrich*, Steinheim
DMSO (dimethyl sulfoxide)	*Merck*, Darmstadt
DTT (Dithiothreitol)	*Sigma-Aldrich*, Steinheim
Dulbeccos Phosphate Buffered Saline	*PAA Laboratories,* Pasching
ECL detection kit	*GE Healthcare*, Munich
EDTA (Ethylene Diamine Tetra Acetate)	*Sigma-Aldrich*, Steinheim
EGTA (Ethylene Glycol Tetraacetic Acid)	*Sigma-Aldrich*, Steinheim
Ethanol	*Carl Roth*, Karlsruhe
Ethidiumbromide	*Carl Roth,* Karlsruhe
Fetal Bovine Serum (FBS)	*PAA Laboratories,* Pasching
Forene® Isofluran	*Abbott GmbH*, Wiesbaden
Formaldehyde [37%]	*Carl Roth*, Karlsruhe
GeneRuler™ 1kb, 100bp Plus DNA ladder	*Fermentas,* St. Leon-Rot
Glycerol	*Carl Roth*, Karlsruhe
Glycin	*Carl Roth*, Karlsruhe
Hepes (N-2-hydroxyethylpiperazine-N'-2-ethanesulfonic acid)	*Carl Roth*, Karlsruhe
Imatinib Mesylate	*Novartis,* Basel, Switzerland
Isopropanol (2-Propanol)	*Carl Roth*, Karlsruhe
Kanamycin A Monosulfat	*Sigma-Aldrich*, Steinheim
KCl (Potassium Chloride)	*Carl Roth*, Karlsruhe
LB-Agar	*Carl Roth*, Karlsruhe
Leupeptin	*Sigma-Aldrich*, Steinheim
L-glutamine	*PAA Laboratories*, Pasching
Lipofectamine™2000	*Invitrogen*, Darmstadt
Lipofectamine™LTX	*Invitrogen*, Darmstadt
Matrigel	*Beckton Dickinson,* Heidelberg
Methanol	*Carl Roth*, Karlsruhe
$MgCl_2$ (Magnesium Chloride)	*Sigma-Aldrich*, Steinheim
Milk powder (low fat)	*AppliChem,* Darmstadt
Mitomycin C	*Sigma-Aldrich*, Steinheim
Mito Serum Extender	*Beckton Dickinson, Heidelberg*
NaAc (Sodium Acetate)	*Carl Roth*, Karlsruhe
NaCl (Sodium Chloride)	*Carl Roth*, Karlsruhe
NaOH (Sodium Hydroxide)	*AppliChem*, Darmstadt
Oxaliplatin	*GRY-Pharma,* Kirchzarten
PEI, Polyethyleneimine	*Sigma-Aldrich*, Steinheim
Penicillin/Streptomycin	*PAA Laboratories,* Pasching
Pfx DNA-Polymerase (5u/µl)	*Roche,* Mannheim
PI (propidium iodide)	*Sigma-Aldrich*, Steinheim
PMSF (Phenylmethylsulfonylfluoride)	*Carl Roth*, Karlsruhe
Polybrene (hexadimethrine bromide)	*Sigma-Aldrich,* Steinheim
Polyethylenimine	*Polysciences, Inc.,* Eppelheim
PonceauS solution	*Sigma-Aldrich*, Steinheim
Protease inhibitor cocktail	*Roche*, Mannheim

Protein A/G PLUS Agarose beads	*Santa Cruz, Heidelberg*
Protein G MicroBeads	*Miltenyi,* Bergisch Gladbach
Puromycin	*Calbiochem*, Darmstadt
REDTaq® Polymerase (1u/µl)	*Sigma Aldrich,* Taufkirch
RiboLock RNase Inhibitor	*Fermentas*, St. Leon-Rot
RNAlater	*Qiagen*, Hilden
Roti® Histofix	*Carl Roth*, Karlsruhe
Rotiphorese-Gel 30 (30% acrylamide/0.8% bisacrylamide)	*Carl Roth*, Karlsruhe
Sodium Citrate (NaCi)	*Carl Roth,* Karlsruhe
SDS (Sodium Dodecyl Sulfate)	*Carl Roth*, Karlsruhe
Staurosporine	*Calbiochem*, Darmstadt
SYBR Green PCR master mix	*Fermentas*, St. Leon-Rot
TEMED (N,N,N',N'-Tetramethylethane-1,2-Diamine)	*Carl Roth*, Karlsruhe
Tris (hydroxymethyl)-aminomethan	*Carl Roth*, Karlsruhe
Triton X-100	*Fluka*, Buchs, Switzerland
Trypan blue	*Sigma-Aldirch*, Taufkirch
Tween-20	*Carl Roth*, Karlsruhe
β-Mercaptoethanol	*Carl Roth*, Karlsruhe
7-Aminoactinomycin D (7-AAD)	*Invitrogen,* Darmstadt

2.1.4 Enzymes

Calf alkaline phosphatase (CIP)	*Roche Diagnostics*, Mannheim
DNase I	*Fermentas*, St. Leon-Rot
Platinum® *Pfx* DNA Polymerase	*Invitrogen*, Karlsruhe
Restriction enzymes	*New England Biolabs*, Frankfurt
RNase A	*Roche Diagnostics*, Mannheim
Taq-Polymerase	*New England Biolabs*, Frankfurt
T4-DNA-Ligase	*New England Biolabs*, Frankfurt

2.1.5 Kits

DNeasy Blood and Tissue kit	*Qiagen*, Hilden
Omniscript® RT kit	*Qiagen*, Hilden
QIAGEN Plasmid Maxi kit	*Qiagen*, Hilden
QIAquick Gel-Extraction kit	*Qiagen*, Hilden
RNase-free DNase set	*Qiagen*, Hilden
RNeasy® Mini kit	*Qiagen*, Hilden

2.1.6 Cell lines

Cell line	*Origin/ATCC number*	*Description*
HEK293T	CRL-11268™	Human embryonal kidney cells
RKO	CRL-2577™	Human epithelial colon carcinoma cells
GIST48	J. Fletcher, Boston, USA	Gastrointestinal stromal tumor cells
GIST882	J. Fletcher, Boston, USA	Gastrointestinal stromal tumor cells
Renca-lacZ	AG Wels, GSH	Murine renal carcinoma cells
NIH/3T3	CRL-1658™	Murine fibroblast cells

2.1.7 Buffers and Media

2.1.7.1 Cell culture

Dulbecco´s modified eagles medium (DMEM)	*Invitrogen*, Karlsruhe
Ham´s F-10 Nutrient Mix	Gibco®, Darmstadt
Luria Bertani (LB) agar, broth	*Invitrogen*, Karlsruhe
Opti-MEM®	*Invitrogen*, Karlsruhe
Roswell Park Memorial Institute (RPMI) medium	*Invitrogen*, Karlsruhe

FACS buffer (3% FCS in DPBS)

2.1.7.2 Molecular biology

Tris borate EDTA (TBE 10x)	
	108 g Tris 55 g boric acid 40 ml [0.5M] EDTA pH 8.0 ad 1 l H2O
DNA loading dye (10x)	
	20% (w/v) glycerol 100mM EDTA 1% SDS 0.25% (w/v) bromphenol blue or 0.25% (w/v) xylenecyanol
GTE solution	
	50mM Glucose 25mM Tris/HCl pH 8.0 10mM EDTA
NaOH-SDS buffer	
	0.2 N NaOH 1% SDS

2.1.7.3 Protein biochemistry

µMacs lysis buffer	
	50 mM Tris-HCl pH 8 150 mM NaCl 1% Triton X 100 1 tablet Complete Mini Protease Inhibitor cocktail

Cell lysis buffer (Stock solution)	
	10mM KCl 1.5mM MgCl2 10mM Tris-HCl pH 7.4

Cell lysis buffer (working solution)	
	9.5 ml stock solution 495 µl 10% SDS 132 µl 100mM PMSF 1 tablet Complete Mini Protease Inhibitor cocktail

5x SDS PAGE sample buffer	
	62.5mM Tris HCl pH 6.8 20% glycerine 2% SDS 0.01% bromphenol blue 50mM DTT (added before use)

CEB buffer	
	20 mM HEPES-KOH pH 7.5 10 mM KCl 1.5 mM $MgCl_2$ 1 mM EGTA 1 mM EDTA 1 µM DTT 250 µM PMSF 1 µg/ml Leupeptin 2 µg/ml Aprotinin

Apoptosome lysis buffer	
	20 mM HEPES-KOH pH 7.5 50 mM NaCl 10 mM KCl 1.5 mM $MgCl_2$ 1 mM EGTA 1 mM EDTA 1 µM DTT 250 µM PMSF 1 µg/ml Leupeptin 2 µg/ml Aprotinin 0,3 % CHAPS

10x SDS-running buffer	
	60g Tris 150g Glycin 75ml SDS (20 %) ad 1 l H2O
10x Transfer buffer	
	58.2 g Tris 29 g Glycin 200 ml Methanol ad 1 l H2O
Blocking buffer	
	TBS (0.1% Tween 20) 5 % skim milk powder
10x AnnexinV-binding buffer	
	0.1 M Hepes-KOH pH 7.4 1.4 M NaCl 25mM $CaCl_2$
Ultra-Turrax lysis buffer	
	30mM Tris-HCl pH7.5 150mM NaCl 1% Triton X 100 10% Glycerol 1mM PSMSF (added before use) 1 tablet Complete Mini Protease Inhibitor cocktail added before use)
X-Gal staining buffer	
	5 mM $K_4[Fe(CN)_6]$ 5 mM $K_3[Fe(CN)_6]$ 2mM $MgCl_2$

SDS-Gel pipetting scheme (for 2 gels):

	10 % running gel	12% running gel	15% running gel	stacking gel
Acrylamide	5 ml	6 ml	7.5 ml	1.25 ml
1.5M Tris-HCl (pH8.8)	3.75 ml	3.75 ml	3.75 ml	-
0.5M Tris-HCl (pH6.8)	-	-	-	1.825 µl
10% SDS	75 µl	75 µl	75 µl	37.5 µl
Aqua dest	6.25 ml	5.25 ml	3.75 ml	4.325 ml
10% APS	100 µl	100 µl	100 µl	100 µl
TEMED	10 µl	10 µl	10 µl	10 µl

2.1.8 Plasmids and Oligonucleotides

2.1.8.1 Sequencing oligonucleotides

Name	Sequence
SFFV	5´-CTGCTTCTCGCTTCTGTTCG-3
T7	5‘-GAATTGTAATACGACTCACTATAG-3‘
pcDNA3.1 rev	5‘-TAGAAGGCACAGTCGAGGCTGATC-3‘
pGIPZ	5´- GCATTAAAGCAGCGTATC -3’
pLKO1.Puro	5´-GACTATCATATGCTTACCGT-3´
pEGFP-N1	5´-GTAACAACTCCGCCCCATTGA-3´

2.1.8.2 Oligonucleotides for cloning

Name	*Sequence*
hFAM96A for BamH1	*5´-AAAGGATCCATGCAGCGGTGTCCG-3*
hFAM96A rev Not1	5´-*AAAGCGGCCGCTCAGTCAGGTTC*-3´
mFAM96A for BamH1	*5´-AAAGGATCCATGGAGCGAGTGTC-3*
mFAM96A rev Not1	5´- *AAAGCGGCCGCTCAGTCCGGCTCG-3´*

2.1.8.3 Oligonucleotides for quantitative real time PCR

All primers were designed using the Sofware Primer 3 (Rozen and Skaletsky, 2000) Version 4.0 (http://frodo.wi.mit.edu/)

Name	*Gene*	*Sequence (5´-3´)*	*Accession no. (nucleotides cds)*
mWT1 for	*WT1*	*ACCCAGGCTGCAATAAGAGA*	NM_144783 (1184-1203)
mWT1 rev	*WT1*	*CCTGGTGTGGGTCTTCAGAT*	NM_144783 (1394-1413)
hGAPDH for	*GAPDH*	*AATGGAAATCCCATCACCATCT*	NM_001256799 (82-103)
hGAPDH rev	*GAPDH*	*CGCCCCACTTGATTTTGG*	NM_001256799 (122-139)
hHPRT for	*HPRT*	*TGACACTGGCAAAACAATGCA*	NM_000194 (411-431)
hHPRT rev	*HPRT*	*GGTCCTTTTCACCAGCAAGCT*	NM_000194 (484-504)

2.1.8.4 Oligonucleotides for genotyping of mouse strains

Oligonucleotides for genotyping of the different conditional knockout strains were designed with the ApE software(http://biologylabs.utah.edu/jorgensen/wayned/ape/).

Name	*Sequence*
FAM96A (5´arm) for	*5´-TACCATGTGCCAACAGAGACC-3´*
FAM96A (3´arm) rev	*5´- ATCTGGCTGTGTAGCCCAGG-3´*
En2 SA rev	*5´- CCTGTCCCTCTCACCTTCTACC-3´*
LacZ for	*5´-CGGTCGCTACCATTACCAGTTG-3´*
LoxP for	*5´-CTAAGTCATCCCGACGGCAG-3´*
LoxP rev	*5´-TCAGGCATAATGGACGGACC-3´*
Cre for	*5´-GACCAGGTTCGTTCACTCATGG-3´*
Cre rev	*5´-AGGCTAAGTGCCTTCTCTACAC-3´*
FLP for	*5´-GAGAAGAACGGCATAGTGCGT-3´*
FLP rev	*5´-GACAAGCGTTAGTAGGCACAT-3´*

2.1.8.5 Lentiviral expression constructs

2.1.8.5.1 *pLKO.1-puro* shRNA vectors

shRNA constructs cloned into *pLKO.1-puro* were purchased from Sigma Aldrich (Steinheim, Germany). Human *FAM96A* (NM_032231) shRNAs were cloned into in the *TRC2* backbone, and murine shRNAs targeting *mFAM96A* into the *TRC1* vector backbone.

Construct	*Mature antisense (5´-3´)*	*Targeted mRNA-region*
hFAM96A sh1	*CAATGAGGTACTGTTGGCGT*	489-509
hFAM96A sh2	*CAAATTAGGTACTACCTTATA*	868-888
hFAM96A sh3	*ATTTATCTCCTGAACTTCCAC*	439-459
hFAM96A sh4	*TTAAATGGTAAACATCGCTGA*	552-572
hFAM96A sh5	*ATTTATCTGCTTATTGATGTC*	622-641
mFAM96A sh1	*TTACAAAGGATTGAAACTAGC*	759-779
mFAM96A sh2	*ATTTGCTCAGAAAGAATCCTC*	1003-1023
mFAM96A sh3	*TGGTGTGAACTTGATAATAAC*	471-491
mFAM96A sh4	*AATGTAGATTTCCAACTTGTG*	570-590
mFAM96A sh5	*CATGTTGACTAGATAGGTGAT*	793-813
TRC shctrl	*TGGTGCTCTTCATCTTGTTG*	Non-targeting

A non-targeting control shRNA for each vector backbone was transduced.

2.1.8.5.2 *pGIPZ*-shRNA vectors

The following constructs were purchased from *Open Biosystems*, Lafayette, USA (pGIPZ shctr) or provided by Prof. Dr. S. Fulda (Institute for Experimental Cancer Research in Pediatrics, J.W. Goethe University Hospital, Frankfurt, Germany) for

lentiviral knockdown of human *Ciao1* (NM_004804) and human *FAM96A* (NM_032231):

Construct name	Clone ID	Mature Antisense	Targeted mRNA-region
pGIPZ-sh1 Ciao1	*V3LHS_300519*	*ACACACTCAAAGTCATCCT*	480-498
pGIPZ-sh2 Ciao1	*V3LHS_300520*	*TCACTGTGTCATCATAGCT*	710-728
pGIPZ-sh3 Ciao1	*V3LHS_300522*	*TGCTTGACATCCTGTGTGT*	651-669
pGIPZ-sh4 Ciao1	*V3LHS_300524*	*TACACACTCAAAGTCATCC*	481-499
pGIPZ-sh5 Ciao1	*V3LHS_300523*	*TCATCAACTTCCCAGACCC*	594-612
pGIPZ-sh1 FAM96A	*V2LHS_138077*	*ATATCAAACAATTACAGGC*	745-765
pGIPZ-sh2 FAM96A	*V2LHS_138078*	*TATAATTAAATCTCGCTTG*	853-871
pGIPZ-sh3 FAM96A	*V3LHS_308911*	*TCTTCTTCATTTATCTCCT*	449-458
pGIPZ-sh4 FAM96A	*V3LHS_308912*	*AAACTTCTAGCGCTTTCTC*	343-361
pGIPZ-sh5 FAM96A	*V3LHS_308913*	*AACCAGATATTCTTCTTCA*	459-477
pGIPZ-sh6 FAM96A	*V3LHS_400981*	*ATAATTAAATCTCGCTTGG*	852-870
pGIPZ-sh7 FAM96A	*V3LHS_400982*	*TAAACATGAGTCTCTGACA*	776-805
pGIPZ-sh8 FAM96A	*V2LHS_138081*	*TAAATTGAGTACATTTGGG*	1032-1050
pGIPZ-shctr	verified negative control	Cat No. # RHS4346	non-silencing

2.1.8.5.3 *LeGoiG2*

For lentivirally-mediated overexpression, murine as well as human *FAM96A* coding sequences were cloned into the *LeGoiG2* vector (Weber et al., 2008) . The empty vector served as a control. http://www.lentigo-vectors.de/

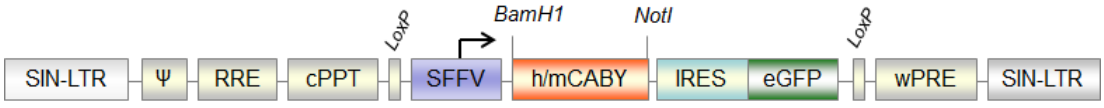

LeGoiG2 vector element description:

SIN-LTR: Self-inactivating long terminal repeat *Ψ*: Psi, packaging signal for DNA into capsid, *RRE*: rev response elemen; *cPPT*: central polypurine tract; *LoxP*: Cre recombinase recognition site; *SFFV*: spleen focus-forming virus promoter; *IRES*:

internal ribosomal entry site; *eGFP*: enhanced green fluorescent protein; *wPRE*: woodchuck posttranscriptional regulatory element

2.1.8.5.4 Ectopic expression plasmids

For transient overexpression in cell lines, the following vectors were used:

Plasmid	*Description*	*Reference*
pcDNA3.1 (+)	Amp^R, empty vector control	*Invitrogen, Darmstadt*
pcDNA 3.1 hFAM96A	Amp^R, expression plasmid for human FAM96A	*S.Bösser, AG Zörnig, GSH, Frankfurt*
pcDNA 3.1 ΔN-FAM96A	Amp^R, expression plasmid for human ΔN-FAM96A	*S.Bösser, AG Zörnig, GSH, Frankfurt*
pcDNA3.1 Flag-hFAM96A	Amp^R, expression plasmid for flag-tagged human FAM96A	*S.Bösser, AG Zörnig, GSH, Frankfurt*
pcDNA3.1 Flag-ΔN-hFAM96A	Amp^R, expression plasmid for flag-tagged human ΔN-FAM96A	*S.Bösser, AG Zörnig, GSH, Frankfurt*
pcDNA3.1 Flag-hAVEN	Amp^R, expression plasmid for flag-tagged human AVEN	*S.Bösser, AG Zörnig, GSH, Frankfurt*
pcDNA3.1 Flag-hFADD	Amp^R, expression plasmid for flag-tagged human FADD	*S.Bösser, AG Zörnig, GSH, Frankfurt*
pcDNA3.1 Myc-APAF1$_S$	Amp^R, expression plasmid for myc-tagged human $APAF1_S$	*S.Bösser, AG Zörnig, GSH, Frankfurt*
M289-Bcl-x_L	Amp^R, expression plasmid for human Bcl-x_L	*Prof. Dr. Dorothee M v. Laer, GSH, Frankfurt*
peGFP N1	Kan^R, green fluorescent protein expression control	*Clontech Laboratories Inc., USA*
pCMV Sport6 Ciao1	Amp^R, expression plasmid for human Ciao1	*Invitrogen, Darmstadt*
mWT1 +/-KTS pCB6+	Amp^R, expression plasmid for murine WT1	*Prof. Holger Scholz, Charité, Berlin*
pCB6+ empty vector	Amp^R, empty vector control	*Prof. Holger Scholz, Charité, Berlin*
pMD2.G (vsv-g)	Amp^R, vesicular stomatitis virus glycoprotein expression	*Addgene Inc., Cambrige, MA, USA*
p8.91 (gag pol)	Amp^R, encapsidation plasmid for viral integration	*(Zufferey et al., 1997)*

2.1.8 Antibodies

2.1.8.1 Non-conjugated antibodies

Antibody	*Origin*	*Dilution*	*Reactivity*	*Host*
anti-FAM96A	Pineda	1:100-500	human, mouse	rabbit
anti-β-ACTIN (C11)	Santa Cruz Biotech.	1:2,000	human, mouse, rat	goat
anti-APAF1	BD Biosciences	1:1,000	human, mouse	rabbit
Anti-EZRIN (3C12)	Invitrogen	1:1,000	human	mouse
anti-FLAG (M2)	Sigma-Aldrich	1:1,000	DYKDDDDK	mouse
anti-rabbit IgG	Zymed Laborat.	1µg	rabbit	goat
Anti-goat IgG	Zymed Laborat.	1µg	goat	rabbit
Anti-Ciao1	Sigma-Aldrich	1:2,000	human, mouse	rabbit
Anti-WT1 (C-19)	Santa Cruz Biotech.	1:1,000	human, mouse, rat	rabbit
Anti-p15 (K18)	Santa Cruz Biotech.	1:1,000	human, mouse, rat	rabbit

2.1.8.2 Conjugated antibodies

Antibody	*Origin*	*Dilution*	*Host*
anti-rabbit HRP	Ge Healthcare, Munich	1:2,000	donkey
anti-mouse HRP	Ge Healthcare, Munich	1:1,000	sheep
anti-goat HRP	Ge Healthcare, Munich	1:1,000	rabbit

2.1.9 Mouse strains

Name	*Genetic background*	*Origin*
NOD-SCID	NOD.CB17-*Prkdcscid*/J	Jackson Laboratory
FAM96A	B6NTac;B6N-A^{tm1Brd} Fam96a$^{tm2a(EUCOMM)Wtsi}$/ WtsiBiat	EUCOMM
CMV-Cre	GO-Tg-Deleter-Cre B6.C-Tg(CMV-cre)1Cgn/J	ZVTE Mainz
FLPeR	GO-Tg-Act-Flp	ZVTE Mainz
FAM96A/lacZ	B6NTac;B6N-A^{tm1Brd} Fam96a$^{tm2a(EUCOMM)Wtsi}$/WtsiBiat GO-Tg-Deleter-Cre B6.C-Tg(CMV-cre)1Cgn/	Georg-Speyer-Haus (AG Zörnig)
FLP/FAM96A	GO-Tg-Act-Flp B6NTac;B6N-A^{tm1Brd} Fam96a$^{tm2a(EUCOMM)Wtsi}$/WtsiBiat	Georg-Speyer-Haus (AG Zörnig)
FLP/FAM96A/Cre	GO-Tg-Act-Flp B6NTac;B6N-A^{tm1Brd} Fam96a$^{tm2a(EUCOMM)Wtsi}$/WtsiBiat/ GO-Tg-Deleter-Cre B6.C-Tg(CMV-cre)1Cgn/J	Georg-Speyer-Haus (AG Zörnig)
C57Bl/6	C57BL/6NCrl	Charles River

2.2 Methods

2.2.1 Molecular biology

2.2.1.1 Transformation of chemocompetent *E.coli*

30 µl of frozen chemocompetent *E.coli* cells (DH5α (*TaKaRa Bio,* Saint-Germain-en-Laye*,* France) or Top10 cells (*Life Technologies,* Darmstadt), stored at -80°C) were thawed on ice, and 1 µg plasmid DNA or 5 µl of a DNA ligation reaction were added. Bacteria were incubated on ice for 30 minutes, and a heat-shock was applied at 42°C for 30 seconds. Subsequently, bacterial cells were returned on ice, and 250 µl of antibiotics-free LB Medium were added, followed by incubation for 1.5 h at 37°C while shaking (750 rpm, Thermomixer). Then 150 µl of the transformed bacterial suspension was plated on agar-plates and incubated overnight at 37°C.

2.2.1.2 Storage of bacteria

Bacterial suspensions were frozen in 50% sterile glycerol and stored until further usage at -80°C.

2.2.1.3 DNA and RNA isolation and analysis

2.2.1.3.1 Small scale plasmid DNA isolation (Mini-prep)

The alkaline lysis method was used for small scale isolation of bacterial plasmid DNA (Birnboim, 1983). During the protocol, cell lysis is induced by a NaOH-SDS-containing buffer. SDS denatures the proteins, whereas addition of NaOH leads to denaturation of chromosomal and plasmid DNA. Subsequent neutralization with potassium acetate causes precipitation of SDS and formation of complexes including chromosomal DNA, denatured proteins and cellular debris, which can be removed by centrifugation. The plasmid DNA remains in the supernatant.

3 ml LB medium (containing 100 µg/ml of Ampicillin) were inoculated with one colony of transformed *E. coli* from an agar plate or a bacterial glycerol stock and incubated at 37°C overnight while shaking at 160 rpm. 1.5 ml of this overnight culture were centrifuged at 12,000 x g for 2 min, the supernatant was discarded and the cell pellet was resuspended in 100 µl of ice-cold GTE solution. After addition of 200 µl freshly prepared NaOH-SDS buffer, the tube was inverted 5 times and

incubated at room temperature for 5 min. Afterwards, 150 µl of ice-cold 5M KOAc were added and mixed carefully by inverting the tubes, followed by incubation for 5 min on ice. After centrifugation at 12,000 x g for 5 min, the supernatant was transferred to a new tube. Plasmid DNA was precipitated after addition of 1 ml 100% ethanol and centrifugation at 12,000 x g for 10 min at room temperature. The pellet was washed with 70% ethanol, and after centrifugation for 5 min at 12,000 x g, the DNA was air-dried and resuspended in 30 µl sterile deionized water containing 0.2 mg/ml RNase A. The isolated plasmid DNA was stored at –20°C.

2.2.1.3.2 Large scale plasmid DNA isolation (Maxi-prep)

For a large scale plasmid isolation, 250 ml of LB supplemented with the respective antibiotic were inoculated with transformed bacteria and grown overnight at 37°C and 160 rpm. After 12 to 16 hours, cells were harvested by centrifugation at 4,500 x g and 4°C for 15 min. Large-scale DNA isolation was performed according to the manufacturer's instructions (Plasmid Maxi Kit, *Qiagen,* Hilden) to isolate plasmid DNA, which was stored at -20°C until further usage. DNA and RNA concentrations were determined by photometric measurement, based on the absorption of DNA at 260 nm, using the NanoDrop™ 1000 spectrophotometer (*Peqlab*, Erlangen). The 260/280nm-ratio is used to determine the purity of the measured DNA or RNA and should be within a range 1.8 to 2.1.

2.2.1.3.3 Polymerase chain reaction

Specific DNA fragments can be amplified by polymerase chain reaction (PCR). A PCR reaction includes denaturation of the template, hybridization of specific primers to the target DNA and repeated elongation cycles during which the DNA fragment is enriched. The elongation time depends on the length of the amplified sequence. Here, 1 min for 1 kb was used.

A standard PCR reaction was set up according to the following composition:

Reagent	*Final concentration*	*Volume (µl)*
10 x Platinum *Pfx* amplification	1 x	5
50 mM $MgSO_4$	1 mM	1
dNTPs (100 mM)	10 µM	2
Forward Primer	20 µM	1
Reverse Primer	20 µM	1
Pfx-DNA-Polymerase	1.75 units/reaction	0,75
template-cDNA-Volume	100ng -1µg	1
sterile, distilled water	ad 50 µl	38,25

A standard PCR for the amplification of FAM96A was performed as follows:

Amplification step		Time	Temperature	Cycle number
Initial denaturation		3 min	95°C	1
Elongation	Dentauring	30 sec	95°C	30 cycles
	Annealing	30 sec	60°C	
	Extension	30 sec	68°C	
Final Elongation		10 min	68°C	1
Cooling		∞	4°C	

Amplified fragments were visualized using UV light following intercalation of ethidium bromide during agarose gelelectrophoresis. The desired amplified DNA was extracted from the gel and purified with the QIAquick gel extraction kit (Qiagen, Hilden).

2.2.1.3.4 Agarose gelelectrophoresis

DNA fragments can be separated according to their size by agarose gelelectrophoresis. This is based on movement of the negatively charged DNA towards the anode in an electric field. The agarose forms a meshwork in which the migration velocity of DNA depends on the size of the fragments. Separated DNA fragments can be visualized by UV light (Helling et al., 1974). PCR products or plasmid DNA were separated in agarose gels containing 1% to 2% of agarose in 0.5 x TBE buffer and 0.5 µg/ml ethidium bromide. Electrophoresis was performed in chambers filled with 0.5 x TBE buffer, and DNA samples were mixed with 10 x DNA loading buffer, loaded onto agarose gels and separated at 120 V. A 1 kb DNA ladder or a 100 bp DNA ladder (*Fermentas*, St. Leon-Rot) were used as DNA size markers.

2.2.1.3.5 DNA extraction from agarose gels

The ethidiumbromide-stained DNA of interest was cut out from an agarose gel with a scalpel. DNA purification was performed using the QIAquick gel extraction kit (*Qiagen*, Hilden) according to the manufacturer's instructions.

2.2.1.3.6 Ligation of DNA

The enzyme DNA ligase catalyzes formation of phosphodiester bonds between 5´phosphates and 3´hydroxyl groups of DNA strands, thereby coupling the ends of DNA fragments with complementary nucleotide overhangs. Vector and insert DNA were ligated in a total reaction volume of 10 µl. The ligation mix contained DNA, 1 µl

T4-DNA-ligase (40u/ml) and 1 µl 10 x ligase buffer. The ligation reaction was performed at room temperature for 1 hour, or at 16°C overnight. Afterwards, 5 µl of the ligation volume were used for transformation of chemocompetent *E.coli*.

2.2.1.3.7 Restriction digest and dephosphorylation of 5´ends

For restriction enzyme digestion of DNA, a reaction mix consisting of the restriction enzyme, a suitable reaction buffer (10x) and, if required, 10% BSA were used. An analytic restriction digest was performed with 1 µg DNA in a volume of 20 µl for at least 1 hour, while preparative digestions were conducted overnight with 10 µg to 20 µg DNA in 50 µl reaction volume at 37°C. DNA fragments were analyzed by agarose gel electrophoresis.
Dephosphorylation of DNA 5´ ends by incubation with Calf intestine phosphatase (CIP) prevents self-ligation of digested DNA. 5´ dephosphorylation of cut plasmid vectors increases efficiency of the ligase reaction with desired inserts. For 5´dephosphorylation of vectors, 1 u CIP was added to the restriction digestion mix.

2.2.1.3.8 Sequencing

Sequencing of DNA was performed with the *AB1377*-sequencer (*Perkin Elmer,* Rodgau) using dye primer chemistry. Sequences were analyzed with the Lasergene software (*Version 8.0, DNAStar*) and NCBI Blast (http://blast.ncbi.nlm.nih.gov/). For sequencing, 0.5 µg DNA or 3 µl Mini-prep DNA and 1 µl sequencing primer (10 µM) were adjusted with sterile water to a total volume of 15 µl.

2.2.1.3.9 RNA Isolation

For isolation of total RNA, cells were harvested mechanically in DPBS and centrifuged (5 min, 450 x g, 4°C). Cell pellets were either resuspended in *RNAlater* stabilization reagent (*Qiagen*, Hilden) and frozen at - 80°C, or used immediately for RNA isolation via the *RNeasy Mini Kit* according to the manufacturer´s instructions (*Qiagen*, Hilden). Cells were lysed using *QIAshredder* columns (*Qiagen*, Hilden), and on-column DNAseI digestion was performed for 15 min prior to elution of total RNA.

2.2.1.3.10 cDNA synthesis

1 µg of total RNA was transcribed enzymatically to cDNA according to the manufacturer´s instructions using the Omniscript® RT Kit (*Qiagen*, Hilden). In a 20 µl volume, an oligo(dT) primer (*Qiagen*, Hilden) was used together with the *RiboLock* RNAse inhibitor (*Fermentas*, St. Leon-Rot). A control reaction with RNA lacking reverse transcriptase was performed (RT-) to exclude sample contamination with foreign DNA.

2.2.1.3.11 Quantitative real time PCR (RT qPCR)

The exact quantity of an mRNA transcript or DNA molecules in a sample (e.g. cultivated cells or tissue samples) can be determined *via* quantitative real time PCR. Isolated DNA can directly be used as a template for qPCR analysis. A reverse transcription reaction has to be performed prior to the analysis of isolated RNA. The obtained cDNA is used for the quantitative PCR reaction. The signal of an intercalating fluorescent dye (SYBR Green 1) is detected at the end of each amplification cycle and directly correlates with the amount of double stranded DNA in the sample. The amount of target cDNA can either be compared to a DNA of known concentration (absolute quantification) or normalized to expression of a certain housekeeping gene (relative quantification). The threshold cycle (Ct) at which the fluorescence signal of the sample is higher than background level is determined for each sample, and the ΔCt value is calculated by subtraction of the Ct of the housekeeping gene from the Ct of the target gene.
To compare the relative abundance of a target cDNA in different samples, the ΔΔCt value is calculated as follows: ΔΔCt = ΔCt (sample 1) - ΔCt (sample 2)
Assuming a doubling of the target sequence in each cycle (PCR efficiency of 2), the relative target sequence abundance can be calculated using the following equation: Fold difference of the target gene compared to the housekeeping gene = $2^{(-\Delta\Delta Ct)}$.
Quantitative real time PCR analysis was performed on a LightCycler® 480 system (*Roche*, Mannheim). Specificity of the RT qPCR was further confirmed by agarose gel electrophoresis and sequencing of the reaction product. The crossing point values for each amplification curve were calculated using the LightCycler® 480 Abs Quant/2nd Derivative Max method (Relative Quantification Software, Roche Applied Science).

A qRT-PCR reaction was set up as follows:

Reagent	Final concentration	Volume (µl)
Forward Primer (10µM)	0,25 µM	1,25
Reverse Primer (10µM)	0,25 µM	1,25
Maxima SYBR Green 1	-	12,5 µl
Template-cDNA	≤ 500 ng	
sterile, distilled water	-	10 µl

All PCR reactions were set up in triplicates, 2 µl of cDNA were added and 24 µl per sample were distributed among a 96 well plate. An RT- as well as a template-lacking control were included.

Amplification step		Time	Temperature	Cycle number
Initial denaturation		15 min	95°C	1
	Dentauring	20 sec	95°C	
Elongation	Annealing	30 sec	60°-62°C	40 cycles
	Extension	30 sec	72°C	
Melting curves		10 sec	50°C	
		10 acquisitions/°C	95°C	
Cooling		10 min	37°C	

2.2.1.3.12 Genomic DNA isolation from mouse tails

Total DNA was isolated from mouse tails using a DNeasy Blood and Tissue Kit according to the manufacturer´s instructions (*Qiagen*, Hilden). Tail tips of 0.3-0.5 cm were lysed overnight in a 56°C water bath in tissue lysis buffer supplemented with proteinase K. Genomic DNA was eluted in a volume of 200 µl and kept at 4°C until further usage.

2.2.1.3.13 Genotyping of a conditional *FAM96A* knockout mouse

Genetically mutated mouse strains serve as a valuable tool to investigate the physiological function of a gene. Constitutive and conditional knockin or knockout mice are generated by targeted incision or excision of a specific DNA sequence into and off their genome. Murine embryonic stem (ES) cells transfected with a targeting vector are positively screened for the correct homologous recombination construct and injected into a diploid blastocyst. This blastocyst is implanted into the uterus of a

pseudo pregnant mouse, giving rise to chimeric animals whose germline is derived from the donor ES cells.

A conditional knockout of a gene can be induced by recombination achieved *via* breeding of animals together with deleter mice that express recombinases of the Cre/*loxP*- or FLP/*FRT*-system that cut and recombine DNA at site-specific recombination target sites (SSRTs: *loxP*- or *FRT*-sites). As approximately 15 % of all gene knockouts are developmentally lethal, a conditional knockout model provides the opportunity to induce a tissue-specific knockout. A conditional *FAM96A* knockout mouse on the C57Bl/6 background was generated by and received from EUCOMM (European Conditional Mouse Mutagenesis Program), a member of the International Knockout Mouse Consortium (IKMC) (Project: 26229; http://www.knockoutmouse.org/search_results?criteria=FAM96A). The targeting vector construct is shown below.

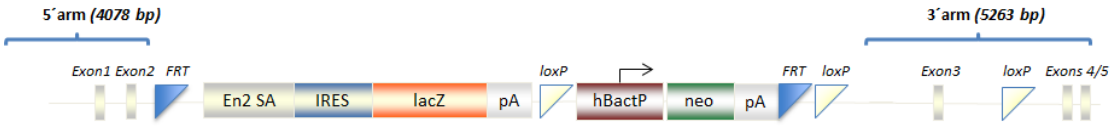

FAM96A targeting vector, description of functional elements*:*

FRT: recombination target site for FLP recombinase; *En2SA*: mouse Engrailed-2 gene splice acceptor; *IRES*: internal ribosomal entry site; *lacZ*: reporter gene; *pA*: Polyadenylation signal; *loxP*: recombination target site for Cre recombinase; *hBactP*: human beta-actin promoter; *neo*: neomycin resistance gene

The conditional knockout is achieved via the so-called “knockout first” strategy where a cassette is inserted into an intron of the target gene, and the knockout is produced at the level of mRNA processing (Testa et al., 2004). A splice acceptor in the cassette is responsible for mRNA-capturing and a polyadenlyation-signal serves as a truncation signal to interfere with mRNA transcription downstream of the cassette. For gene targeting of murine *FAM96A*, Exon 3 was floxed (flanked by loxP sites), and a cassette upstream of the floxed region was inserted that is flanked by *FRT*-sites. As shown above, the targeting cassette contains a splice acceptor (*En2 SA*), an internal ribosomal entry site (*IRES*) between splice acceptor and *lacZ* reporter gene as well as a polyadenlyation signal (*pA*). For selection of embryonic stem cells, the human β-actin promoter (*hBactP*) was cloned in front of a neomycin resistance gene and another polyA signal flanked by *loxP* and *FRT*-sites. Genotyping of the heterozygous *FAM96A* mice was performed by conventional PCR. Here, a three-primer strategy served to discriminate between the wildtype (wt) allele and the allele containing the inserted cassette (red arrows). In heterozygous

mice, two fragments were obtained after amplification, one for the wt allele (945 bp) and another for the inserted cassette (408 bp). A 5´-3´-fragment that contains the inserted cassette is not amplified under these conditions, due to the large fragment size of 7.9 kb.

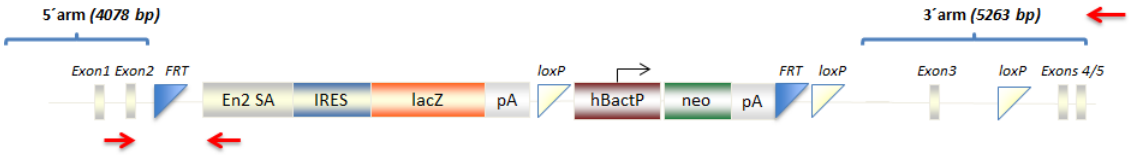

Mating between heterozygous *FAM96A* mice and transgenic *CMV-Cre* animals that ubiquitously express the Cre recombinase under the control of the human cytomegalovirus promoter generates reporter mice in which the truncation of the *FAM96A* gene can be monitored in all tissues of the animal. The strategy for genotyping of *FAM96A/lacZ* mice is shown below. Three PCR reactions were carried out of which the first distinguished between the wt allele and insertion of the targeting cassette (*FAM96A* PCR, red arrows). In a second PCR reaction, occurrence of *Cre recombinase* DNA was determined and the third PCR served to confirm the deletion of Exon 3 (*LacZ* PCR, green arrows). A fragment of 404 bp was generated if Exon 3 and the selection marker were deleted after Cre-recombination.

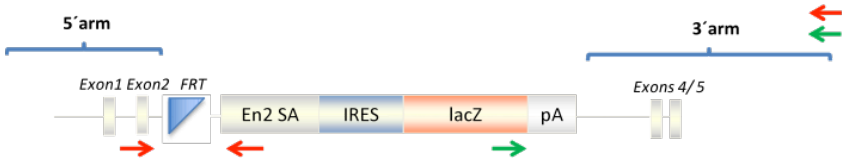

Cross-breedings of heterozygous *FAM96A/lacZ* mice gave rise to homozygous knockout reporter animals that were genotyped following the same strategy.

The targeting cassette was deleted by recombination with FLP-recombinase at the *FRT*-sites. The resulting *FLP/FAM96A* mice were genotyped *via* three different PCR reactions.

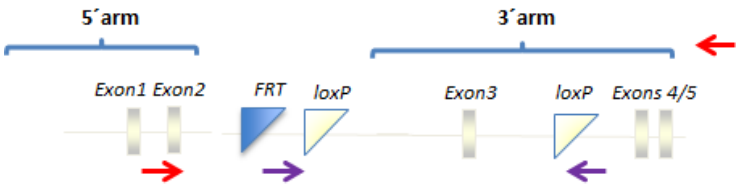

The first PCR was performed to investigate the absence of the targeting cassette by primers that bind in the 5´ and 3´ arm of the vector (961 bp, red arrows). In a second reaction, occurrence of *Flp-recombinase* DNA was analyzed. In a third PCR reaction, wt alleles were distinguished from the targeted, floxed alleles by

amplification of the remaining loxP sites (269 in wt compared to 301 bp in targeted allele, purple arrows).

To produce a null allele, heterozygous *FAM96A* mice were crossbred with FLPeR mice prior to exposition to the Cre recombinase. Heterozygous *FLP/FAM96A* mice from the first mating were bred to *CMV-Cre* mice to achieve a complete knockout of Exon 3 without the reporter cassette. The remaining transcript that consists mainly of Exons 1 and 2 is *in silico* predicted to not to be recognized by non-sense mediated decay (NMD). Heterozygous mice were genotyped by amplification of the wildtype allele (945 bp, red arrows) and in addition, a fragment of 342 bp was generated from the knockout allele. Only the smaller fragment was amplified in homozygous knockout animals.

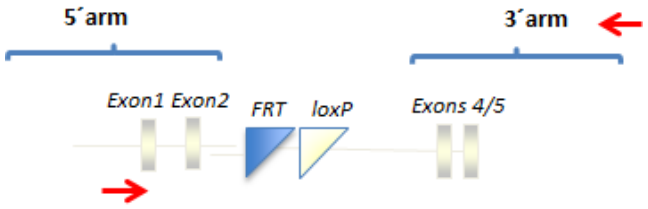

PCR reactions using genomic DNA from mouse tails were set up as follows:

Reagent	***Volume (µl)***				
	FAM96A(1x)	***FLPer(1x)***	***Cre(1x)***	***LoxP(1x)***	***LacZ(1x)***
isolated DNA	4	2	5	4	4
dNTP-mix (2.5mM	3	3	3	3	3
Forward (10µM)	1.5	1.5	1.5	2	2
Reverse (10µM)	1.5	1.5	1.5	2	2
En2 SA rev (10µM)	1.5	/	/	/	/
10 x PCR buffer	2.5	2.5	2.5	2.5	2.5
REDTaq Polymerase	1.5	1.5	1.5	1.5	1.5
H_2O	9.5	13	10	10	10

For genotyping of *FAM96A*, *FAM96A/lacZ* and *FLP/FAM96A* mice, the following PCR programs were used:

Amplification step	***Temperature***			***Time (min)***	***Cycle number***
	FAM96A	***LacZ***	***LoxP***		
Denaturing	95°C	95°C	95°C	3	1
Primer hybridization	95°C	95°C	95°C	0.5	
Primer hybridization	55°C	55°C	55°C	0.5	3
Primer hybridization	72°C	72°C	72°C	0.5	
Denaturing	95°C	95°C	95°C	0.5	
Annealing	62°C	60°C	60°C	0.5	35
Extension	72°C	72°C	72°C	0.5	
Final Extension	72°C	72°C	72°C	4	1
Cooling	4°C	4°C	4°C	∞	

PCR programs to detect *FLP*- and *Cre recombinase* transgenes are depicted below:

Amplification step	***Temperature***		***Time (min)***		***Cycle number***
	FLP	**Cre**	**FLP**	**Cre**	
Denaturing	95°C	95°C	3	3	1
Denaturing	95°C	95°C	1	0.5	
Annealing	58°C	55°C	1	0.5	35
Extension	72°C	72°C	1	0.5	
Final Extension	72°C	72°C	4	4	1
Cooling	4°C	4°C	∞	∞	

2.2.2 Protein biochemistry

2.2.2.1 Protein isolation from cellular lysates

Cells were harvested and washed once with 1ml of DPBS prior to centrifugation for 5 min at 450 x g and 4°C. Pellets were resuspended in a suitable volume of 1x protein lysis buffer and incubated for 10 min on ice. Lysates were then sonicated (Sonifier 250, Branson; Duty cycle 30%, Output 5) and centrifuged for 15 min at 15,700 x g and 4°C. Pellets were discarded and protein concentration in the supernatant was determined by the Bradford assay.

2.2.2.2 Protein extraction from tumor and tissue material

A piece of tumor or murine tissue was cut from the solid mass with a scalpel and transferred into a tube (12,0/75mm, Greiner) filled with 1 ml of Ultra-Turrax lysis buffer. The tumor or tissue sample was homogenized, transferred into an eppendorf tube and centrifuged at 15,700 x g for 10 min at 4°C. Protein concentration of the supernatant was analyzed according to the Bradford protocol.

2.2.2.3 Protein quantification using the Bradford protocol

Protein concentration of cellular lysates was determined spectrophotometrically via the Bradford assay (Bradford, 1976). The reagent *Coomassie Brilliant Blue* G-250 binds to cationic and unpolar amino acid residues, which shifts the reagent's absorption maximum from 470 nm to 595 nm. The extent of absorption at 595 nm is proportional to the protein amount in the lysate, and using a standard curve of known concentrations, the total protein amount can be quantified. 400 µl of deionized water were supplemented with 0.5 µl of protein lysate and 100 µl of Bradford reagent, followed by a 5 min incubation and subsequent measurement.

2.2.2.4 SDS PAGE

Separation of proteins according to their molecular weight is achieved by sodiumdodecyl-sulfate polyacrylamide gel electrophoresis. Disulfide bonds are reduced due to addition of ß-Mercaptoethanol or DTT to the 5 x sample buffer, and

proteins are denatured by SDS in the running buffer and an initial denaturation of cellular lysates for 5 min at 95°C. Gels were run in 1 x SDS-running buffer using the Mini Protean II system (*BioRad*, Munich) at 90 V for the first 20 min (stacking gel) and at 130 V for the separation gel.

2.2.2.5 Transfer of proteins onto nitrocellulose membranes

Proteins separated by SDS PAGE were transferred onto 0.45 µm nitrocellulose membranes using a TE77X semi-dry transfer unit (*Hoefer Pharmacia Biotech Inc.*, San Francisco). Whatman papers were soaked in 1 x transfer buffer. 3 layers of Whatman paper were placed on top of the anode of the chamber, followed by a nitrocellulose membrane, the SDS gel, 3 Whatman papers and the cathode of the blotting chamber on top. Protein transfer was performed at 0.8 mA/cm^2 for 2 hours. After blotting, membranes were stained with PonceauS solution to confirm equal transfer and loading of proteins from the gel.

2.2.2.6 Immunodetection of blotted proteins

To prevent unspecific binding of antibodies, the membranes were blocked in TBS-T (0.1% Tween in 1xTBS) supplemented with 5% skim milk powder for 1 h at room temperature, before they were incubated in TBS-T plus skim milk with primary antibodies overnight at 4°C. The membranes were then further washed 3 x 30 min with blocking buffer and incubated with peroxidase-conjugated secondary IgG antibodies in TBS-T plus 5% skim milk for 1 h at room temperature. Protein bands were visualized by chemiluminescence with the ECL kit (*GE Healthcare*, Munich).

2.2.2.7 Co-immunoprecipitation analysis *via* antibody-coupled beads

2 to 4 x10^6 HEK293T cells were seeded in 10 cm^2 or 14.5 cm^2 dishes 48 h prior to harvesting in DPBS. 24 h afterwards, cells were either transfected with PEI or left untransfected. Lysates were prepared by resuspending the pellets in 500 µl to 1 ml of ice-cold CEB buffer, followed by incubation for 10 min on ice. After 30 strokes with a Dounce homogenizer (*VWR*, Leicestershire, UK) and centrifugation at 15,700 x g for 15 minutes, pre-clearing of the lysates was performed by incubation with equilibrated protein A/G-agarose beads for at least 2 h in an overhead rotator at

4°C. Beads were equilibrated by washing them three times with CEB buffer and centrifugation steps for 3 min at 830 x g and room temperature in between the washing steps. Meanwhile, 1 µg of the appropriate antibody was coupled to equilibrated agarose beads for 4 h at 4°C in TBS/3%BSA. Coupled beads were washed three times with apoptosome lysis buffer, centrifuged for 3 minutes at 830 x g, and immune complexes were collected overnight at 4 °C. Immune complexes were washed three times with apoptosome lysis buffer prior to boiling in 5x SDS PAGE sample buffer for 5 minutes at 95°C. Precipitates were analyzed by SDS PAGE and visualized *via* immunodetection.

2.2.2.8 Co-immunoprecipitation via Protein G µMacs beads

The pelleted cells were taken up in 1 ml of µMacs lysis buffer and incubated on ice for 10 min. After centrifugation of the lysate at 15,700 x g for 15 minutes at 4°C, protein concentration of the supernatant was determined by Bradford assay. 1-3 mg of total protein in a cellular lysate and 1-3 µg of the corresponding antibody were mixed for precipitation together with 50 µl Protein G MicroBeads (*Miltenyi Biotec*, Bergisch Gladbach). Complexes were incubated for 30 min on ice and subsequently added to freshly equilibrated µ columns in a magnetic field. Washing and elution were carried out according to the manufacturer´s instructions, and the precipitated protein complexes were separated by SDS PAGE and visualized by Western blotting and immunodetection.

2.2.3 Cellular assays

2.2.3.1 Cell culture and transfections

HEK293T, NIH/3T3 and RKO cells were cultured in Dulbecco's modified Eagle's medium (DMEM) supplemented with 10% fetal bovine serum, 1% L-Glutamine and 1% Penicillin/Streptomycin. Murine Renca-lacZ renal carcinoma cells were cultured in Roswell Park Memorial Institute medium (RPMI) 1640 containing the same supplements. GIST48 (kindly provided by J. Fletcher, Boston, USA) were cultured in Ham´s F-10 medium supplemented with 18% FBS, 1% Pen/Strep, 1% L-Glutamine, 7,5 mg Bovine Pituitary Extract and 1,25 mg Mito^{TM} plus Serum Extender. GIST882 (kindly provided by J. Fletcher, Boston, USA) were cultured in RPMI 1640 containing

15% of heat-inactivated FBS, 1% L-Glutamine and 1% Penicillin/Streptomycin. All cell lines were cultured at an atmosphere of 5% CO_2 at 37 °C.

2.2.3.2 Freezing and thawing of cells

Adherent cells were washed, trypsinized and pelleted by centrifugation for 5 min and 450 x g. Then, cells were resuspended in 1 ml of 90% FBS supplemented with 10% of sterile DMSO. The suspension was slowly cooled down to -80°C in a freezing container (*Nalgene*, Roskilde, Denmark).
For gentle thawing of cells, cells were incubated in a water bath at 37°C and mixed with 10 ml complete growth medium. Cells were then centrifuged for 5 min at 450 x g and room temperature to remove DMSO and subsequently taken up in culture medium.

2.2.3.3 Counting cell numbers (Neubauer Hematocytometer)

Total cell numbers in a suspension were quantified by manual counting of cells in a hematocytometer. 10 µl of cell suspension were transferred to one chamber, and 16 small squares (1 corner square) were counted under a microscope. The number of cells per ml was calculated by multiplying the counted number of cells with 10^4. Cell viability was additionally determined by trypan blue staining of cells in a ratio of 1:1.

2.2.3.4 Polyethyleneimine (PEI)-mediated transfection

Transfection *via* the polymer is most efficient when the ratio between positively charged amine nitrogens in PEI and negatively charged phosphates of the DNA backbone is in a range of 9-13.5 (Boussif et al., 1995). According to this, the transfection protocol was set up as follows:
1 µg DNA = 3nmol phosphate; 1 µl 10mM PEI (monomer) = 10nmol amine nitrogens
A ratio of 9 corresponds to 27nmol nitrogen amines per 1 µg DNA, therefore 2.7 µl of 10mM PEI working solution were used to transfect 1 µg of DNA. DNA and PEI were diluted in 150 µl DPBS in separate eppendorf tubes. Both solutions were mixed and incubated at room temperature for 20-30 min. Cells were washed and

FBS-free medium was added. After 4-6 hours in the incubator, the medium was replaced by different medium containing FBS.

2.2.3.4 Lipofectamine-2000^{TM}- and Lipofectamine LTX-mediated transfection

Lipofectamine 2000- and Lipofectamine LTX-mediated transfection were carried out following the manufacturer´s instructions. Medium was replaced by other medium lacking antibiotics for 6 hours during the transfection of DNA. For Lipofectamine LTX transfections, Plus Reagent and Lipofectamine were added in a ratio of 1:1 in order to achieve higher transfection efficiencies.

2.2.3.5 Lentiviral transduction of cells

Lentiviral transduction was used to introduce expression constructs for shRNAs or cDNA into mammalian cells in order to knock down or overexpress a certain target gene (Sumimoto and Kawakami, 2007). Advantages to use lentiviral vectors are, amongst others, highly efficient DNA transfer, the possibility to achieve stable long-term expression due to integration into the host genome, and the ability of lentiviruses to infect non-dividing, slowly proliferating cells. 2 x 10^6 HEK293T cells were transfected with 1.625 µg of p8.91 (*gag/pol*), 0.875 µg pMD2.G (*env*) and 2.5 µg overexpression or shRNA constructs for the production of lentiviral particles. 48 hours post-transfection, 2 x 10^5 target cells seeded in 6 well plates were infected with filtered virus-containing supernatant (0.45µm filter), together with polybrene at a concentration of 8 mg/ml, by centrifugation for 1 hour at 340 x g and 32°C (spin infection). 4-6 hours later, medium was changed, and the infection procedure was repeated the next day. 2 µg/ml of the antibiotic puromycin (0.5 mg/ml) served as the selective agent for infected cells. Alternatively, cells were sorted using a FACS cell sorter (*FACSAria, BD,* Pharmingen).

2.2.4 Apoptosis assays

2.2.4.1 Viability stainings

Cell viability was determined by staining of dead cells with DNA-intercalating agents such as Propidium iodide (PI) or 7-Aminoactinomycin D (7-AAD). Living cells

exclude these dyes, whereas due to changes in membrane integrity, dying cells are stained. Intracellular single cell staining can be quantified by FACS analysis (Philpott et al., 1996).

Cells were seeded at 1-2 x 10^5 cells per well in a 6 well plate 24 to 48 hours prior to induction of apoptosis by UV-irradiation, recombinant Fas ligand or one of several chemotherapeutics. Supernatant and cells were harvested in FACS tubes, filled with DPBS and centrifuged for 5 min at 450 x g and 4°C. Cells were harvested and stained for 20 min with propidium iodide (50 µg/ml) in DPBS supplemented with 3% FBS or 7-AAD (4 µg/ml) for 20 min in the dark. PI- or 7-AAD-positive (dead) cells were quantified using FACS analysis (FACS *Calibur*, FACS *Scan*).

Cell line	***Treatment***	***Concentration***	***Incubation period (h)***
Renca-lacZ	Mitomycin C	30 µg/ml	24
RKO	Mitomycin C	15 µg/ml, 10 µg/ml, 4µg/ml	20, 6, 12
Renca-lacZ	Oxaliplatin	100µM	24
RKO	Oxaliplatin	100µM	20
RKO	Staurosporine	1µM	6
RKO	Fas ligand	40 ng/µl, 1µg/µl anti-Flag, 0.1 µg/µl Cycloheximide	6
Renca-lacZ	Rad-001 (Everolimus)	10nM, 50nM, 100nM, 500nM, 1µM	30-48
NIH/3T3	Fas ligand	20 ng/µl, 1µg/µl anti-Flag, 0.1 µg/µl Cycloheximide	6
NIH/3T3	UV-irradiation	70, 100, 120 and 150 mJ	6
RKO	UV-irradiation	70, 100, 120 and 150 mJ	6
GIST48	Staurosporine	1µM	18
GIST882	Imatinib Mesylate	10µM	24

2.2.4.2 Cell cycle profiling using the Nicoletti protocol

During apoptosis, DNA is cleaved by Caspase activated DNAse (CAD), and fragments of about 200 bp and multiples of 200 bp are generated. Intercalating agents such as propidium iodide (PI) can bind specifically to nucleic acids and stain them. This intracellular staining can be analyzed cytometrically in ethanol-fixed cells. This method allows cell cycle profiling and quantification of the apoptotic subG1 fraction within a population of cells (Nicoletti et al., 1991; Riccardi and Nicoletti, 2006). Cells are stained after fixation with ethanol and after addition of RNase A. The DNA content of a cell is proportional to the PI intensity after RNAse digestion

and, due to fixation, fragmented DNA of the apoptotic cells generates a subG1 peak that is illustrated in a cell cycle profile.

1 x 10^5 RKO cells per well were seeded in 6-well plates. For induction of cell death, cells were irradiated with UV or treated with chemotherapeutics (such as mitomycin C and oxaliplatin). After an accordant incubation time, cells were harvested, washed with DPBS and fixed by gentle addition of ice-cold 70% ethanol prior to incubation at 4 °C for at least 24 h. This was followed by a washing step with 38mM sodium citrate (pH 7.4) and centrifugation for 5 min at 4°C and 400 x g. Cells were then stained for 20 min with propidium iodide (50 µg/ml) in 38mM sodium citrate plus 5 µg/ml RNaseA at room temperature in the dark. The apoptotic subG1 fraction of RKO cells was quantified by FACS analysis (FACS Calibur or FACS Scan) using the *CellQuest Pro* software (*BD Biosciences*, Pharmingen). Fluorescence intensity in the FL-2A channel was quantified using the doublet discrimination module (DDM). 20,000 events were acquired for each sample, and a gate was set on the cell population present in a FL2-A/FL2-W dot plot, so that the cell cycle profile could be visualized in a FL2-A histogram.

2.2.4.3 AnnexinV staining of apoptotic cells

During the onset of cell death, phosphatidylserine (PS) is exposed at the outer leaflet of the plasma membrane to mark the dying cells for phagocytosis. Fluorescently-labeled Annexins bind to phospholipids, preferentially PS, in a calcium-dependent manner and can thereby serve as a marker for early apoptotic cells. Together with a viability dye (PI or 7-AAD) detecting membrane disintegrity, early (AnnexinV-positive) and late apoptotic cells (double positive) can be distinguished from necrotic cells that stain only positive for PI or 7-AAD (Zhang et al., 1997)

2 x 10^5 NIH/3T3 were seeded in 6 well plates, and after adhesion for 24 hours, apoptosis was induced by several stimuli of the intrinsic or extrinsic apoptosis pathway. Cells were incubated for 6 hours and afterwards, the supernatant as well as living cells were harvested and transferred to FACS tubes. Tubes were filled with PBS, and the samples were centrifuged for 5 min at 4°C and 450 x g. Cells were subsequently stained with PI (50 µg/ml) and AnnexinV-FITC (2 µl/sample) in 100 µl of AnnexinV-binding buffer for 20 min at room temperature in the dark. Another 400 µl of binding buffer were subsequently added to the stained samples, and AnnexinV- and PI-single-stained as well as double positive cells were quantified by FACS analysis (FACS Calibur) using the CellQuestPro software (*BD Biosciences*, Pharmingen).

20,000 events were acquired for each sample and visualized by quadrant stats in a FL1-FL2 dot plot.

2.2.5 Animal work

2.2.5.1 Mice

Non-obese-diabetic/severe-combined immunodeficient (NOD-SCID) mice were bred in the animal facility of the Georg-Speyer-Haus, fed food and water *ad libitum,* and were housed in individually ventilated cages under pathogen-free-like conditions. All xenograft experiments were performed in compliance with the guidelines for animal experimentations.

2.2.5.2 Tumor xenograft experiments

Subcutaneous xenograft experiments were performed in non-obese-diabetic/severe-combined immunodeficient (NOD/SCID) mice, and the lentivirally transduced tumor cells were injected into the left flank of 8- to-12-week old animals. Tumor cells were applied either in 100 µl of DPBS or in 100 µl of a Matrigel suspension at a ratio of 1:1 in DPBS. Tumor growth was quantified twice to three times a week with external calipers for 5-8 weeks. Tumor size was calculated as follows: tumor volume [mm^3] = length x $(width)^2/2$. When the tumor reached a size of 70-150 µl, mice were treated intraperitoneally with 3mg/kg of mitomycin C once a week.

2.2.5.3 X-Gal staining of mouse tissues

Tissues were excised and washed once in DPBS and stored in fixative solution (Roti® Histofix) overnight at room temperature. Prior to staining, tissues were washed four times for at least 30 minutes in DPBS. Tissues were stained overnight to 40 hours in X-Gal staining buffer supplemented with 1mg/ml X-Gal (50mg/ml) at 37°C and gentle shaking (30 rpm) in the dark and washed three times afterwards. Positive staining of tissues was documented with a digital camera (Nikon COOLPIX3700; Panasonic, Lumix).

2.2.6 *In silico* comparative genomic hybridization

Chromosomal aberrations can be screened in several tumor entities, and comparative genomic hybridization data are pooled in certain databases of which the largest one currently is the Progenetix database (Baudis and Cleary, 2001; du Manoir et al., 1993; Kallioniemi et al., 1993) (http://www.progenetix.org/cgi-bin/pgHome.cgi). It contains anonymized information from 29, 743 human cancer patients.

3. Results

3.1. Interaction of FAM96A and APAF-1

FAM96A was isolated as an interaction partner of APAF-1 in a yeast two hybrid screen performed with a mouse thymoma cDNA library and *CED-4* or different *APAF-1* constructs as baits. Several investigations on the protein-protein interaction of FAM96A and APAF-1 were performed previously in the group of Prof. Zörnig (R. Pick, S. Mateus-Fernandez, K. Völp, unpublished data), and further verification of the binding was one focus of this work. Therefore, *APAF-1$_S$* (1-1194), the shortest of the five APAF-1 isoforms that lacks the extra WD40 repeat and the 11 aa insert at the N-terminus, was co-transfected together with Flag-tagged expression vectors for the APAF-1-binding protein AVEN, FAM96A and Fas-associated protein with Death Domain (FADD) as a negative control into HEK293T cells (**Fig. 3.1 A**). After protein precipitation *via* a specific anti-Flag-antibody, an interaction of APAF-1 could be confirmed with its well-known interactor AVEN as well as with FAM96A. APAF-1 was not detected following FADD-precipitation.

Endogenous APAF-1 was successfully co-precipitated following precipitation of overexpressed Flag-FAM96A (**Fig. 3.1 B**) and after incubation of the endogenous protein lysate with a purified polyclonal anti-FAM96A-antiserum (Immunogen: YDLIRTIRDPEKPN**)** (**Fig. 3.1 D**). Rabbit IgG (IP control) served as a negative control for unspecific antibody binding. A moderate co-precipitation of Flag-tagged FAM96A was achieved following precipitation of overexpressed, Myc-tagged APAF-1$_S$ (Immunogen: REALEKDIKTSYIMDH) **(Fig. 3.1 C**). FLICE inhibitory protein (FLIP)-precipitation, as a negative control, confirmed specific interaction of both proteins.

Binding site mapping of recombinant FAM96A on APAF-1 was performed to confirm previous data from immunoprecipitation of truncated APAF-1-deletion mutants that suggested an interaction of FAM96A with the nucleotide binding domain (NBD) of APAF-1. Bacterially expressed recombinant FAM96A was purchased from RiNA, Berlin. APAF-1ΔWD40 was spotted on a nitrocellulose membrane in linear 18mer peptides with an offset of 1 or 3 amino acids. Recombinant FAM96A was incubated on the two different membranes overnight, and 5 potential binding peptide candidates could be identified of which one is located in the NOD, one in the NBD, one in the HD1, one within the WHD and two in the HD2-domain of APAF-1 (data not shown).

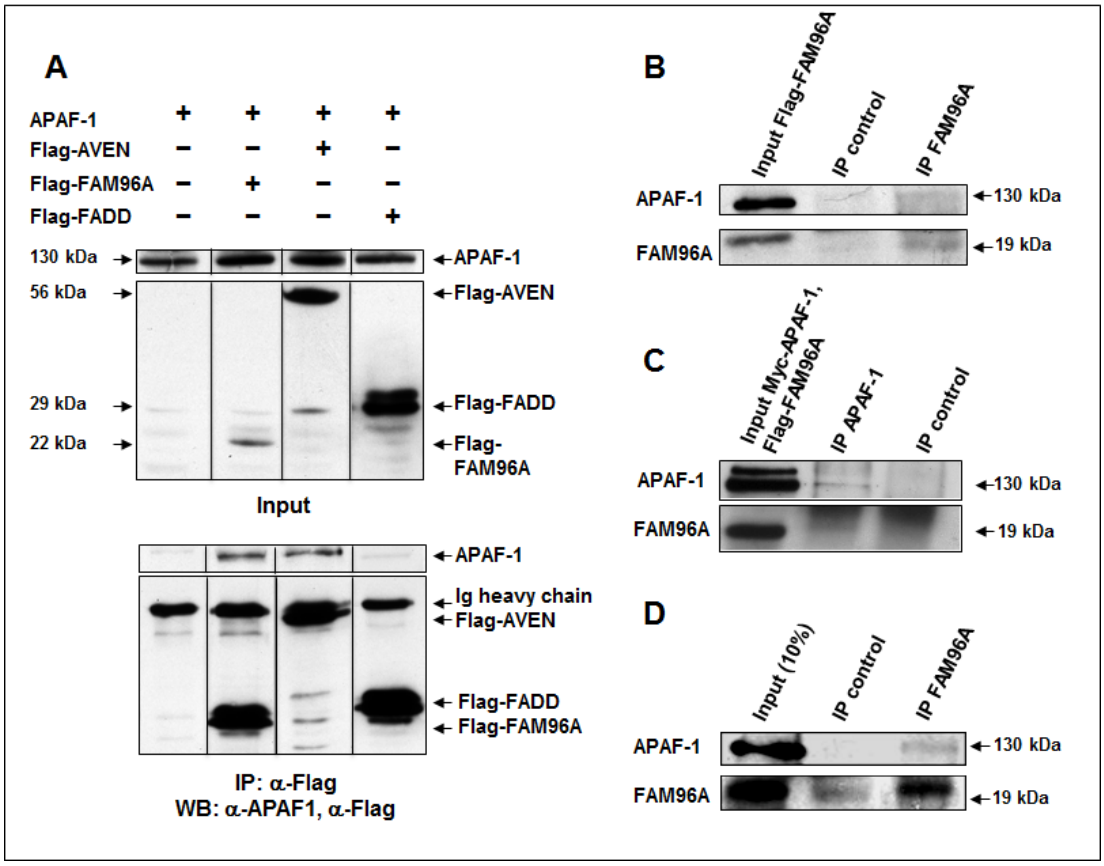

Figure 3.1: Co-immunoprecipitation experiments of FAM96A and APAF-1
The interaction of FAM96A and APAF-1 was investigated after transient over-expression of one or both binding partners in HEK293T cells (A-C). For this purpose, 2 x 10^6 cells were co-transfected with Flag-tagged *pcDNA3.1* constructs together with *APAF-1*$_S$. 24 hours later, proteins were immunoprecipitated *via* their Flag-tag (A). Successful precipitation was achieved with the known APAF-1 interaction partner AVEN and FAM96A. Flag-FADD served as a negative control for APAF-1-interaction. Endogenous APAF-1 was co-precipitated following overexpression of *Flag-FAM96A* (B) and following precipitation of endogenous FAM96A using a purified anti-FAM96A-antiserum (D). Rabbit IgG served as a negative control (IP control). Precipitation of APAF-1 was achieved *via* an antibody recognizing the C-terminus (APAF-1 K20) (C), and an anti-FLIP antibody served as a negative control (IP control).

3.2 Functional involvement of FAM96A in the intrinsic apoptosis pathway

3.2.1 Consequences of stable overexpression of human and murine FAM96A in cancer cell lines and its influence on cell death

Transfection of human *FAM96A*, followed by UV-induced killing of RKO cells, resulted in an increase in apoptotic cell numbers compared to empty vector control-transfected cells (Mateus-Fernandez, data not shown). To confirm these preliminary data obtained by transient overexpression of *FAM96A* in RKO cells, lentiviral

constructs for stable ectopic upregulation of human and murine *FAM96A* were generated. Coding sequences of *FAM96A* were cloned into the *LeGoiG2* vector that controls transgene expression by the *SFFV* promoter, and the inserted target sequence is followed by a 3´ *IRES-eGFP* element. The GFP-reporter gene activity resembles transgene expression and allows sorting of cells with homogeneous expression levels. Cytostatic drugs such as mitomycin C or oxaliplatin are widely used in chemotherapy for treatment of colon and renal cancer and were therefore used to treat the virus-transduced cells.

3.2.1.1 Ectopic expression of FAM96A in human colon cancer cells

A polyclonal population of *FAM96A*-transduced RKO cells was analyzed for a potential involvement of FAM96A in modulating the intrinsic apoptosis pathway. The lentivirus-transduced cell population was separated from non-transduced cells by FACS sorting (**Fig. 3.2 A**), and upregulation of FAM96A in the GFP-positive cells was analyzed over several passages by immunoblotting. Ectopic expression of FAM96A was stable up to passage 8 after initial sorting (**Fig. 3.2 B**) of the cells. The empty *LeGoiG2* vector served as a negative control. Following overexpression of hFAM96A, untreated cells displayed no enhanced numbers of dead cells compared to controls. To investigate the influence of FAM96A on apoptosis induction, the intrinsic pathway was induced *via* treatment of cells with the cytostatic chemotherapeutics oxaliplatin (**Fig. 3.2 C**) and mitomycin C (**Fig. 3.2 D**). Upon upregulation of FAM96A, the susceptibility of the cells was significantly increased upon treatment with oxaliplatin, and a moderate pro-apoptotic influence of FAM96A could also be observed after incubation with mitomycin C.

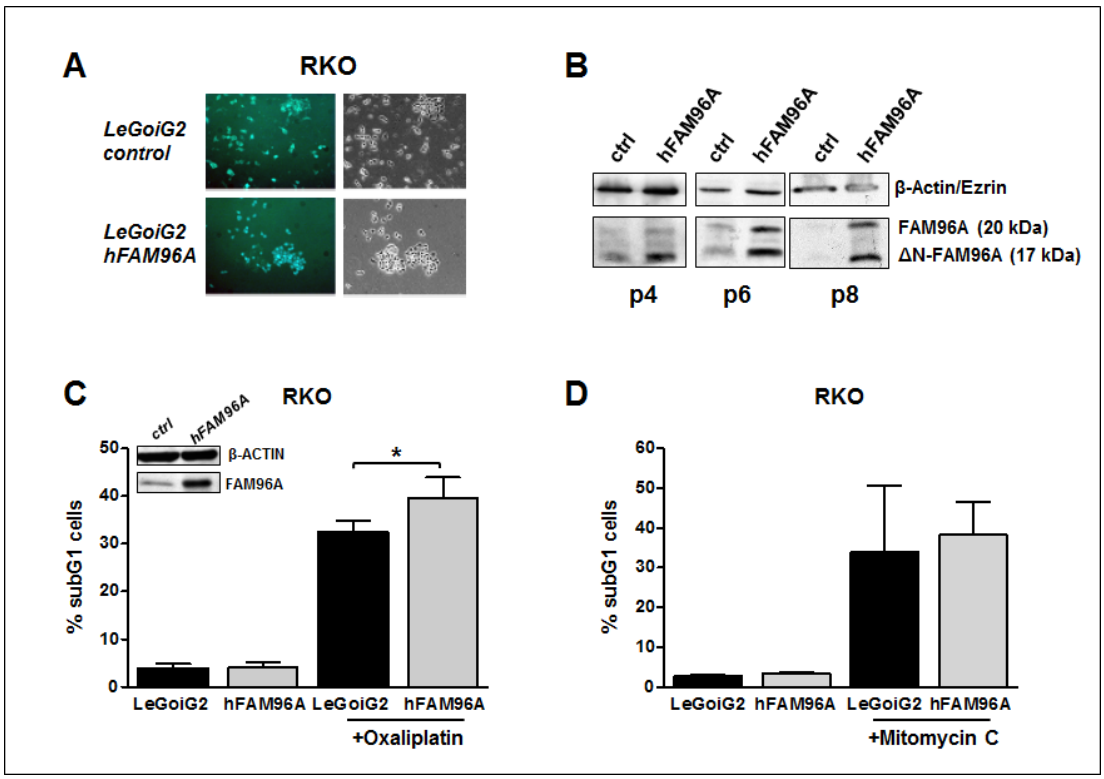

Figure 3.2: Stable overexpression of human FAM96A in RKO cells
2 x 10^5 RKO cells were stably transduced with viral particles containing a *hFAM96A* cDNA construct and compared to empty vector-infected cells as a control. GFP-positive cells were sorted (A), and long-term stability of expression was investigated by immunoblotting over a period of 8 passages (B). Intrinsic apoptosis was induced *via* treatment of the RKO cells with 100µM oxaliplatin (C) or 15 µg/ml mitomycin C (D) for 20 hours and investigated using a Nicoletti-assay. C: n=6; *=p<0.05, D: n=4; unpaired student´s t-test; Mean ± SD.

3.2.1.2 Ectopic expression of murine FAM96A in renal cancer cells

Murine *FAM96A* was stably introduced into the genome of Renca-lacZ (RLZ) cells following lentiviral transduction. Cells were sorted and compared to empty *LeGoiG2*-vector-transduced cells (**Fig. 3.3 A**). Protein upregulation was monitored over several passages and diminished during proliferation of the renal cancer cells (**Fig. 3.3 B**). Apoptosis sensitivity of infected cells was therefore investigated until passage 7 *post transduction*. Elevated cell death was observed in PI-exclusion stainings among the untreated cell population when FAM96A was upregulated (**Fig. 3.3 C**). The intrinsic pathway of apoptosis was induced by treatment of Renca-lacZ with mitomycin (MMC) and oxaliplatin (**Fig. 3.3 C**). *FAM96A*-overexpressing cancer cells displayed a significantly increased susceptibility to treatment with cytostatic drugs compared to controls.

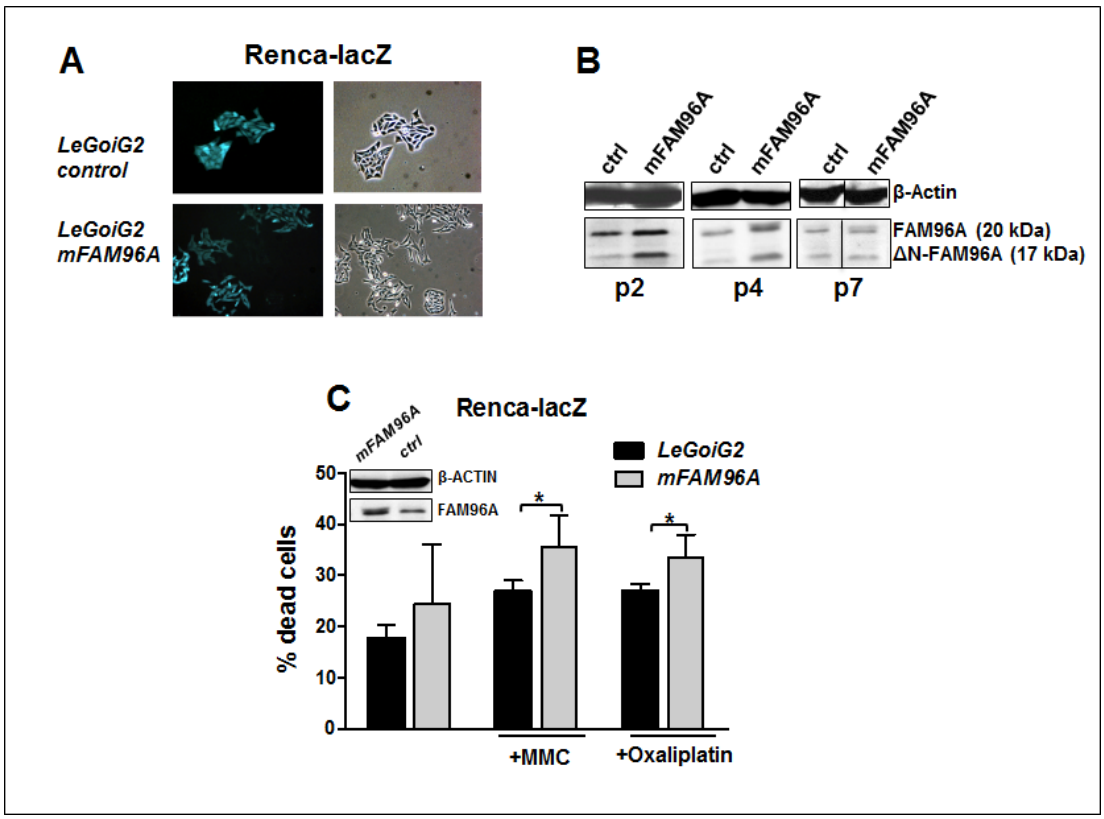

Figure 3.3: Influence of stable ectopic expression of murine FAM96A on apoptosis in Renca-lacZ cells
2 x 10^5 Renca-lacZ (RLZ) were transduced with *mFAM96A-LeGoiG2* and compared to empty vector-transduced cells as a control. After sorting of the clonal population (A), protein expression was investigated by immunoblotting over 7 passages (B). PI-exclusion stainings were performed after treatment of RLZ with 30 µg/ml mitomycin C and 100µM oxaliplatin for 24 hours. C: n=7; *=p<0.05, unpaired student´s t-test; data are presented as Mean ± SD.

3.2.1.3 Influence of murine and human FAM96A upregulation on tumor growth *in vivo*

After the pro-apoptotic influence of *FAM96A* on intrinsic apoptosis was confirmed in cell culture experiments, subcutaneous tumor xenograft experiments were performed to investigate the consequences of FAM96A expression on tumor growth *in vivo*. *LeGoiG2-FAM96A* and empty vector-transduced RKO and RLZ cells were injected into the right flank of nonobese diabetic/ severe combined immunodeficient (NOD/SCID) mice, and tumor growth was monitored over several weeks. Additionally, mice injected with *FAM96A*- and empty vector transduced tumor cells were treated with mitomycin C intraperitoneally (*i.p.*) once a week. Tumor growth was significantly reduced in both xenograft experiments comparing untreated *FAM96A* groups to *LeGoiG2* control groups (**Fig 3.4 A, D**). At the last day of the

xenograft experiment, tumors were excised, and elevated FAM96A expression was confirmed *via* immunoblotting of tumor material or GFP-fluorescence under a stereomicroscope (*Leica*, Wetzlar) (**Insets, Fig**. **3.4 A, D**).

Mitomycin C treatment of mice that were injected with RKO cells was started at a tumor volume of 70 mm^3 (day 0). Chemotherapeutic mitomycin C treatment once to twice a week displayed slight beneficial effects on tumor growth in the control groups (**Fig. 3.4 B**). However, in the groups with FAM96A-overexpressing cells, mice treated with mitomycin C did not benefit from treatment compared to their untreated controls. The relative tumor volume of treated mice was reduced upon upregulation of FAM96A compared to control vector-transduced tumors, as depicted by Figure 3.4 C. Interestingly, of the 14 injected tumors in the FAM96A group, only 5 tumors successfully engrafted, while in the control group, 4 out of 14 tumors did not expand.

Tumor growth was impaired when murine *FAM96A* was introduced into Renca-lacZ cells and compared to controls (**Fig. 3.4 D**). Additional chemotherapeutic treatment of tumor-bearing mice with mitomycin C was started when the tumors had reached a size of 150 mm^3, but a beneficial effect from the treatment could not be observed (**Fig. 3.4 E**). Due to the high degree of ulceration of Renca-lacZ tumors, 15 of the 32 mice had to be sacrificed at this time point. Relative tumor volumes for all mice in mitomycin C-treated groups are indicated in Figure 3.4 F. The relative tumor growth under mitomycin C treatment was not affected when FAM96A was overexpressed compared to control cells.

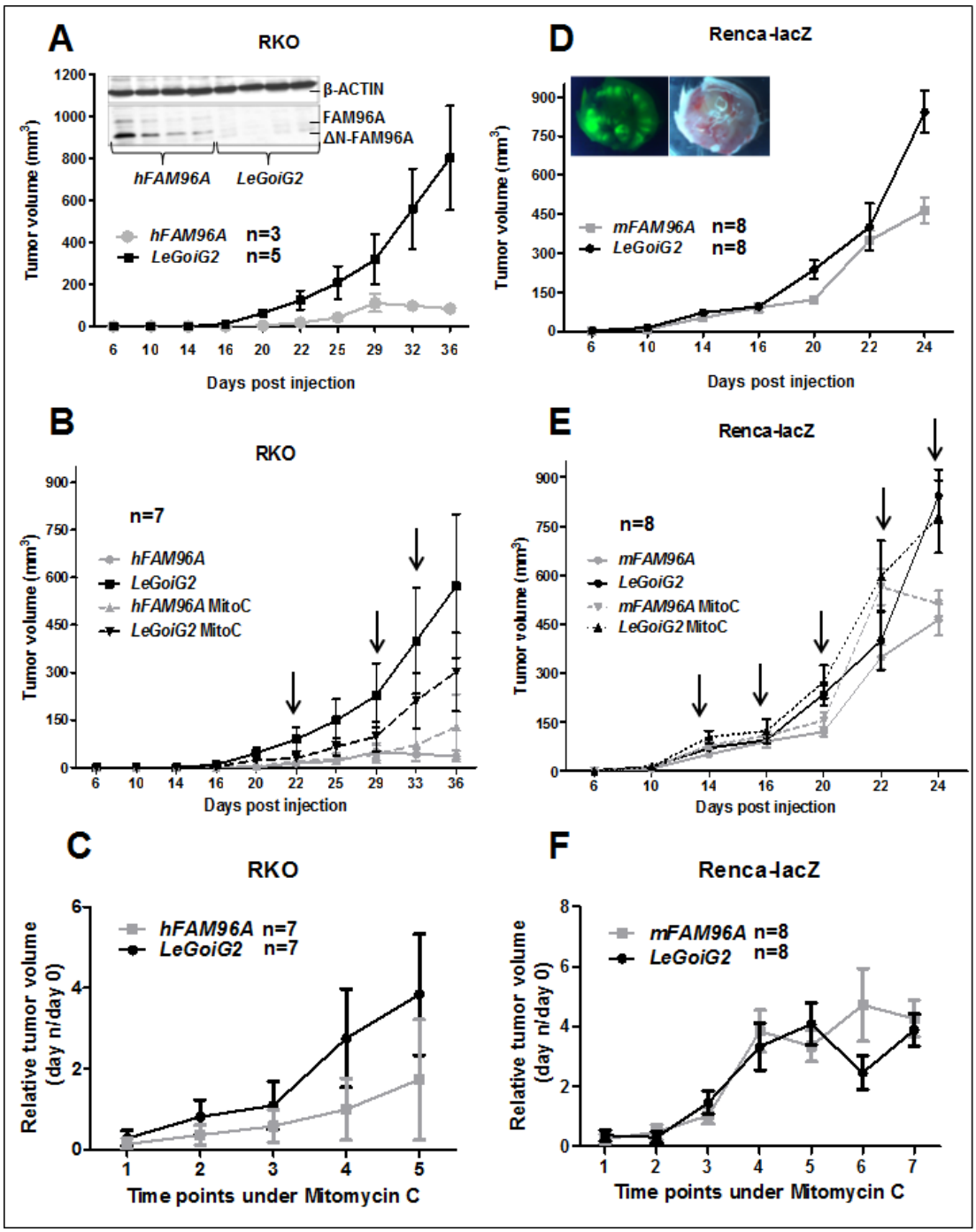

Figure 3.4: Influence of *FAM96A* upregulation on tumorigenicity of RKO and Renca-lacZ cells

4 x 10^6 RKO/mouse stably transduced either with *FAM96A* or the empty *LeGoiG2* vector were supplemented with matrigel (1:1), injected subcutaneously into the flank of NOD/SCID mice (RKO: n=7 mice/group), and tumor growth was monitored twice weekly for 36 days (A, B, C). Tumor growth was significantly reduced at 20 and 36 days *post injection (p.i.)* comparing non-treated mice injected with *FAM96A*-overexpressing cells to mice with control vector-transduced cells ($p<0.05$). Once the tumor volume had reached 70 mm^3, two groups of mice were injected *i.p.* weekly with 3 mg/kg mitomycinC/100µl DPBS (arrows) (B). The relative tumor growth at days of measurement (twice a week; day 0 = first time point of mitomycin C injection, tumor volume 70 mm^3) under mitomycin C (Time points under Mitomycin

C) treatment is depicted in C. Excised tumors were analyzed for FAM96A protein expression by immunoblotting (Inset, A). 1 x 10^6 transduced Renca-lacZ cells/mouse were injected into NOD/SCID mice (n=8 mice/group), and tumor development was measured for 24 days (D). Mice were treated intraperitoneally once a week with 2 mg/kg mitomycin C/100µl DPBS starting at a tumor volume of 150 mm^3 (day 0) (E). Highly significant ($p<0.01$) differences in tumor growth were observed at days 20 and 24 *p.i.* in the untreated groups and in between the treated groups at day 24 *p.i.* ($p<0.05$). Arrows indicate time points of mitomycin C treatment. Relative tumor volumes were calculated for mitomycin C-treated mice; start of treatment: day 0; days of monitoring twice weekly from day 0= Time points under Mitomycin C (F). GFP-fluorescence was investigated in isolated tumors (Inset, B). Data are presented as Mean ± SEM; unpaired student´s t-test.

3.2.2 Consequences of shRNA-mediated silencing of endogenous murine and human *FAM96A* on intrinsic apoptosis

To further investigate whether *FAM96A* is required for efficient induction of intrinsic apoptosis, polyclonal murine and human gene knockout cell lines were generated by lentiviral transduction. Transduced cells were selected with the antibiotic puromycin, and two separate vector systems were applied for reduction of human FAM96A *in vitro*. The *pLKO.1-puro* constructs (*Sigma Aldrich*) contain a puromycin selection cassette, whereas in the *pGIPZ* vector (*Open Biosystems*), an *IRES* element is inserted between a *tGFP* reporter and the puromycin resistance gene. A corresponding control vector, containing a non-targeting control shRNA, was transduced for both vector systems. Following infection of human and murine cells, sensitivity to induction of intrinsic apoptosis was analyzed.

3.2.2.1 Lentiviral, short-hairpin mediated knockdown of murine *FAM96A*

To induce efficient lentivirus-mediated downregulation of FAM96A protein levels, 5 individual shRNAs were investigated for their knockdown potential in the murine fibroblast cell line NIH/3T3. Upon transduction of the *sh4 (mFAM96A sh)* construct, reduction in protein expression of FAM96A and ΔN-FAM96A was most efficient compared to the other four introduced shRNAs (**Fig 3.5 A**). Long-term stability of *FAM96A* depletion under constant selection pressure was investigated by immunoblotting of the cells in later passages (data not shown) (**Inset, Fig. 3.5 B,** passage 2 post transduction). Viability assays were performed to analyze sensitivity to UV irradiation of knockdown cells compared to the non-targeting control population. Susceptibility of untreated cells was largely reduced in the knockdown

cells as measured by PI-exclusion stainings. Upon UV-mediated induction of cell death in increasing doses, a significant desensitization towards irradiation could be observed comparing knockdown cells to control vector transduced NIH/3T3 (**Fig 3.5 B**). Surprisingly, no dose-dependency of the UV-induced killing upon application of 70, 100, 120 and 150 mJ was detected. As simple viability stainings do not provide information whether apoptotic or necrotic cell death is occurring, an additional AnnexinV/PI assay was performed. Early (AnnexinV positive/PI negative) and late apoptotic cell death (AnnexinV and AnnexinV/PI positives) was severely diminished in cells expressing low levels of *FAM96A* (**Fig. 3.5 C** and **D**). Killing *via* the extrinsic pathway of apoptosis, however, when induced by treatment of cells with recombinant Fas ligand, remained unaffected after reduction of FAM96A expression.

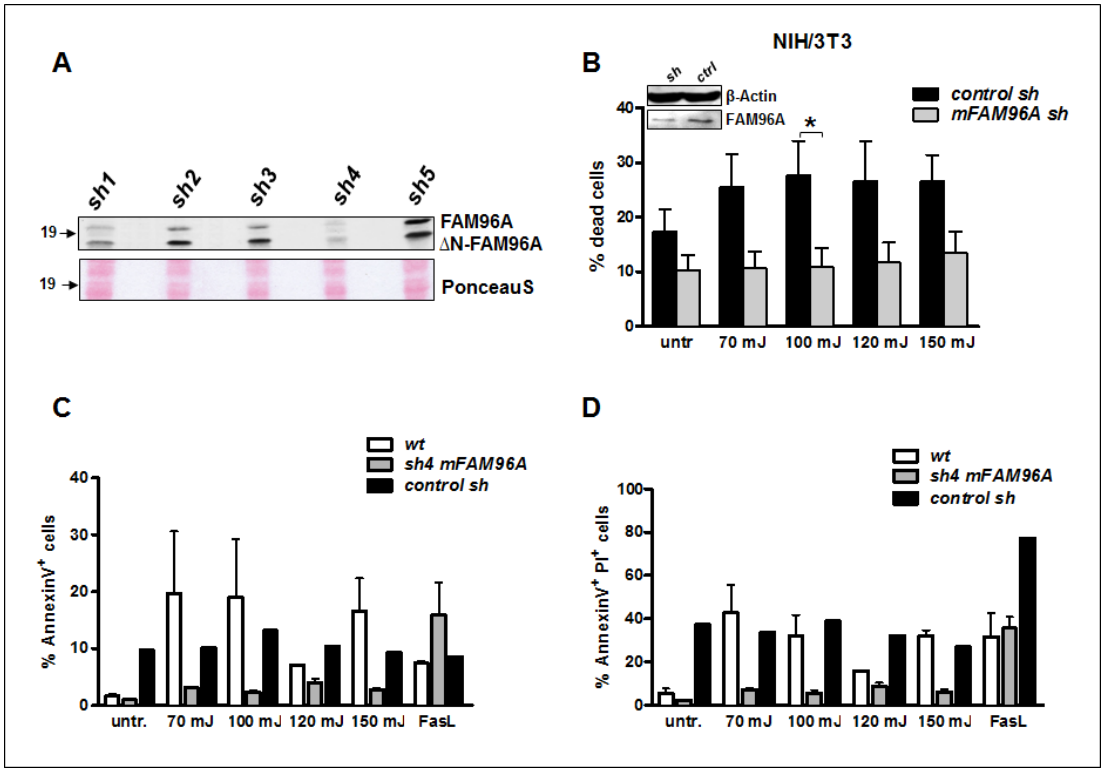

Figure 3.5: Influence of *FAM96A* knockdown on apoptosis of NIH/3T3
Endogenous murine *FAM96A* was reduced by short hairpin RNA delivered *via* lentiviral transduction of NIH/3T3 cells. 5 different vector constructs were analyzed for their knockdown efficiency and a significant reduction in protein levels of *FAM96A* was achieved by the *sh4* construct (A). The sh4 construct was compared to non-targeting control vector-transduced NIH/3T3 in viability stainings following UV-irradiation of cells with four different doses. PI-staining was carried out 6 hours after apoptosis induction. Data from two independent transductions are represented as Mean ± SEM; n=4; * = $p<0.05$, unpaired student´s t-test (B). Apoptosis of NIH/3T3 was investigated in an AnnexinV/PI staining (AnnexinV-positive cells: C, AnnexinV- and Pi-positive cells: D). Cells were treated for 6 hours with four different

doses of UV or Fas ligand. Wild type cells were compared to control vector-transduced and *mFAM96A* knockdown cells. n=2 (*control sh*: n=1); Mean ± SEM.

3.2.2.2 Consequences of FAM96A downregulation in human colon cancer cells

To demonstrate an influence of human FAM96A on intrinsic apoptosis, 5 different shRNA constructs (*pLKO.1-puro*) were investigated in two independent transductions for their efficiency to reduce FAM96A protein levels in the colon cancer cell line RKO. Of the five different constructs, the *sh4 (hFAM96A sh)* construct was most effective in transcriptional interference (**Fig 3.6 A**). A significant reduction in ΔN-FAM96A protein expression was achieved by all 5 constructs. The result of 6 independent cell killing assays from two separate transductions is depicted in Fig. 3.6 B. Knockdown cells were compared to non-targeting control vector-transduced cells (*control sh*) in Nicoletti apoptosis assays. A significant decrease in intrinsic cell death could be observed in FAM96A-depleted cells after treatment with increasing doses of UV (**Fig 3.6 B**). Additionally, 8 shRNA constructs in the *pGIPZ* vector (Open Biosystems) were analyzed for their *FAM96A* knockdown potential and compared to the corresponding non-targeting vector control (**Fig 3.6 C**). All of the constructs induced efficient protein reduction in early passages and the two most promising candidate cell lines were analyzed for their sensitivity towards intrinsic cell death. While the *sh1* construct reduced FAM96A protein levels in low passages, FAM96A expression levels were restored as soon as passage five was reached after transduction (data not shown), although cells were cultured under constant selection pressure by puromycin. Long-term knockdown stability could be confirmed in *sh5-FAM96A* transduced RKO cells. These cells were compared to *sh1* and non-targeting *(sh control)* vector-transduced cells in a Nicoletti apoptosis assay. Cell death was induced *via* treatment of the cells with mitomycin C (Mito C) or UV irradiation. Here, a diminished susceptibility of the knockdown cells towards apoptosis induction could be observed (**Fig 3.6 D**), as described for the *pLKO.1-puro* transduced RKO and NIH/3T3 cells.

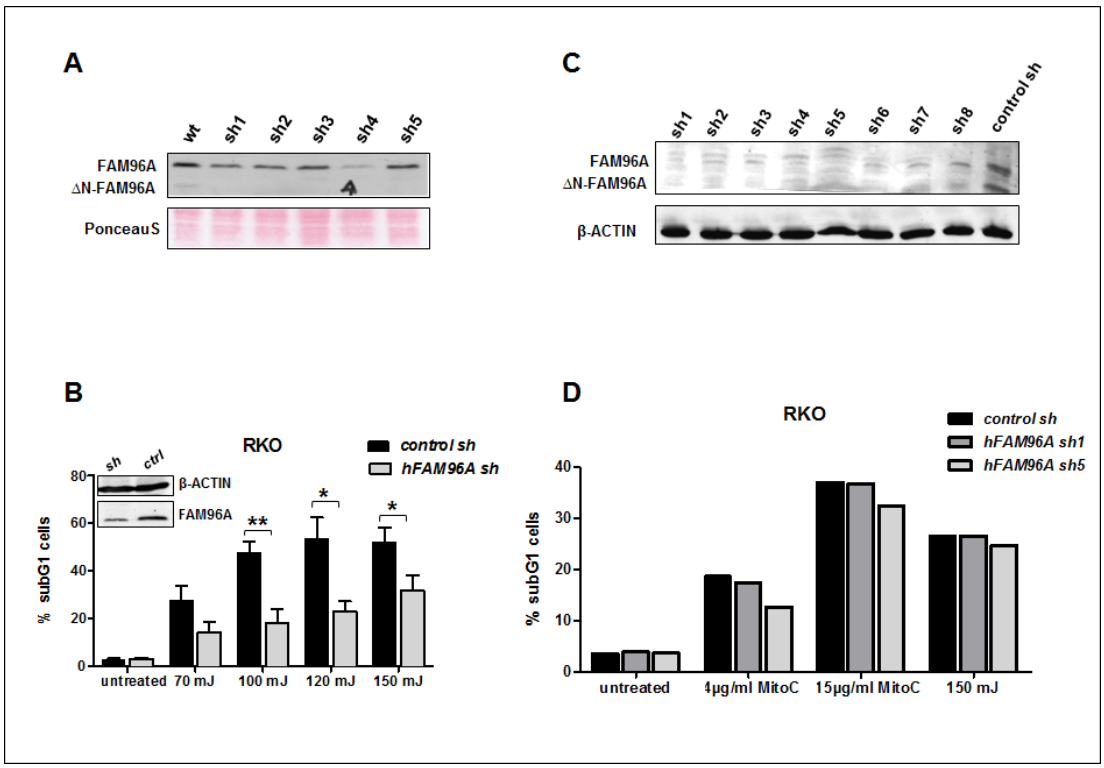

Figure 3.6: Consequence of FAM96A depletion for cell death of RKO cells
For stable lentiviral knockdown of *FAM96A* in the colon cancer cell line RKO, 5 different shRNA constructs cloned in the vector *pLKO.1-puro* were analyzed for their efficiency to reduce FAM96A protein levels. The *sh4* construct (*hFAM96A sh*) was most effective in FAM96A depletion (A). In a Nicoletti assay, the subG1 fraction of *FAM96A* knockdown (*sh* = sh4, passage 4 *post transduction*) cells was quantified by FACS and compared to non-targeting shRNA-transduced control cells (*control sh*) 6 hours after irradiation (2 x 10^5 RKO cells, 70, 100, 120 and 150 mJ UV); n=6 (two independent transductions); * = p<0.05, unpaired student´s t-test; Mean ± SEM (B). 8 different shRNA constructs cloned in the *pGIPZ* vector were investigated for their capability to induce efficient knockdown of *FAM96A* in passage two after transduction of RKO cells (C). Antibiotic selection was performed with 2 µg/ml puromycin. Cells transduced with the *sh5* construct were investigated in a Nicoletti assay and compared to the *sh1* knockdown cell line and the non-targeting *pGIPZ* control. 2 x 10^5 RKO were treated with 4 or 15 µg/ml mitomycin C for 20 hours, or with 150 mJ UV for 6 hours (D). Fixed cells were stained with PI prior to cell cycle profiling by flow cytometry; n=1.

3.3 Functional investigations on the potential antagonistic role of the smaller isoform ΔN-FAM96A

Due to an alternative in-frame startcodon 32 amino acids downstream of the first *FAM96A* translational start site, a second, N-terminally truncated isoform is generated. Previous studies were performed suggesting an antagonistic, anti-apoptotic role for the smaller isoform of human FAM96A (Pick, 2006). This

assumption was further addressed in the course of this study. Therefore, RKO cells were transiently transfected with an efficiency of 60-70% with ectopic expression constructs (**Fig. 3.7 A**) for full length as well as the truncated isoform of human *FAM96A* in the *pcDNA3.1(+)* vector, and their effect on apoptosis was investigated (**Fig 3.7 B**). Transfected RKO cells were treated with mitomycin C (Mito C) and compared to wild type and empty vector-transfected controls. A pro-apoptotic influence could be observed, when either full-length or the smaller isoform of *FAM96A* were expressed (**Fig 3.7 B**). As the assumed antagonistic effect of the smaller *FAM96A* isoform could not be confirmed, further analysis of the functional role of *ΔN-FAM96A* and its interaction with APAF-1 was performed by Jennifer Jung (Jung, 2012).

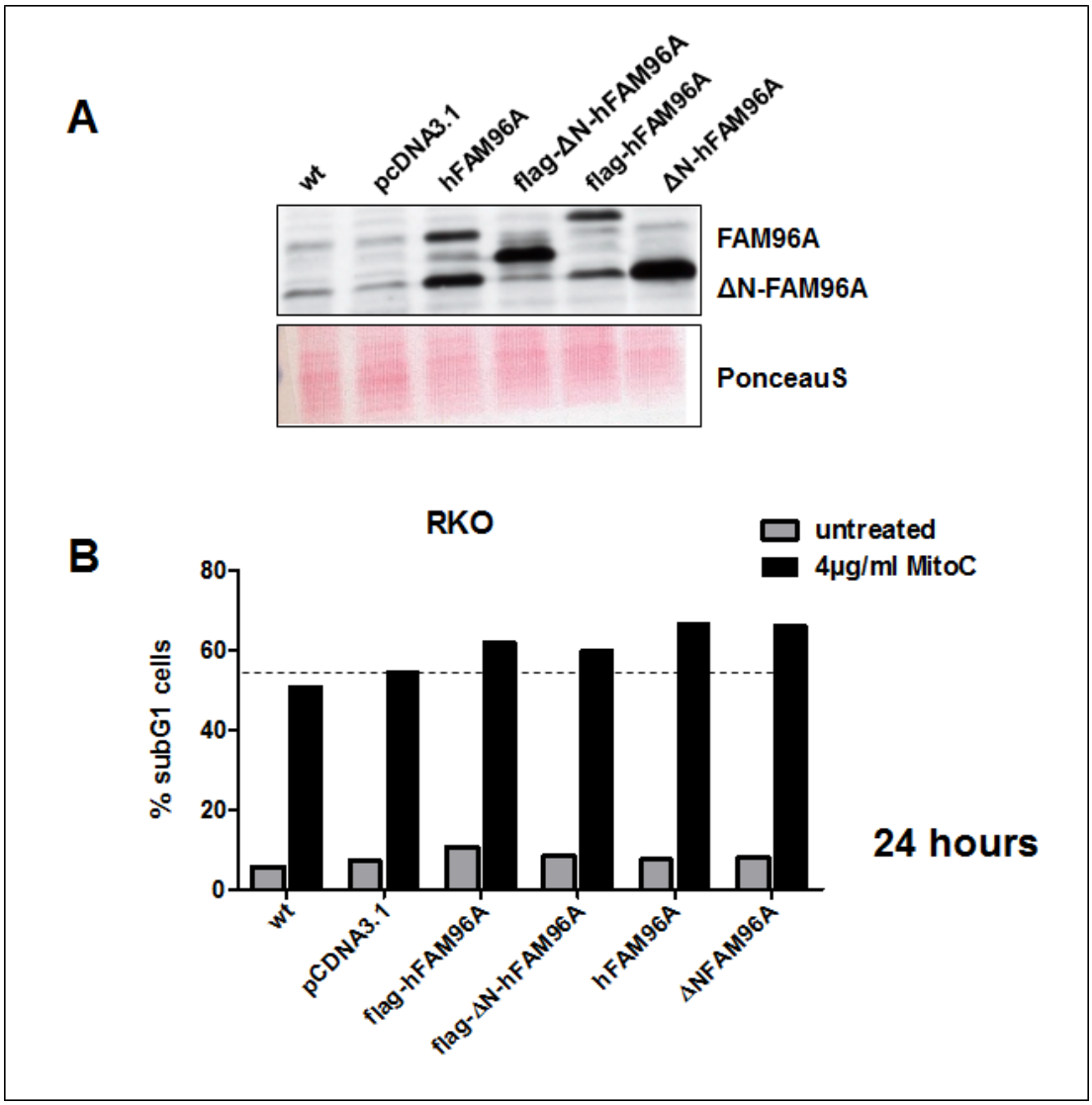

Figure 3.7: Influence of *ΔN-FAM96A* on mitomycin C-induced cell death
2 x 10^5 RKO cells were seeded 24 hours prior to transient transfection with *pcDNA3.1* expression constructs for full length and *ΔN-FAM96A*. 48 hours later, apoptosis was induced by treatment with 4 µg/ml mitomycin C (Mito C) for 24 hours

(B). Cells were then fixed in 70% ethanol for at least one day, followed by subsequent staining with propidium iodide and RNaseA treatment. The subG1-fraction was quantified by flow cytometry (B); n=1.

3.4 Consequences of ectopic FAM96A expression on the cell cycle profile

A potential influence of *FAM96A* overexpression on the cell cycle distribution of cancer cells was investigated in Renca-lacZ cells. Additionally, the G1-arrest-inducing chemotherapeutic agent Rad-001 (Everolimus) was added to the culture medium of Renca-lacZ cells in increasing concentrations. Everolimus belongs to the mTOR-pathway inhibitors, diminishes cellular proliferation and is used as a second-line treatment of advanced and metastasizing renal cell carcinoma (George and Bukowski, 2009). An efficient G1-arrest was introduced in wild type, control vector- and *FAM96A*-transduced Renca-lacZ cells with Rad-001 at a concentration of 10nM. Although cells transduced with *mFAM96A* displayed a marginally increased G1-arrest upon mTOR-inhibition, no significant changes due to upregulation of *FAM96A* in RLZ compared to wild type or empty vector-transduced cells could be observed (**Fig**. **3.8 A**). mTOR-inhibition also increases apoptosis sensitivity in cancer cells by inhibition of the p53-target p21 (Beuvink et al., 2005). Therefore, Rad-001 was analyzed for its dose-dependent sensitization of Renca-lacZ cells to apoptosis. Due to G1-arrest induction, cell killing was reduced compared to untreated cells upon application of Rad-001 in different concentrations. No significant differences in apoptosis sensitivity upon cell-cycle inhibition of the renal cancer cells stably transduced with *FAM96A* could be observed compared to empty vector controls. However, intrinsic apoptosis was not triggered by combinatorial treatment with a DNA-damaging agent.

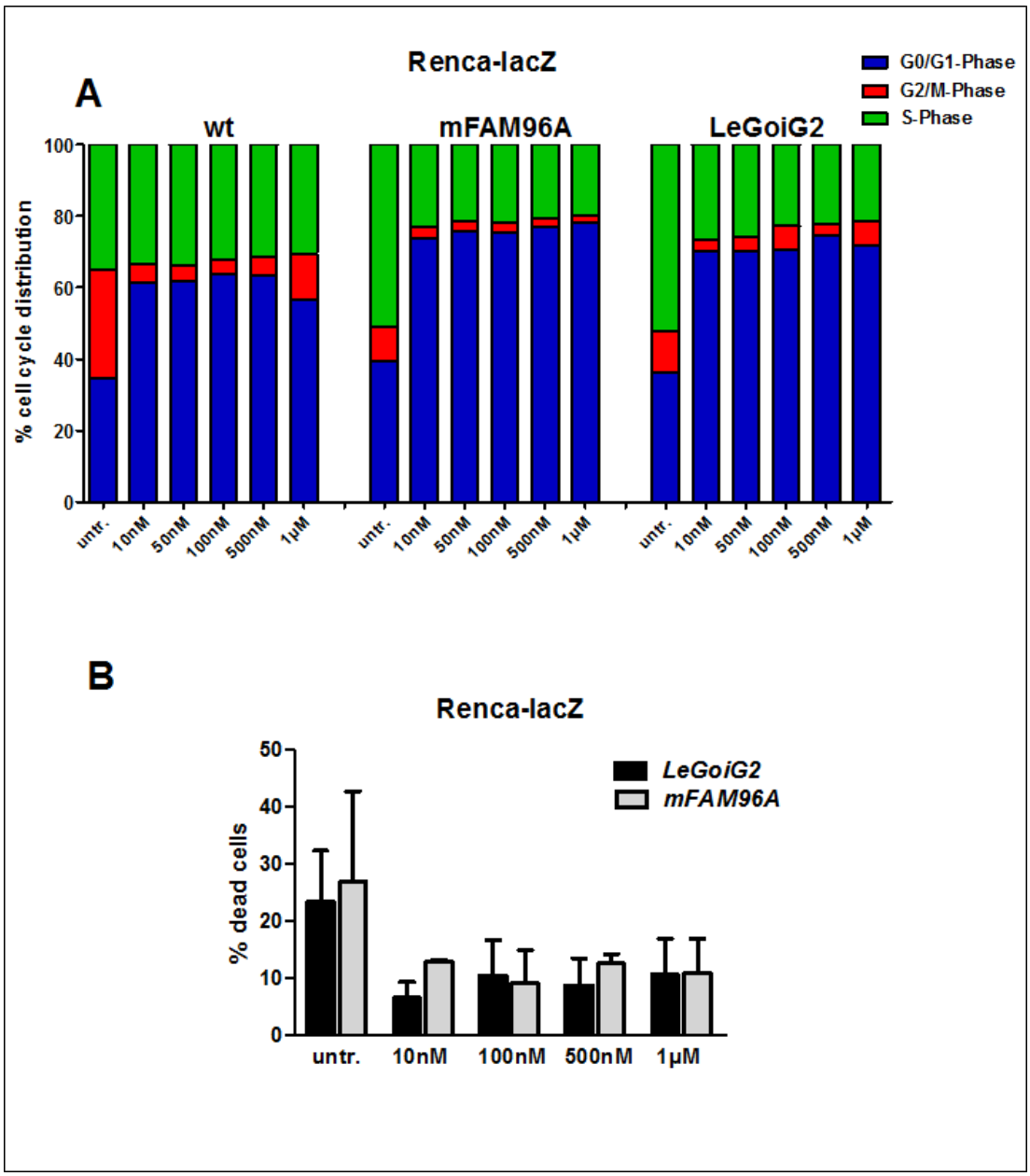

Figure 3.8: Analysis of cell cycle distribution and apoptosis of FAM96A over-expressing Renca-lacZ following mTOR inhibition

2 x 10^5 *LeGoiG2mFAM96A* or *LeGoiG2*-transduced and non-transduced Renca-lacZ cells were seeded in 6 well plates. 24 hours later, G1-arrest was induced by increasing concentrations of Rad-001 (Everolimus) for 30 hours (A). Cells were fixed in ethanol for at least 24 hours, stained with PI, and cell-cycle distribution was analyzed by flow cytometry; n=1. Induction of apoptosis in the Rad-001-treated and untreated cells was quantified by PI-exclusion after 30-48 hours of treatment (B), data are presented as Mean ± SD; n=2.

3.5 Correlation of FAM96A expression with tumorigenicity

Since a pro-apoptotic role for FAM96A was observed *in vitro* and a significant negative effect of increased FAM96A expression was observed on tumor growth *in vivo*, a tumor-suppressor function of the protein can be assumed. Mutation or deletion of the protein would increase the probability of tumor formation or progression. To investigate potential deletions within the *FAM96A* locus in tumors, an *in silico* analysis of a comparative genomic hybridization (CGH) database was conducted. CGH is a method to analyze chromosomal aberrations such as insertions or deletions within a certain locus in a genome wide manner (du Manoir et al., 1993; Kallioniemi et al., 1993).

3.5.1 FAM96A is downregulated in gastrointestinal stromal tumors

The progenetix database (http://www.progenetix.org/cgi-bin/pgHome.cgi) provides CGH data of 29,743 cancer patients and 364 distinct tumor entities. The most profound deletion of the *FAM96A* locus (chromosome 15q22.31) was observed in 48.8 % of gastrointestinal stromal tumors (GIST). This *in silico* result about copy number aberrations (CNAs) was then further investigated by real time PCR analysis and immunohistochemistry of two different cohorts of GIST patient samples. In the first cohort, *FAM96A* mRNA levels were found to be diminished in 29 of 31 GIST independent of tumor grading (low risk, borderline, high risk or metastasis). Quantitative real time PCR with GIST material was performed in collaboration with Kurt Zatloukal (Institute for Pathology, University of Graz) (data not shown). Reduced protein levels were also observed when comparing 4 GIST samples to normal tissue from small intestine (material provided by Pathology department, University of Heidelberg; Pick, 2006). In a second cohort, FAM96A expression in biopsies from 53 different GIST cancer patients was investigated by immunohistochemistry by Dr. Abbas Agaimy (Institute for Pathology, Erlangen) (**Fig. 3.9 A**). Tumor samples were derived from different areas of the gastrointestinal tract and, regardless of the cancer origin, none of the samples indicated positive staining for FAM96A. An example is represented by Figure 3.9 B. While normal liver tissue displayed strong cytosolic staining for FAM96A, GIST samples lacked protein expression.

When normal small intestine was analyzed by IHC, FAM96A protein was observed to be co-expressed together with the tyrosine kinase KIT in interstitial cells of Cajal (ICC), the precursor cells of GIST (Corless et al., 2011) (**Fig. 3.9 C**). FAM96A expression decreases at some point during gastrointestinal stromal tumor development. Independent of KIT expression, FAM96A was also highly represented in a KIT-negative interstitial cell (red asterisk, **Fig. 3.9 C**). In order to narrow down the time point of *FAM96A* loss during GIST tumorigenesis, mRNA levels were investigated *via* quantitative real time PCR in sorted ICC and ICC stem cells (ICC-SC) from the gastric *tunica muscularis* of BALB/c mice (T. Ordog, Rochester, data not shown). The findings confirmed high expression of *mFAM96A* in both cell types compared to the unsorted cell population. Furthermore, a tumorigenic, immortomouse-derived clonogenic ICC-SC population that underwent malignant transformation was compared to its nontumorigenic precursor cell line for expression of *mFAM96A*, and decreased mRNA levels were observed in the transformed cells (T. Ordog, data not shown). According to these data, loss of *FAM96A* occurs simultaneously with malignant transformation of ICC stem cells.

A

No	GIST site	Type	Risk
1	Stomach body	Mix	VLR
2	Stomach body	Spindle	IR
3	Duodenum	Spindle	LR
4	Antrum	Epithel	HR
5	Stomach body	Spindle	HR
6	Antrum	Epithel	IR
7	Fundus/cardia	Spindle	HR
8	Fundus	Spindle	VR
9	Antrum	Mix	LR
10	Stomach body	Spindle	IR
11	Stomach	Spindle	HR
12	Sigmoid	Mix	HR
13	Fundus	Spindle	LR
14	Stomach body	Mix	HR
15	Antrum	Spindle	LR
16	Small intestine	Spindle	LR
17	Antrum	Spindle	LR
18	Stomach body	Epithel	
19	Fundus, Cardia	Mix	
20	Antrum	Epithel	LR
21	Stomach body	Spindle	VLR
22	Fundus	Spindle	VLR
23	Stomach body	Spindle	IR
24	Mesentery (EGIST)	Mix	HR
25	Body	Epithel	LR
26	Body	Spindle	IR
27	Body	Spindle	LR
28	Duodenum	Spindle	LR
29	Jejunum	Mix	IR
30	Duodenum	Mix	IR
31	Stomach	Epithel	NA
32	Body	Spindle	NA
33	Antrum	Mix	IR
34	body	Spindle	NA
35	body	Spindle	NA
36		Epithelioid	HR
37	SI	Mix	HR
38	Peritoneal MTS	Epithelioid	malig
39	stomach	Spindle	
40	antrum	epithelioid	
41	Small intestine	Spindle	LR
42	Small intestine	Spindle	VLR
43	Stomach	Epithelv chordoid	LR
44	Proximal jejunum	Spindle	LR
45	Duodenum	Mix	HR
46	Stomach cardia	Spindle	IR
47	Fundus	Spindle	LR
48	Small intestine	Spindle	VLR
49	Small intestine	Mix	HR
50	Fundus	Mix	HR
51	Body	Mix	LR
52	SI/ omentum	Mix	HR
53	NA	Epithelioid	NA

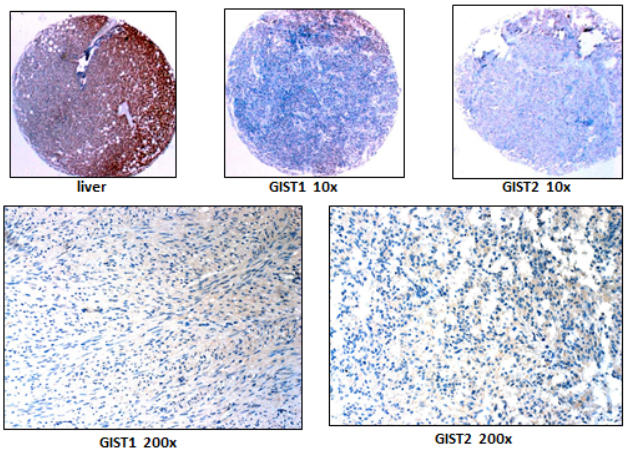

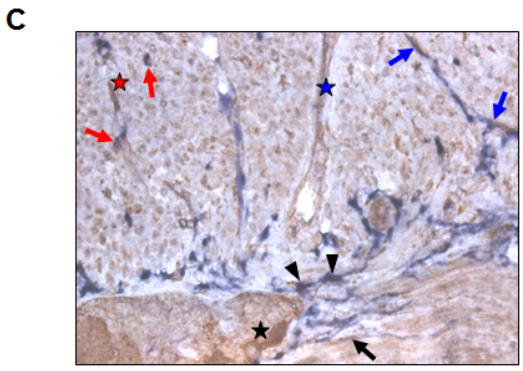

Figure 3.9: Immunohistochemical analysis of FAM96A protein expression in GIST precursor cells and GIST patient material
Immunostaining of normal small intestine *gastric tunica muscularis* tissue reveals co-expression of KIT (blue) and FAM96A (brown) in the precursor cells of GIST, the interstitial cells of Cajal (ICC) (A): double-labeled myenteric ICC (black arrowheads), intramuscular ICC in longitudinal muscle (black arrow), intramuscular ICC in circular muscle (red arrows) and ICC within intermuscular septa (blue arrows). FAM96A was also detected in some myenteric ganglion cells (black asterisk), intramural blood vessels (blue asterisk) and KIT^{-} interstitial cells (red asterisk). Magnification: 400x. Expression of FAM96A was analyzed in tumor tissue samples from 53 GIST patients of various origins within the GI tract of which none stained positive, in contrast to liver tissue, which served as a positive control (B, C).

3.5.2 Re-introduction of FAM96A into gastrointestinal stromal tumor cell lines

As loss of *FAM96A* occurs during GIST tumorigenesis, the consequences of its re-expression in established GIST cell lines were one focus of further studies. For this purpose, two GIST cell lines, GIST48 and GIST882, were kindly provided by S. Bauer (University hospital, Essen, Germany). While GIST882 is a tumorigenic, imatinib-sensitive cell line that harbors an uncommon, homozygous, primary

activating mutation in Exon 13 of the *c-kit* receptor which codes for the ATP-binding region (K642E), GIST48 was established from an imatinib-resistant GIST that, in addition to the usual primary, imatinib-sensitive, homozygous Exon 11 mutation (V560D), has acquired an additional, heterozygous, secondary Exon 17 mutation (D820A, within the activation loop) which resulted in imatinib resistance. The secondary mutation was acquired while the patient was treated with imatinib and confers therapy resistance. When endogenous FAM96A protein expression was investigated in these two cell lines, residual amounts of FAM96A could be detected *via* immunoblotting in the GIST48 cell line, whereas GIST882 cells completely lack FAM96A expression in contrast to a colon carcinoma (RKO) and two glioblastoma cell lines (U87, T98G) (**Fig. 3.10**).

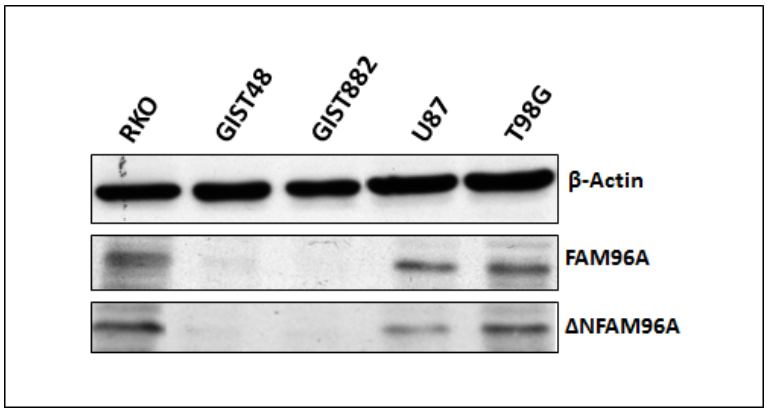

Figure 3.10: Analysis of FAM96A protein expression in GIST cell lines
FAM96A protein expression was explored in two different established GIST cell lines, GIST48 and GIST882, and compared to one colon cancer and two glioblastoma cell lines. 150 µg of total protein lysate were loaded on a SDS gel and analyzed by immunoblotting with a polyclonal anti-FAM96A antiserum. Anti-β-Actin was used as a control for protein loading.

Upon transient or stable re-introduction of *FAM96A*, both GIST cell lines displayed increased susceptibility to induction of cell death with and without staurosporine or imatinib treatment (**Fig 3.11 A, C, D**).

A modest increase in 7-AAD positive cells upon imatinib treatment was achieved in GIST882, and was enhanced in *FAM96A* expressing cells compared to controls 24 hours after treatment (**Fig. 3.11 A**). When imatinib was incubated for 72 hours on GIST882 cells in a later passage *post transduction*, no difference between controls and cells that were expressing increased FAM96A amounts could be observed (**Fig. 3.11 B**). Interestingly, when later passages of both GIST cell lines re-expressing *FAM96A* were investigated for their pro-apoptotic nature, no differences compared to controls could be observed although FAM96A expression was retained.

In case of GIST48, transient re-introduction of FAM96A increased “basal” cell death even without apoptosis induction. Unspecific kinase-inhibition by staurosporine significantly induced cell death in the imatinib-resistant GIST48 cells (**Fig 3.11 C**), whereas the state-of-the art treatment for KIT-positive GISTs, Imatinib Mesylate, had only a slight influence on cell killing, as expected (**Fig 3.11 D**). However, an increased susceptibility of GIST48 due to stable introduction of *FAM96A* again uncovered the pro-apoptotic nature of the protein.

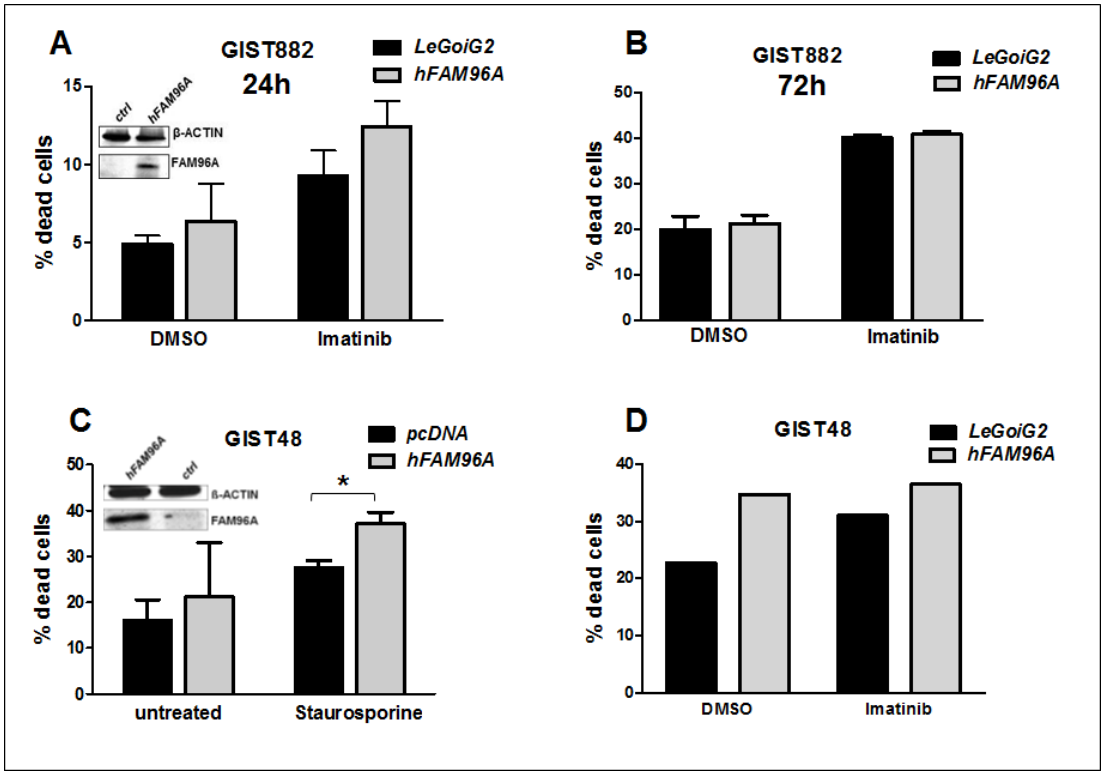

Figure 3.11: Consequences of re-expressing *FAM96A* in GIST cell lines
The effect of re-introducing *hFAM96A* in GIST cell lines was investigated in GIST882 and GIST48 cells. 1.5 x 10^5 GIST882 cells stably transduced with *FAM96A* or the empty *LeGoiG2* vector were incubated with DMSO or 10µM Imatinib Mesylate for 24 hours. Cell death was analyzed by flow cytometry following 7-AAD staining; n=4; Mean ± SEM (A). Re-expression of *FAM96A* was confirmed by immunoblotting (inset). 1.5 x 10^5 GIST882 stably transduced with *FAM96A* or the empty *LeGoiG2* vector were incubated with DMSO or 10µM Imatinib Mesylate for 72 hours. Cell death was analyzed by flow cytometry following 7-AAD staining; n=3; Mean ± SEM (B). 1.5 x 10^5 GIST48 cells were transiently transfected with *hFAM96A-pcDNA3.1* and *pcDNA3.1* as a control, and 48 hours later, apoptosis was induced by treatment with 1µM staurosporine for 18 hours. PI-staining of the cell population was analyzed by FACS (C). FAM96A expression was confirmed by immunoblotting (inset). *, $p < 0.05$; n=3; Mean ± SEM. 1.2 x 10^5 GIST48 were seeded following transduction with *FAM96A* or the empty *LeGoiG2* vector prior to incubation with 10µM of imatinib or DMSO as solvent control for 48 hours. Subsequently, viability staining with 7-AAD and flow cytometric analysis were performed (D); n=1.

3.5.3 Re-establishment of FAM96A protein expression in GIST882 cells and its influence on tumor growth *in vivo*

To further investigate the observed pro-apoptotic effects of FAM96A retrieval in GIST cell lines, a subcutaneous tumor xenograft experiment was performed in NOD/SCID mice using GIST882 cells. GIST882 cells stably transduced with the *LeGoiG2* control vector or the *LeGoiG2-hFAM96A* construct were sorted for GFP expression by flow cytometry (**Fig. 3.12 A**). Stable expression of FAM96A in the transduced cells was further confirmed by immunoblotting (**inset Fig. 3.11 A**), and tumor propagation was monitored for 83 days following tumor cell injection. Interestingly, in the *hFAM96A*-transduced group, only 5 of the 9 injected tumors successfully engrafted, whereas 8 of 9 control tumors started growing. Upon re-introduction of *FAM96A*, the tumor volume was significantly reduced compared to controls (**Fig. 3.12 B**). Additionally, only three of the expanding tumors ever reached a palpable tumor volume of 70 mm^3 (day 0) during 83 days of monitoring (**Fig. 3.12 C**). As a consequence, the relative tumor volume (tumor volume (tv) at day n/tumor volume at day 0), as presented by Fig. 3.12 C, was severely decreased, and growth deceleration is indicated by an increased time period of the *FAM96A* tumors before reaching a volume of 70 mm^3 compared to the control tumors. The tumor burden of excised tumors at the end of the experiment was significantly reduced in *hFAM96A*-expressing GIST882 compared to empty vector control tumors (**Fig. 3.12 D**). Tumors of both groups were GFP-positive at the last day of monitoring (data not shown). As a result, re-introduction of FAM96A significantly reduces GIST tumorigenicity *in vivo*.

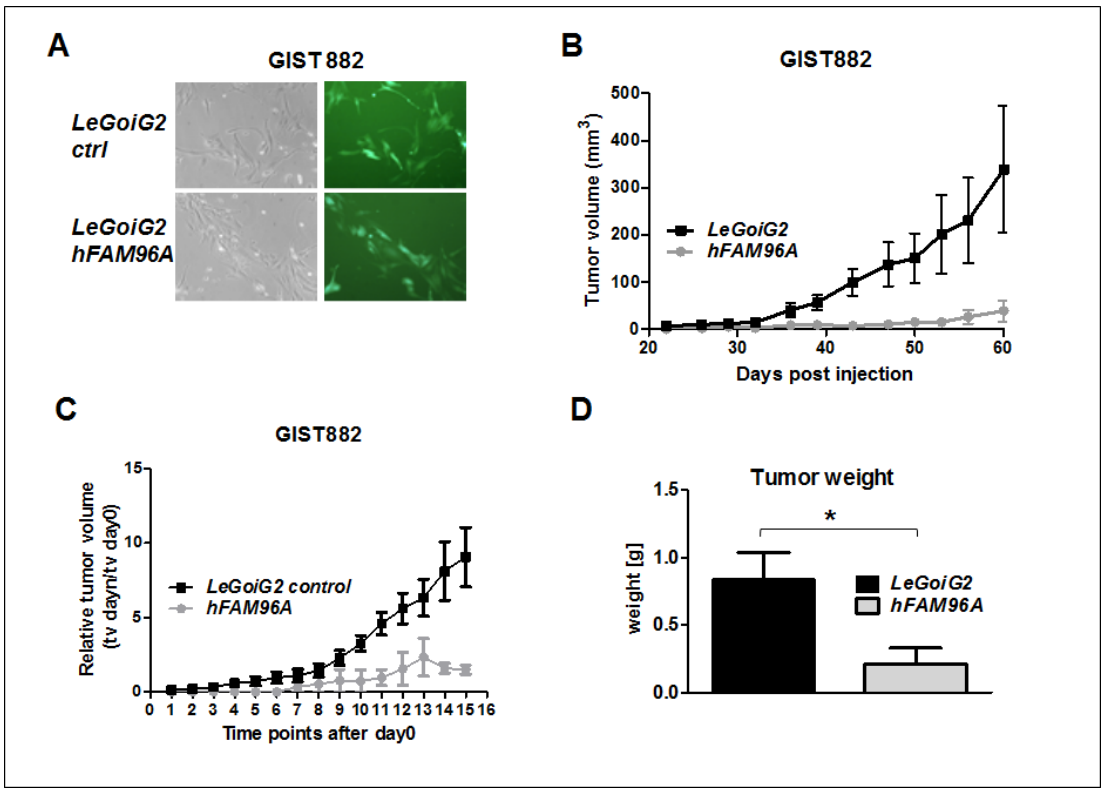

Figure 3.12: Consequences of FAM96A re-introduction for tumorigenicity of the GIST882 cell line

7.7 x 10^6 GIST882 cells lentivirally transduced either with *FAM96A* or empty *LeGoiG2* vector (A) were subcutaneously xenografted into the right flank of NOD/SCID mice (B). Successful engraftment was detected in 8 of 9 mice injected with empty vector-transduced cells, and in 5 of 9 mice injected with *FAM96A*-overexpressing cells. Tumor growth was significantly reduced in the *hFAM96A*-group compared to the control at 39, 43, 47, 50, 56, 67, 70, 74 and 77 days *post injection*; *=p<0.05; unpaired student´s t-test; Data are presented as Mean ± SEM (B). Relative tumor volume at day 0 (tumor volume (tv) of 70 mm^3) was reached at a significantly increased latency when *FAM96A* was re-introduced. Only 3 of the 5 engrafted tumors ever reached 70 mm^3. Relative tumor volume (tv at day n/tv at day 0) (day n = time point of measurement after day 0; tumors monitored twice during one week) (C). Tumor weight of *hFAM96A* tumors (n=5) compared with control tumors (n=6) at day 83 *post injection*; *=p<0.05; unpaired student´s t-test (D). Data presented as Mean ± SEM.

3.5.4 Protein expression of FAM96A in tumor vs. normal tissue biopsies

To further evaluate the general tumor-suppressive potential of the pro-apoptotic protein FAM96A, its expression was analyzed in multi-tumor tissue arrays by IHC. Biopsies of 2 mm in diameter from several tumor entities and normal tissue sections were incubated with a purified polyclonal anti-FAM96A antiserum. Tissue arrays were kindly provided by the NCT (National Center for Tumor Diseases, Heidelberg) and IHC was performed by R. Rieker (Institute for Pathology, Erlangen).

3.5.4.1 FAM96A is reduced in several cancer entities

Patient samples representing 18 different tumor entities were analyzed for FAM96A expression and compared to normal tissue material. Tumor biopsy punches of 2 mm in diameter were spotted on a microscope slide and incubated with an anti-FAM96A antiserum (**Fig. 3.13 A**). FAM96A protein levels were reduced in most of the tumor material investigated**.** Blue staining indicates weak expression (score 1) of the protein, whereas brownish staining suggests high tissue abundance (score 3). A strong expression in macrophages of lung and spleen was observed. This finding confirms existing microarray data on *FAM96A* mRNA expression (Chen et al., 2012). All normal tissues displayed an intermediate (score 2) to strong (score 3) FAM96A expression, while the protein abundance was between weak (score 1) and intermediate in most tumor tissues analyzed (**Fig. 3.13 B**). Protein levels of FAM96A in patient samples were not changed in tumor material derived from colon, bile duct, prostate, uterus and ovary when compared to corresponding normal tissue.

A

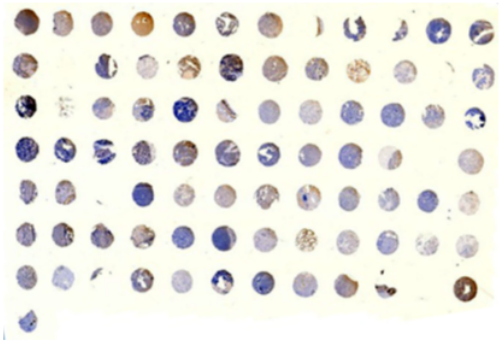

B

Tissue	Mean score	
	Normal	Tumor
Kidney tubuli	3	1
Brain	2	1.33
Parotis	3	1.5
Testes	1	1.25
Thyroid	1	1.8
Lung	x	1
Lung macrophages	3	2
Esophagus	1	1.08
Stomach	2	1.2
Colon	1	1
Bile duct	2	2
Hepatocytes	2	1.33
Gall bladder	2	1
Pancreas	1	1.67
Bladder	3	1
Prostate	1	1
Uterus	2	2
Ovary	1	1

Figure 3.13: IHC analysis of a multi-tumor array to compare FAM96A protein levels to normal tissue

In a multi-tumor tissue array, several tumor entities were investigated for their FAM96A expression and compared to normal tissue samples. Punched biopsy samples of 2 mm in diameter were transferred to microscope slides and incubated with the respective antibody (A). 18 different tumor entities and nonmalignant precursor tissues were compared for their FAM96A expression (B). Mean values are presented; Scoring: 1: low, 2: intermediate, 3: strong expression, x: not analyzable

3.5.5 FAM96A expression in kidney and bladder compared to transformed tissue

The patient material analyzed in multi-tumor tissue arrays revealed a strong reduction of FAM96A protein expression in renal (RCC) and transitional cell carcinoma (TCC). 4 RCC samples were compared to 27 normal kidney punches and 6 bladder samples to 3 TCC. As an example, high expression in the normal bladder epithelium is indicated by the brownish staining in the cytoplasm of cells (**Fig. 3.14 A**), while the protein was hardly detectable in transitional cell carcinoma. Loss of FAM96A expression in tumor tissue compared to normal kidney was also observed for samples from renal cell carcinoma (**Fig 3.14 B**). A potential influence of FAM96A as a tumor-suppressor in renal cell carcinoma was investigated in Renca-lacZ cells.

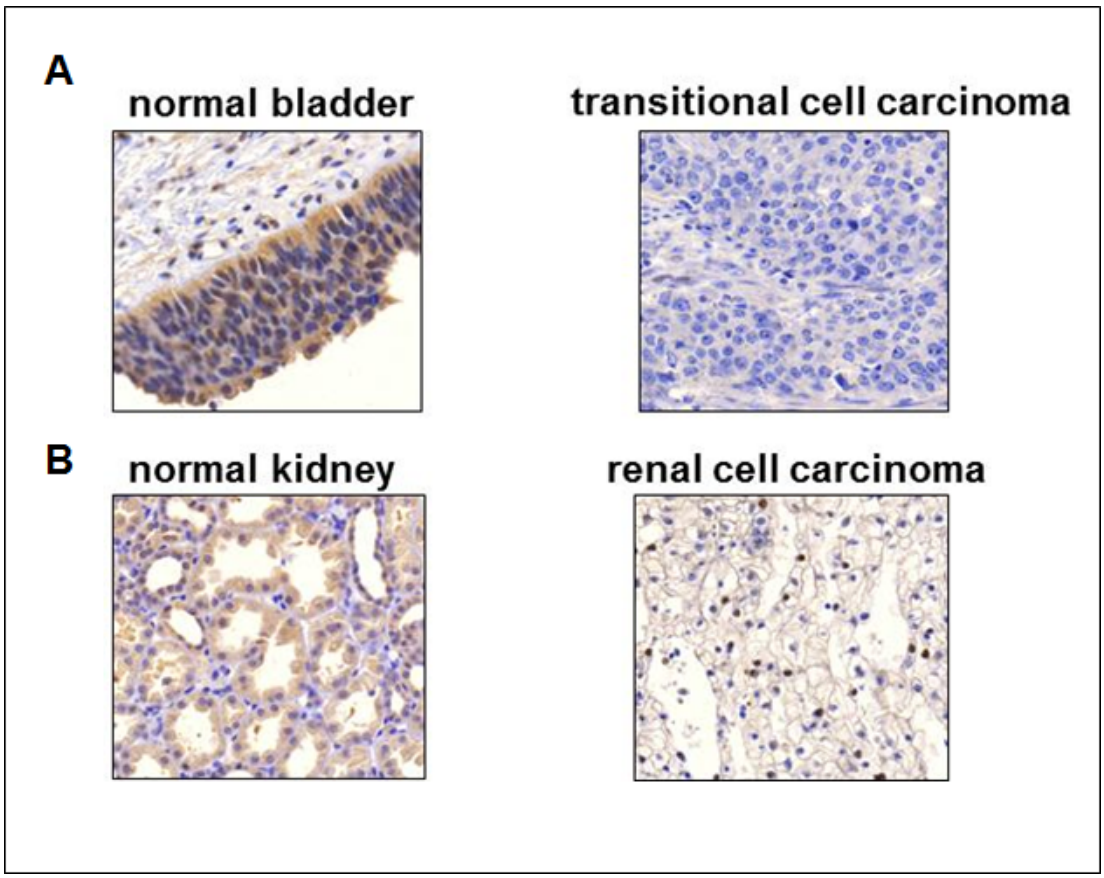

Figure 3.14: Immunoreactivity of an anti-FAM96A-antiserum in renal and bladder cancers compared to their tissues of origin
6 different bladder biopsies were incubated with anti-FAM96A antiserum and compared to 3 transitional cell carcinoma punches (A). Brownish staining indicates strong immunoreactivity of the polyclonal anti-FAM96A antiserum in the cytosol of the bladder epithelial cells. 27 normal kidney biopsies were compared to 4 renal carcinoma samples for their FAM96A expression levels. Representative pictures of the tumor and normal tissue sections are presented in B.

3.6 The interaction of FAM96A with the cytosolic iron sulfur cluster assembly protein Ciao1

In a global yeast-two hybrid screen for disease-associated genes, the interaction of human FAM96A and Ciao1 was first described (Rual et al., 2005). During the course of our investigations, the structure of FAM96A was resolved and its interaction with Ciao1 was verified by Chen et al. (Chen et al., 2012). Ciao1 is a 38 kDa, WD40 repeat-containing protein that plays a major role in cytosolic iron sulfur cluster assembly and is assumed to be involved in DNA metabolism (Ito et al., 2010; Srinivasan et al., 2007; Stehling et al., 2012; van Wietmarschen et al., 2012). A polyclonal anti-Ciao1 antibody (Immunogen: SVLNSHTQDVKHVVWHPSQELLASA-

SYDDTVKLYREEED-DWVCCATLEGH) was investigated for its specificity of detecting human and murine Ciao1 (**Fig. 3.15 A**). In case of murine Ciao1, background staining is higher than for its human homolog, as a second, unspecific band occurred for the NIH/3T3 lysate.

The interaction of FAM96A with Ciao1 was confirmed by co-immunoprecipitation of Ciao1 by Flag-tagged FAM96A with an anti-Flag antibody (**Fig. 3.15 B**). An anti-Cyclin D2 antibody of the same IgG subtype served as a negative control for the co-immunoprecipitation. A "beads only" control was added to exclude potential unspecific protein interaction with the agarose beads.

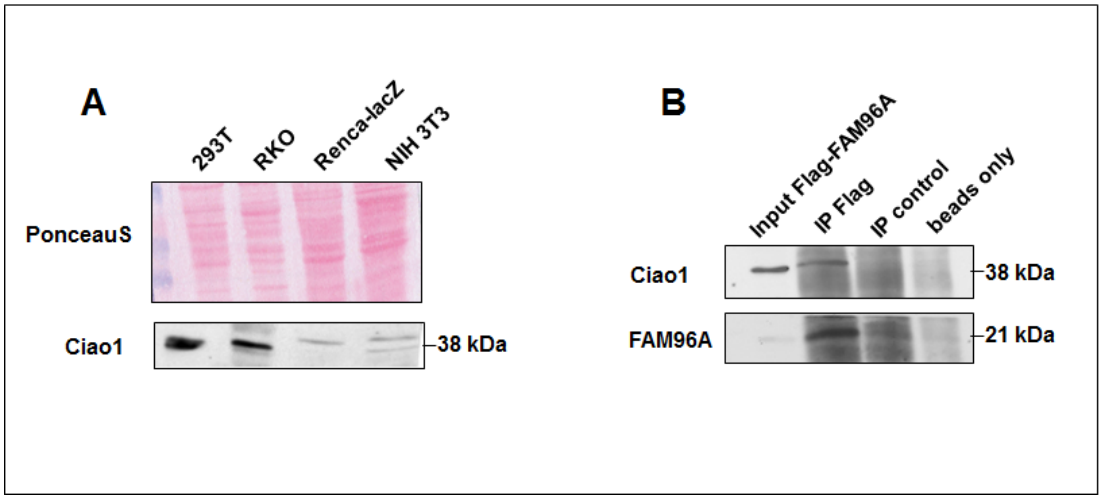

Figure 3.15: Overexpressed, Flag-tagged FAM96A interacts with endogenous Ciao1

The specificity of a polyclonal anti-Ciao1 antibody for detection of the human and murine protein (38 kDa) was analyzed by immunoblotting. 100 µg of total protein lysate per lane were loaded on a SDS gel (A). 2 x 10^6 HEK293T cells were seeded 24 hours prior to transfection of Flag-tagged *FAM96A*. After immunoprecipitation of overexpressed FAM96A *via* an anti-Flag antibody coupled to Protein A/G agarose beads, endogenous Ciao1 was successfully co-precipitated. An anti-Cyclin D2 antibody of the same isotype and agarose beads served to ensure the specificity of the binding (IP control, beads only). n=4, one representative immunoprecipitation is depicted in B.

3.7 A possible involvement of Ciao1 in the intrinsic cell death pathway

As an interaction partner of FAM96A, an involvement of Ciao1 in the regulation of the mitochondrial cell death pathway can be envisioned. Ciao1 might facilitate apoptosome formation in collaboration with FAM96A, or it could intervene in the APAF-1/FAM96A interaction and thereby antagonize FAM96A function directly or indirectly. Therefore, apoptosis assays upon upregulation and reduction of Ciao1

were performed to investigate a potential role of Ciao1 in intrinsic apoptosis and a possible interplay of the two binding partners in apoptosis regulation.

3.7.1 Co-expression of both interaction partners and consequences for apoptosis sensitivity

In order to investigate a potential function of Ciao1 as an adaptor protein linking FAM96A to APAF-1 *in vivo* and facilitating intrinsic apoptosis, *Ciao1* was transiently introduced into RKO cells which already stably overexpressed FAM96A (**inset, Fig. 3.16**). Empty vector-transduced cells served as a negative control (*RKO ctrl*). An empty vector (*pcDNA3.1*) was transfected for comparison to transient Ciao1-overexpression into the colon cancer cells. Intrinsic apoptosis was activated in RKO cells by UV-irradiation, mitomycin C treatment or incubation with staurosporine. Although a pro-apoptotic influence of FAM96A could be observed, a general reduction of cell death upon Ciao1 upregulation was obvious for all chosen apoptotic treatments (**Fig. 3.16**). This rather anti-apoptotic effect occurred independently of simultaneous FAM96A upregulation. These findings indicate an antagonistic rather than a collaborative function of Ciao1 in FAM96A-regulated mitochondrial cell death.

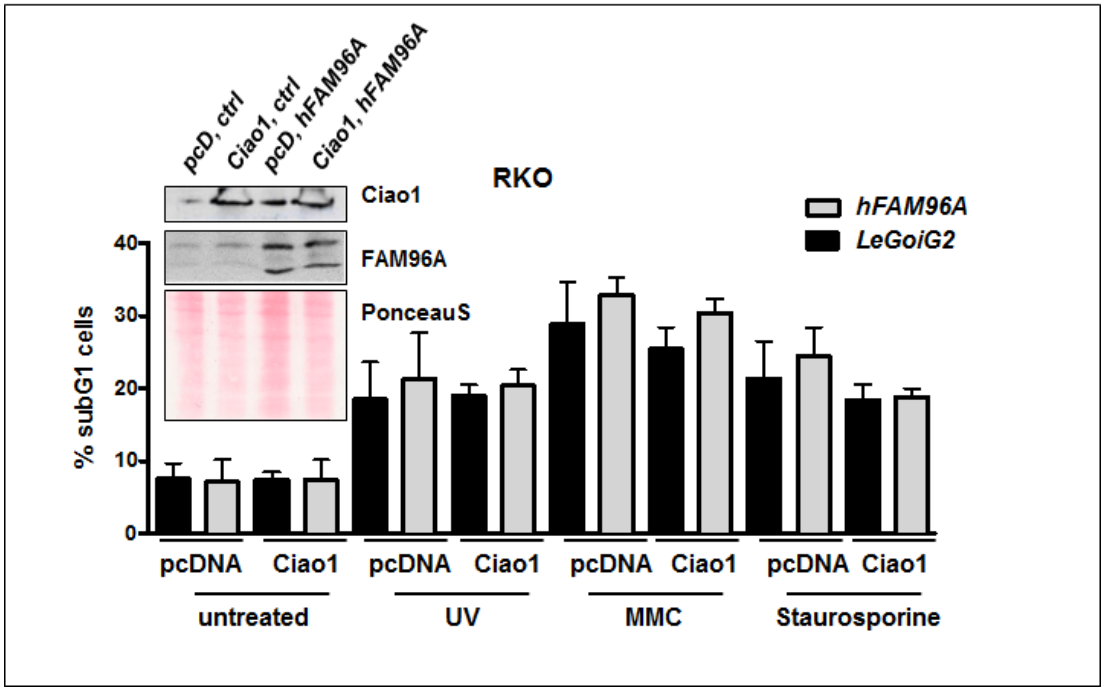

Figure 3.16: Influence of Ciao1 on intrinsic apoptosis of FAM96A-overexpressing colon carcinoma cells
2 x 10^5 RKO cells transduced with *hFAM96A* or the empty *LeGoiG2* vector were transfected with *pcDNA3.1 (pcD)* as a control or *hCiao1*. 24 hours later, apoptosis was induced by treatment of RKO cells with 100 mJ UV irradiation, 1µM of the kinase inhibitor staurosporine for 6 hours, or overnight treatment with 6 µg/ml mitomycin C (MMC). RKO cells were fixed with 70% ice-cold ethanol prior to PI-staining and quantification of apoptosis by flow cytometry. SubG1 fractions of cells in three independent experiments are presented as Mean ± SD.

3.7.2 Influence of a *Ciao1* knockdown on FAM96A-influenced mitochondrial cell death

To further investigate the observed antagonistic role of Ciao1 and whether its expression is of functional relevance for the FAM96A-induced increase in cell death, shRNA-mediated downregulation of *Ciao1* in RKO cells was conducted. For this purpose, 5 different lentiviral shRNA constructs were analyzed for their capability to reduce Ciao1 levels following lentiviral transduction (**Fig. 3.17 A**). Severely diminished mRNA transcription was achieved by the *pLKO.1-puro sh3* and *sh5* constructs. The *sh5*-vector-mediated *Ciao1* knockdown, however, lost its stability during passaging of RKO cells (**Fig. 3.17 B**), while protein depletion in the *sh3*-transduced cells remained stable under puromycin selection. Stable control cells

were generated *via* transduction of a non-targeting *control shRNA* and were compared to knockdown cells for their sensitivity towards apoptotic treatments.

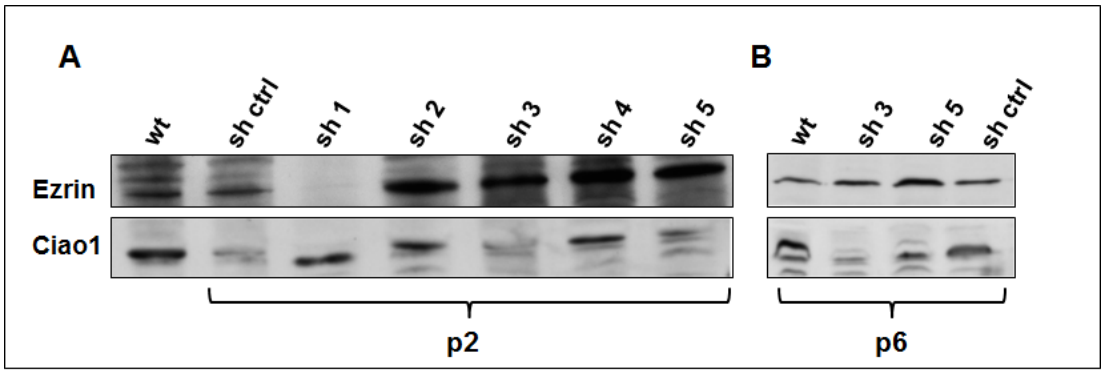

Figure 3.17: Ciao1 knockdown-stability in RKO cells between passage 2 to passage 6 *post transduction*
2 x 10^5 RKO cells were stably transduced with 5 different shRNA constructs to achieve a *Ciao1* knockdown. Reduction was most efficient in *sh3* and *sh5* knockdown cells selected with 2 µg/ml puromycin (A). The long-term knockdown stability was investigated by immunoblotting with a Ciao1-specific antibody in passage 2 (A) and 6 *post transduction* (B). 80 µg of total lysate/lane were used for protein analysis, and Ezrin was chosen to verify equal loading.

Human *FAM96A* or the empty vector *pcDNA3.1* were transiently introduced into *Ciao1*-depleted cells, and cell death was analyzed by Nicoletti assays. An efficient increase in FAM96A protein levels upon simultaneous *Ciao1* knockdown was confirmed by immunoblotting (**inset Fig. 3.18**). Cell death was induced by UV-irradiation (120 and 150 mJ), mitomycin C (MMC), staurosporine or recombinant Flag-tagged Fas ligand (FasL) treatment. The result of two independent Nicoletti assays is depicted by Figure 3.18. FAM96A overexpression increased susceptibility towards intrinsic cell death induction *via* UV-irradiation or mitomycin C treatment in the non-targeting vector-transduced cells compared to *pcDNA* empty vector-transfected controls. Ectopic expression of *FAM96A* had no such effects on the *Ciao1* knockdown cell lines. *Ciao1* reduction increased susceptibility towards cell death in untreated and treated cells in both knockdown cell lines compared to non-targeting control cells, independently of simultaneous *FAM96A* upregulation. According to these data derived upon Ciao1 protein overexpression and reduction, the CIA protein Ciao1 exhibits an anti-apoptotic function.

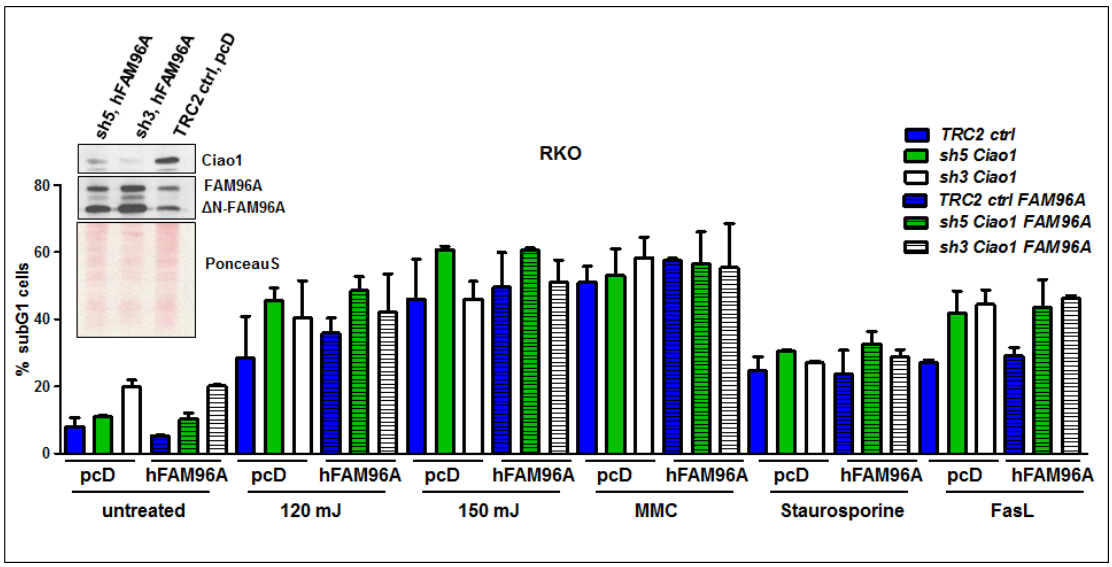

Figure 3.18: Influence of *Ciao1*-reduction and simultaneous *FAM96A* overexpression on RKO cell death
2 x 10^5 RKO cells with a *Ciao1* knockdown were transfected with *hFAM96A-pcDNA3.1* or the empty *pcDNA3.1* vector as a negative control. 24 hours after transfection, cell death was induced by 120 or 150 mJ UV irradiation for 6 hours, mitomycin C (MMC; 10 µg/ml) for 12 hours, staurosporine 1µM (6 hours) or recombinant Flag-tagged Fas ligand (40 ng/ml, together with 1µg/µl anti-Flag antibody and 0.1 µg/µl Cycloheximide for 6 hours). Cells were harvested, fixed in 70% ethanol prior to PI-staining and analyzed by flow cytometry. Hatched bars = *FAM96A*-transfected; Data represent Mean ± SEM of two independent Nicoletti assays.

3.8 Functional interplay of Ciao1 and FAM96A in the regulation of the transcription factor WT1?

The transcription factor WT1 plays an important role during nephrogenesis and is mutated in childhood nephroblastoma. The interaction between WT1 and Ciao1, and the Ciao1-mediated inhibition of transcriptional activation was first described by Johnstone et al. (Johnstone et al., 1998).

3.8.1 Can FAM96A interfere with the interaction of Ciao1 and WT1?

Ciao1 binds to both proteins, FAM96A and WT1, and therefore, a simultaneous interaction of all three proteins cannot be excluded and was investigated during this study. As a first approach to analyze the potential cytosolic assembly of the three proteins, immunoprecipitations were performed. Ciao1 alone (0) or together with

FAM96A (1) were overexpressed in HEK293T cells to analyze whether FAM96A interferes with the WT1/Ciao1 interaction. A reduction of co-precipitated WT1 upon Ciao-1 immunoprecipitation was expected in the presence of FAM96A overexpression. Upon precipitation of Ciao1, no influence of simultaneous overexpression of FAM96A on the interaction with WT1 could be observed in two independent experiments (**Fig. 3.19**). As a control for specific interaction, an anti-p15 antibody of the same isotype was used. Here, an unspecific precipitation of FAM96A with the p15 antibody was observed.

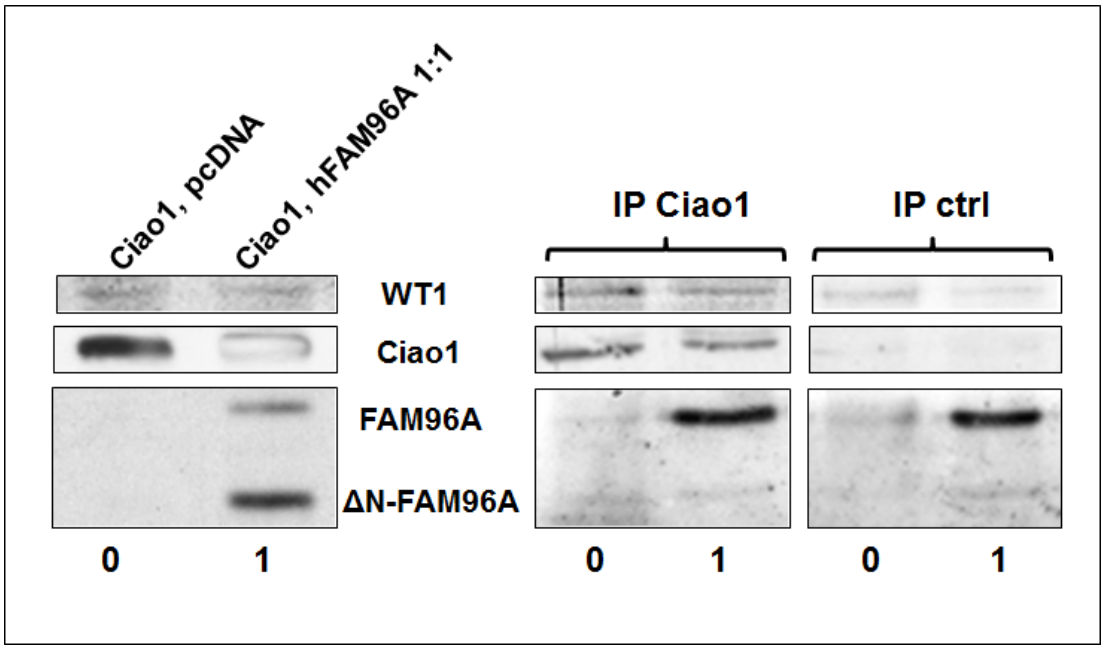

Figure 3.19: Influence of FAM96A expression on the WT1/Ciao1 interaction
Ciao1 only (0) or *Ciao1* and *FAM96A* in a ratio of 1:1 (1) were introduced into 2 x 10^6 HEK293T cells. 24 hours later, cells were harvested and co-immunoprecipitation of Ciao1 was performed *via* antibody-coupled protein A/G agarose beads. An anti-p15 antibody served as a control for specific interaction. An unspecific precipitation of FAM96A occurred with the p15 antibody. n=2

3.8.2 Ciao1-mediated modulation of the transcriptional activity of WT1

The epidermal growth factor family member Amphiregulin (AREG) was described as a *bona fide* target of the transcription factor WT1 (Lee et al., 1999) and served as a readout for WT1 activity in Luciferase assays. The influence of *Ciao1* and *FAM96A* on WT1 activity following overexpression of both proteins was investigated (Jung, 2012). WT1-mediated activation of the AREG promoter was significantly increased upon transient *Ciao1* upregulation. Synchronous FAM96A expression had only moderate antagonistic influence and -in 5-fold excess- reduced WT1 activity.

The influence of Ciao1 and FAM96A on the regulation of WT1 target genes was further investigated on mRNA level by quantitative real time PCR. The *WT1* promoter is subjected to autoregulation by its own protein (Malik et al., 1994; Rupprecht et al., 1994). Therefore, a potential influence of Ciao1 and FAM96A on *WT1* promoter-suppression and mRNA expression was investigated. The two different isoforms derived from alternative splicing of the WT1 transcription factor that are involved in transcriptional regulation (-KTS, WT1 B) and RNA processing (+KTS, WT1 D) were transiently overexpressed in HEK293T cells. Simultaneously, Ciao1 and FAM96A expression were increased and the overexpressed *WT1* mRNA levels were quantified by real time PCR. A significant increase in *WT1* mRNA upon expression of the –KTS as well as the +KTS isoform could be observed that was largely reduced in the presence of overexpressed Ciao1 alone and in collaboration with its binding partner FAM96A. Ectopic expression of FAM96A together with WT1 resulted in slight, but insignificantly reduced mRNA expression of *-KTS* (**Fig. 3.20**), while mRNA-levels of the *+KTS* isoform were marginally increased. FAM96A exhibited only minor influence on the Ciao1-mediated reduction in *WT1*-mRNA levels of both isoforms.

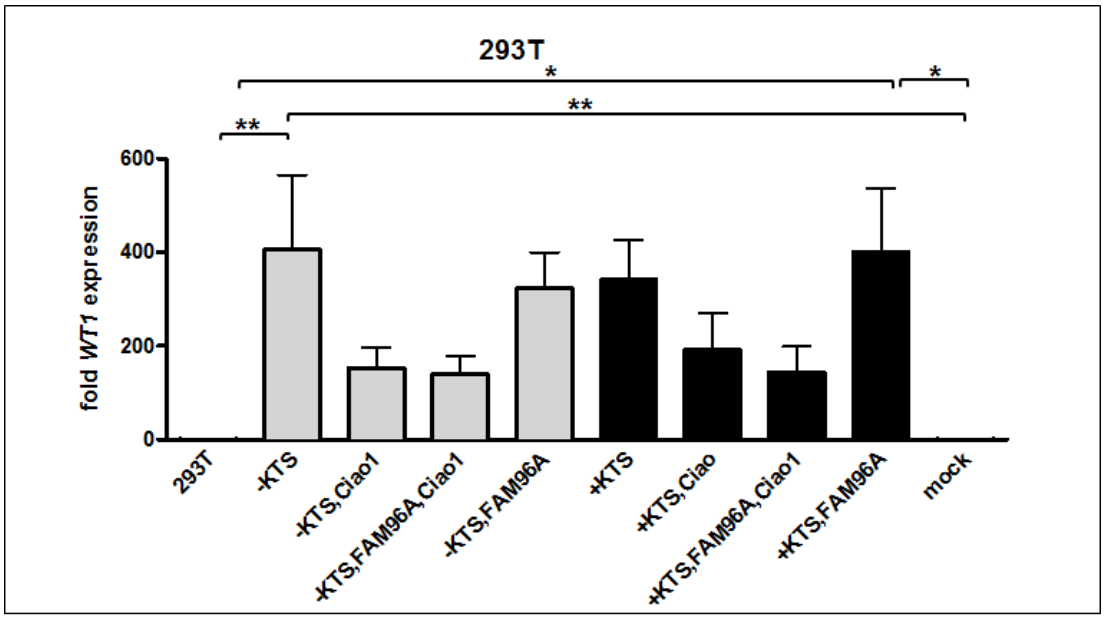

Figure 3.20: Analysis of *WT1* mRNA levels following *Ciao1* and *FAM96A* over-expression

2 x 10^5 HEK293T cells were seeded 24 hours prior to transfection with murine *WT1 -/+ KTS* isoforms (B and D), *Ciao1* and *FAM96A*. 30 hours after transfection, cells were harvested, and mRNA expression of transfected *WT1* was investigated by real time quantitative PCR using total RNA preparations. The relative quantification was performed with mean expression levels of human *GAPDH* and *HPRT*. GFP-transfected cells were used as a control (mock). *–KTS*, wt and *mock*: n=4, *+KTS*:

n=3; data are presented as Mean ± SD, one-way analysis of variance (ANOVA), Bonferroni post-test.

3.9 Analysis of a conditional *FAM96A* knockout mouse model

To study the physiological function of *FAM96A*, a conditional knockout mouse model (EUCOMM Project: 26229) was generated. The targeting vector construct is depicted below.

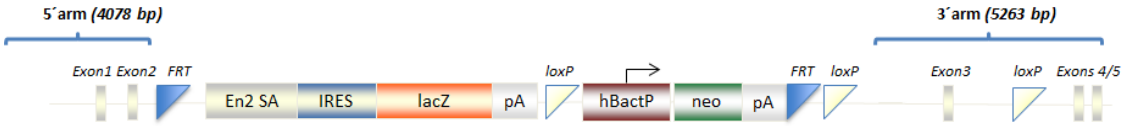

Exon 3 of the *FAM96A* transcript was flanked by *loxP*-sites and after site-specific recombination due to activity of the Cre recombinase, a truncated *FAM96A* mRNA containing the first 2 Exons is left. The efficient trapping of this transcript is expected to be warranted due to the insertion of the En2 SA and a polyadenlyation signal within the reporter cassette (Skarnes et al., 2011; Testa et al., 2004). The *lacZ* gene is inserted to indicate *FAM96A* promoter activity within mouse tissues. The transcript produced originating from the first two remaining exons is predicted to give rise to a newly generated full length protein of 22.7 kDa (http://web.expasy.org/cgi-bin/compute_pi/pi_tool; theoretical pI 8.67; and 19 kDa (pI 8.32) for the alternative, truncated protein sequence: **M**ERVSGLLSWTLSRVLWLSGFSEHGAAWQPRI**M**EE-KALEVYDLIRTIRDPEKPNTLEELEVVTESCVEVQEINEDDYLVIIKFTPTVPHCSLAT LIGPRSRKPKKKNPNKEDKRPRTAFTAEQLQRLKAEFQTNRYLTEQRRQSLAQEL GTRKIWTLENSAPLPPPPLTLLAEAAWNKAGVRLSICYFPPYCRLLAM (in red: 101 putatively generated “nonsense” amino acids).

In knockout mice generated from site-specific recombination from the *FRT* sites using the FLP recombinase, prior to Cre recombinase-mediated truncation of Exon 3, a dedicated transcript of 102 amino acids is generated (**M**ERVSGLLSWTLSRVLWLSGFSEHGAAWQPRI**M**EEKALEVYDLIRTIRDPEKPNT LEELEVVTESCVEVQEINEDDYLVIIKFTPTVPHCSLATLIVGNLHF). The last 6 amino acids are newly translated and derived from translocation of Exon 4. Importantly, a new in-frame stop codon is generated within the next to last exon (Exon 4) and the transcript is not recognized by non-sense mediated decay (NMD). As the novel stop codon is located within the last 50 bp of the second last exon, the exon junction complex cannot interact with the translation termination factors and

the protein is synthesized. The theoretical molecular weight of the newly translated protein is 11.697 kDa (pI 4.62, (http://web.expasy.org/cgi-bin/compute_pi/pi_tool) and the second and smaller putative protein derived from transcription from the alternative start codon (*ΔN-FAM96A*) has a predicted size of 8.04 kDa (pI 4.3). This mouse line was established, but not analyzed during this study.

Heterozygous *FAM96A* mice containing one targeted allele were crossbred to *CMV-Cre* mice on a C57Bl/6 background. The constitutively active *CMV*-promoter was chosen to achieve deletion of the floxed *FAM96A* Exon in every tissue of the progeny. In a second mating, heterozygous *FAM96A*$^{+/-}$*/lacZ* mice expressing the Cre recombinase (*FAM96A/lacZ*) were inbred, resulting in homozygous *FAM96A/lacZ* Exon 3 knockout animals. As the complete knockout or knockdown of *FAM96A* is lethal in yeast (Peter Kötter, Frankfurt University), *Drosophila melanogaster* (Pascal Meier, University College London) and *Danio rerio* (Mathias Hammerschmidt, Cologne University) (unpublished data), embryonic lethality was also presumed for the homozygous knockout in mice. Surprisingly, mice were born and vital.

3.9.1 Reporter gene expression within transgenic *FAM96A/lacZ* animal tissues

No obvious phenotype was observed in the homozygous *FAM96A/lacZ* (*FAM96A*$^{-/-}$) reporter animals. From homo- and heterozygous female Exon 3-knockout mice that contain a *lacZ*-reporter cassette in front of the targeted gene region, tissues were removed and analyzed for lacZ expression *via* X-Gal-staining (**Fig. 3.21**). A wild type C57Bl/6 mouse and a heterozygous *FBP1/lacZ* gene trap mouse served as controls for *lacZ* reporter-expression in tissues. The C57Bl/6 mouse served as a negative control, whereas the *FBP1* gene trap mouse was chosen as a positive control for X-Gal staining. While some background staining occurred in ileum, thymus, and uterus of wt animals, homozygous *FAM96A*$^{-/-}$ mice displayed the most intensive reporter activity in comparison to heterozygous animals in most tissues investigated. Intensive lacZ-activity was observed in lymphatic organs of homozygous animals (thymus and spleen**, Fig. 3.21**). A strong promoter activity of the *FAM96A* promoter was also observed within the ileum of *FAM96A*$^{-/-}$ animals compared to *FAM96A*$^{+/-}$, FAM96A$^{+/+}$ and the FBP1$^{+/-}$ tissue. *FBP1* promoter activity in the murine brain was observed to be much higher compared to *FAM96A* promoter activity according to X-Gal staining intensity (**Fig. 3.21**). Livers and mesenteric lymph nodes excised from wt C57Bl/6, heterozygous *FAM96A/lacZ* and *FBP1/lacZ* control mice compared to the homozygous *FAM96A*$^{-/-}$ animal displayed no difference in staining intensity due

to high background staining. No staining was observed in heart and lung of all the animals. According to these data, the *FAM96A* promoter is active almost ubiquitously in mouse tissues. Staining conditions should be improved, as overnight incubation in X-Gal solution yielded strong background staining in ileum, mesenteric lymph nodes, liver, uterus and thymus of the animals.

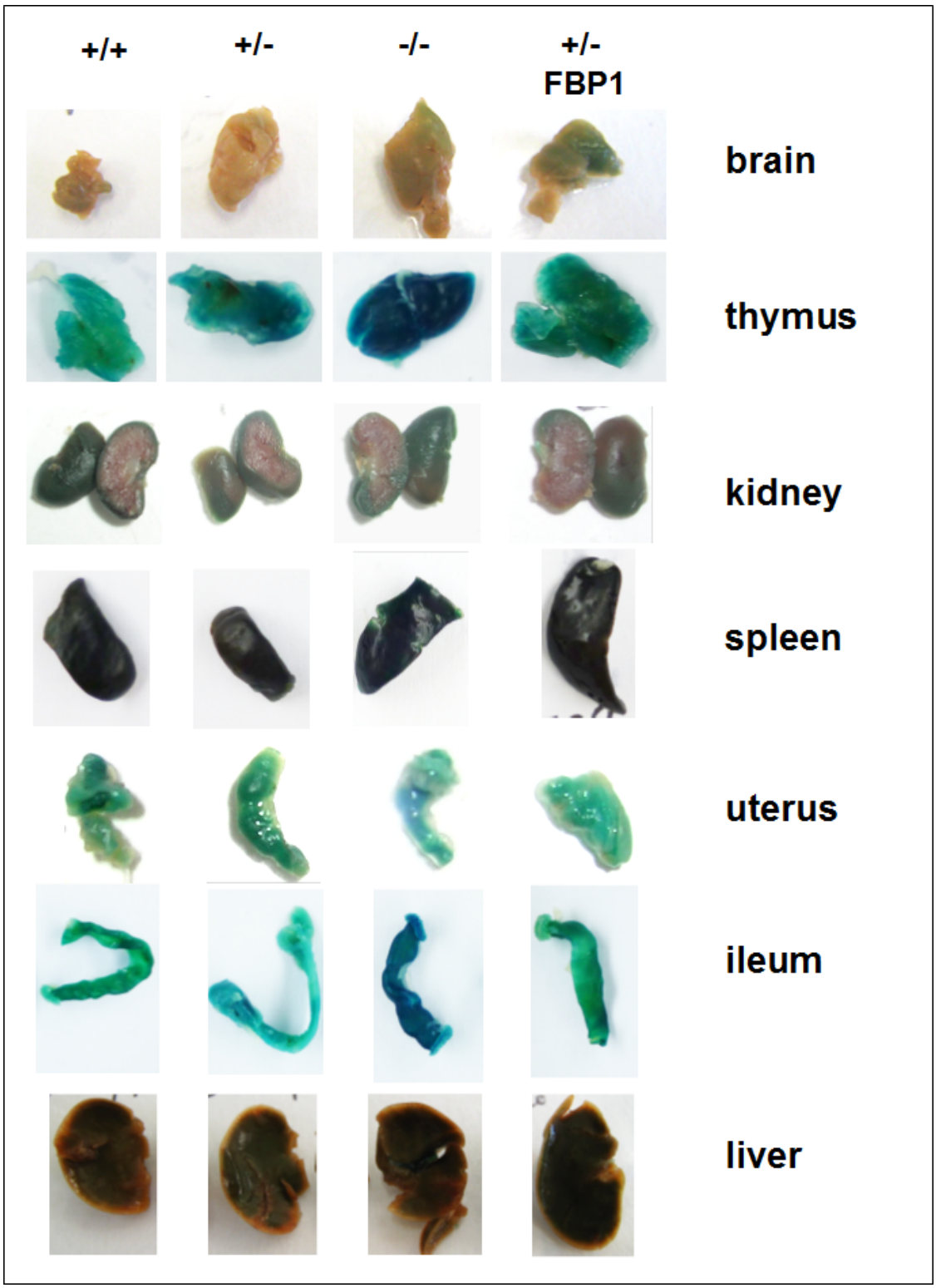

Figure 3.21: Analysis of lacZ reporter activity in *FAM96A* knockout mice via X-Gal-staining of murine tissues

Tissue samples prepared from a female wt C57Bl/6, heterozygous (+/-) and homozygous (-/-) *FAM96A/lacZ* knockout, and an *FBP1/lacZ* gene trap animal as a positive control were analyzed for lacZ expression following fixation and overnight to 40 hours staining with X-Gal. Picture documentation followed washing of the stained tissues with DPBS. Afterwards, all tissues were bed in Roti Histofix for long-term storage.

4. Discussion

Defects within the apoptotic pathways lead to severe pathologies in an organism, such as neurodegenerative diseases and cancer, or fundamental developmental defects during embryogenesis (Los et al., 1999; Schafer and Kornbluth, 2006). Oncogenic mutations in genes that regulate intrinsic apoptosis are common in malignancy and are responsible for initial neoplastic outgrowth, treatment failure and metastization (Lowe and Lin, 2000). Targeting of deregulated anti-apoptotic molecules involved in malignancy and restoration of pro-apoptotic activities are considered suitable approaches to induce cell death for cancer therapy (Lowe and Lin, 2000; Pick, 2006). The identification of novel pro- and anti-apoptotic effectors is indispensable from the development of further treatment strategies to overcome consistent mutational adaptations conferring malignant resistance.
One aim of this project was to functionally characterize the APAF-1 binding protein FAM96A and to elucidate its pro-apoptotic potential that had been observed in preliminary investigations (Pick, 2006).

4.1 Function of FAM96A in apoptosis and cancer

4.1.1 FAM96A is involved in the intrinsic apoptosis pathway

Evasion of the apoptotic program is a hallmark of cancer and the intrinsic apoptosis pathway is often deregulated in neoplasms (Hanahan and Weinberg, 2000). Reactivation of this cell death pathway is in the focus of current research. FAM96A was discovered as an APAF-1 interaction partner in a YTH screen for the *C. elegans* homolog of APAF-1, CED-4 and for several truncated versions as well as full length APAF-1_S as baits (Völp, unpublished). The small protein FAM96A was observed to bind to APAF-1 in GST-pulldown experiments and preliminary co-immuno-precipitation analyses (Pick, 2006; Mateus-Fernandez, unpublished). This study verified the interaction of the two proteins. Binding of FAM96A to APAF-1 could be confirmed for overexpressed as well as endogenous proteins within cellular lysates (**Fig. 3.1**). The binding site of FAM96A was mapped to the NOD of APAF-1_S. If FAM96A would bind to the WHD (**Fig. 4.1**), or any other domain within the NOD of APAF-1 that is in close contact with the nucleotide-binding region, it could serve as a scaffold protein for conformational changes or facilitate nucleotide exchange on APAF-1 during apoptosome formation. Whether FAM96A binds only to the monomeric form or can interact with the apoptosome complex remains unresolved.

Upon induction of apoptosome formation in cellular lysates by the addition of Cytochrome c and dATP and subsequent size exclusion chromatography, FAM96A was found within high molecular weight fractions together with APAF-1, but this could also result from aggregation of FAM96A oligomers (data not shown). Furthermore, the stoichiometry of FAM96A bound to APAF-1 needs clarification. Oligomeric proteins such as FAM96A can co-exist in more than one state *in vivo* (Ali and Imperiali, 2005; Chen et al., 2012). Therefore, either one of the two different domain-swapped dimers, major or minor dimer, or the monomeric FAM96A protein might interact with APAF-1. Oligomerization of FAM96A could potentially occur in response to a certain stimulus, probably the release of mitochondrial factors during apoptosis, and increase the affinity of this conformational state of FAM96A for APAF-1. A transient interaction of FAM96A with APAF-1 is likely because the protein has not been identified as an integral part of the apoptosome so far (**Fig 4.1. (1)** and **(2)**). Recombinant co-expression of both interaction partners might reveal a potential scaffolding function of FAM96A on monomeric APAF-1. This function could have a significant influence on the drastic conformational changes within APAF-1 during the initial steps of apoptosome formation (**Fig. 4.1 (1)**). Heptamerization of the platform for caspase activation can be triggered *in vitro* by addition of Cytochrome c and dATP to WD40-depleted APAF-1 (Riedl and Shi, 2004). The addition of FAM96A could facilitate or enhance oligomerization and thereby induce a stronger response to stimulation of the intrinsic pathway. The pro-apoptotic, cell-cycle regulator Parcs (pro-apoptotic protein required for cell survival) has been suggested to maintain APAF-1 in an activatable conformational state, however, was not observed to be directly involved in apoptosome formation as an integral component (Sanchez-Olea et al., 2008).

A model for a stabilizing function of monomeric FAM96A on APAF-1 is presented in Figure 4.1 (1).This stabilization could also be conferred by binding of one of the two different domain-swapped dimers. Furthermore, FAM96A might be able to stabilize the apoptosome complex as an integral part (3). Whether the protein is found within the heptameric complex can be analyzed in the future by induction of apoptosome formation and size exclusion analyses involving subsequent immunoprecipitation of complex proteins or functionally by monitoring of caspase activity in cellular lysates lacking FAM96A.

In silico predictions and recent reports suggest a function for the DUF59 domain as an ATPase (Lezhneva et al., 2004; Schwenkert et al., 2010). This suggestion was addressed during this study using recombinantly expressed proteins in an ATPase activation assay. An intrinsic ATPase activity of FAM96A could not be observed in

one single experiment performed (data not shown). FAM96A could, however, serve as a nucleotide exchange factor during apoptosome formation (Fig. **4.1 (4)**, **(5)**). This assumption needs to be further addressed. It would be interesting to analyze whether the small protein can bind to radioactively labeled nucleotides. Unknown nucleotide exchange factors interacting with APAF-1 have been mentioned in recent reports (Bao et al., 2007; Bao and Shi, 2007), but have not been identified so far. Nucleotide exchange on APAF-1 *in vitro* is described to be enhanced by PHAPI, CAS and HSP70, but if this is due to facilitated apoptosome formation assisted by the three proteins, or whether one of them is a nucleotide exchange factor remains unresolved until now (Kim et al., 2008). The occurrence of additional adapter proteins complexed with APAF-1 has been frequently cited in literature (Benedict et al., 2000; Hill et al., 2004). Another pro-apoptotic APAF-1 interactor, NAC (NB domain and CARD) enhances caspase activation upon binding to the CARD domain of APAF-1 after unfolding of the autoinhibited protein during complex formation (Chu et al., 2001). Caspase-9 recruitment has been reported to be drastically enhanced by HCA-66, a protein that can bind to APAF-1 in its monomeric and oligomerized state, but has no influence on the oligomerization process *per se* (Piddubnyak et al., 2007). Nucling is a pro-apoptotic molecule that binds to APAF-1 and is assumed to translocate the protein together with Caspase-9 from the cytoplasm to the nucleus (Sakai et al., 2004). Alpha-fetoprotein and acetylcholinesterase are pro-apoptotic proteins that can indirectly influence apoptosome formation (Schafer and Kornbluth, 2006).

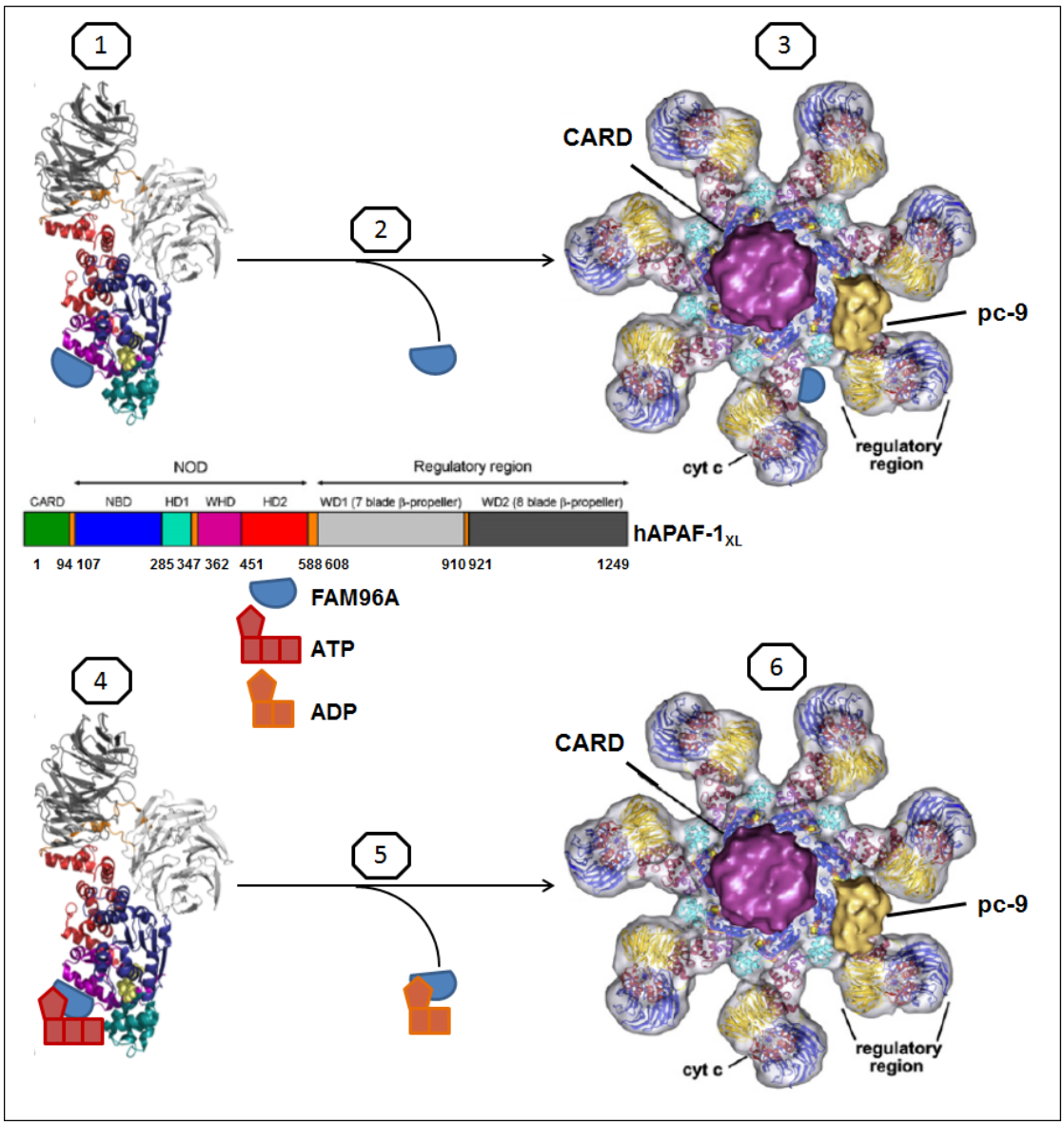

Figure 4.1: Model for the potential involvement of FAM96A during intrinsic apoptosis
1: scaffolding function of FAM96A (monomer or dimers) on the activated APAF-1 monomer; 2: short transient interaction facilitating conformational changes during oligomerization of the complex; 3: integral scaffolding function within the complex (pc-9: pro-Caspase-9); 4: nucleotide exchange factor function transferring ATP to the monomeric protein (before or after Cytochrome c binding); 5: nucleotide exchange factor bound to ADP; 6: ATP-bound apoptosome lacking FAM96A. Adapted from Reubold and Yuan et al., 2012.

The *in silico* predicted molecular weight of FAM96A is 18.355 kDa. The fact that the protein is detected at a higher MW by immunoblotting implies that it might be subjected to posttranslational modifications which remain undefined until now. 6 potential phosphorylation sites are located within FAM96A (Serine 124, Threonine 46, 55, 84, Tyrosine 77, 117) as predicted by the NetPhos 2.0 Server (http://www.cbs.dtu.dk/services/NetPhos/). Two lysine residues (52, 113) are

predicted *in silico* for glycosylation (http://www.cbs.dtu.dk/services/NetGlycate/). Post-translational modifications also play an important role in regulation of the tumor suppressor p53, coordinating its interactions and subcellular localization (Green and Kroemer, 2009). Histone-deacetylase (HDAC) inhibitors were used to stabilize p53 in preclinical experiments in cancer cells, but have not been established in clinical studies so far (Lane et al., 2010). Investigations about the posttranslational regulation of FAM96A might be of interest in the future.

4.1.2 Functional investigations on the pro-apoptotic role of FAM96A

This work aimed to characterize the physiological function of FAM96A. Preliminary results from transient FAM96A overexpression in RKO cells indicated a sensitization of cells towards stimulation of the intrinsic apoptosis pathway (Mateus-Fernandez, unpublished). This observation was further addressed by stable lentiviral *FAM96A* overexpression using the *LeGoiG2* vector in several cancer cell lines. The pro-apoptotic function of FAM96A could be confirmed in cell killing assays (**Figs. 3.2** and **3.3**) upon stable overexpression of the protein. FAM96A upregulation successfully increased the sensitivity of cancer cells towards drug treatment with chemotherapeutics. Increased intrinsic apoptosis upon FAM96A overexpression could be verified in cell culture when RKO and Renca-lacZ cells were treated with mitomycin C or oxaliplatin. Both DNA crosslinking agents are currently in use or were used in the clinics to treat colorectal as well as renal cancer (Adrain et al., 1999; Jin et al., 1992; Porta et al., 2004; Powles et al., 2008; Stein and Arnold, 2012). The anticancer effects of oxaliplatin are optimized in combinatorial treatment with 5-fluorouracil and folic acid (FOLFOX) (Stein et al., 2012), nevertheless, significant pro-apoptotic effects were observed when the agent was used as standalone intervention together with simultaneous FAM96A overexpression. Statistically significant increases in cell death were observed for both chemotherapeutics in Renca-lacZ cells and for oxaliplatin-treated RKO cells when FAM96A expression was increased compared to empty vector-transduced control cells. The overexpression of FAM96A in Renca-lacZ cells was not stable, most probably due to the induction of apoptosis in cells expressing high levels of the protein.

Vice versa, when murine fibroblast (NIH/3T3) and human colon cancer (RKO) cells were depleted of FAM96A *via* lentivirus-mediated shRNA transduction and compared to control vector-transduced cells, a significant desensitization towards UV-mediated killing could be detected (**Figs. 3.5** and **3.6**). Two separate vector

systems for the human *FAM96A* knockdown served to verify the apoptosis resistance-conferring consequence of FAM96A downregulation.

In line with the *FAM96A* knockdown experiments, morpholino-mediated knockdown in zebrafish embryos also significantly reduced the sensitivity towards UV-induced cell death (M. Hammerschmidt, Cologne University, **Fig. 4.2**).

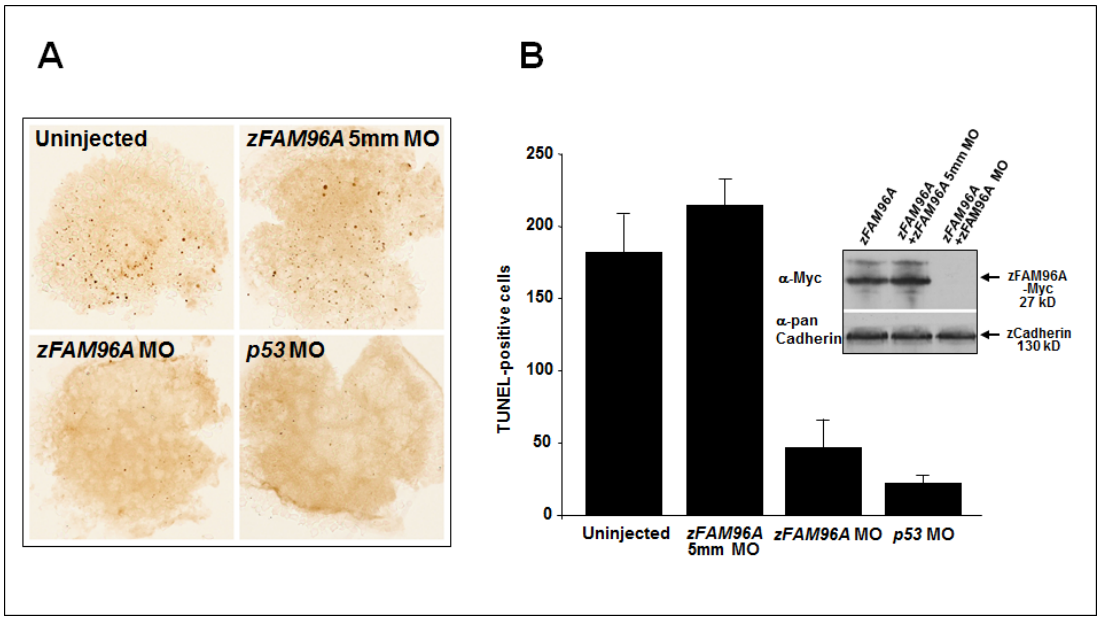

Figure 4.2: TUNEL assay with morpholino-injected zebrafish embryos after UV irradiation

Antisense morpholino oligonucleotides targeting *zFAM96A* (*zFAM96A MO*) or *p53* (*p53 MO*; positive control) were injected into 1-2-cell zebrafish embryos (0-1 hours post fertilization; hpf). Embryos injected with a morpholino bearing 5 mismatch mutations (*zFAM96A* 5mm MO) and uninjected embryos served as negative controls. At 4 hpf, the sphere-stage embryos were subjected to UV irradiation (20 s; 50 mJ/cm^2). (*A*) Apoptotic cells detected by TUNEL staining (dark brown dots) at 8 hpf in representative whole embryos. (*B*) Apoptotic cells counted in 3 UV-irradiated zebrafish embryos. Data are means ± SD. Inset: Verification of knockdown efficiency by Western immunoblotting. To this end, zebrafish embryos were injected with an *in vitro*-transcribed Myc-tagged *zFAM96A* mRNA alone or in combination with *zFAM96A* MO or *zFAM96A* 5mm MO. Embryonic protein lysates prepared at 6 hpf were analyzed using an anti-Myc antibody. Cadherin was used as a loading control.

Increased protein levels of FAM96A were not observed to influence cell cycle distribution in one single experiment performed. Susceptibility towards G1-arrest induction by Rad-001 was observed to be moderately, but not significantly increased upon upregulation of FAM96A in Renca-lacZ cells (**Fig. 3.8**). Here, a combinatorial

treatment of the cells with an apoptotic stimulus, prior to G1-arrest induction will be useful in future experiments.

An antagonistic, anti-apoptotic role for the smaller isoform of FAM96A has been suggested (Pick, 2006). However, preliminary results from this work (**Fig. 3.7**), together with other recent observations, suggest a rather pro-apoptotic function of ΔN-FAM96A (Jung, 2012). This supports the assumption that the C-terminus of the protein might be responsible for its pro-apoptotic function (Pick, 2006). It would be interesting to differentiate between the two FAM96A isoforms and their contributions to apoptosome formation. A specific interaction of the smaller isoform of FAM96A with APAF-1 is assumed, but could not be detected so far (Jung, 2012). The longer isoform was observed to be primarily involved in regulation of the intrinsic pathway and thereby with tumorigenicity. Differential expression of two different isoforms of ZO-2, another tumor-suppressor protein with the 2 isoforms ZO-2 A and C (which differ in 23 amino acids at the N-terminus) is assumed to play a role in pancreatic adenocarcinoma, where only the shorter isoform is expressed (Chlenski et al., 1999; Gonzalez-Mariscal et al., 2012). A rescue experiment performed by exclusive overexpression of the truncated isoform after an efficient *FAM96A* knockdown (removing both endogenous isoforms) would clarify the proposed pro-apoptotic function of ΔN-FAM96A.

4.1.3 Conclusions about the potential tumor-suppressor function of FAM96A

If FAM96A is considered to function as a pro-apoptotic protein with tumor-suppressive potential, its expression should decrease or completely vanish during oncogenesis. Other tumor suppressor proteins such as p53, Rb, PTEN, BRCA1/2 or APC play key roles in development, tissue homeostasis and cancer inhibition and are frequently mutated in tumors (Berger et al., 2011). Here, the *in vivo* tumor-suppressive potential of the apoptosis-regulating protein FAM96A was initially investigated in subcutaneous xenograft experiments in NOD/SCID mice. The tumorigenicity of lentivirally transduced human colon and murine renal cancer cells, which displayed increased protein expression of FAM96A, was compared to empty vector- transduced cells. When these cells were injected subcutaneously into NOD/SCID mice, and tumor development was monitored over several weeks, an impaired tumor growth could be observed in human colon as well as murine renal cancer cells upon increased protein expression of FAM96A (**Fig. 3.4**). Additionally, mice were treated with mitomycin C. Overexpression of FAM96A compared to

control vector transduction successfully reduced resistance towards chemotherapeutic treatment in the colon cancer cell line and it decreased its tumorigenicity *in vivo*. The effect of simultaneous application of anticancer therapy and overexpression of FAM96A should however be investigated in more detail. In the case of the renal tumor xenograft, treatment with the cytostatic mitomycin C was started as soon as the tumor volume had reached 150 mm^3, a value that can be considered as too high for these rapidly expanding tumors. In case of the RKO colon cancer tumor xenograft, only two mice of the seven animals within the mitomycin C-treated FAM96A group showed engraftment of the cancer cells. The relative tumor volume of mitomycin C-treated RKO cells was reduced when FAM96A expression was simultaneously increased. Interestingly, the overall engraftment of RKO cells within the two groups of mice (treated and untreated, 7 animals per group) which overexpressed FAM96A was largely impaired. Only 5 out of 14 injected tumors successfully proliferated, while the 9 other mice did not display any engraftment *post injection*.

4.1.3.1 Loss of FAM96A is important for GIST tumorigenesis, and its re-introduction increases susceptibility to apoptosis of GIST cell lines

A correlation of FAM96A expression with tumorigenicity was observed specifically in gastrointestinal stromal tumors, where FAM96A protein levels were found to be either poor or completely absent, as shown by immunoblotting and IHC (**Figs. 3.9** and **3.10**). A loss of *FAM96A* in this tumor entity was initially observed by CGH, indicating deletions within the *FAM96A* locus with a frequency of around 50% for all GIST present in the CGH database. This was verified on mRNA as well as protein level in two separate GIST patient cohorts (Agaimy, Erlangen; Zatloukal, Graz, unpublished). The reduction of FAM96A in the different primary tumor samples, which were analyzed by quantitative real time PCR (data not shown) and IHC, was found to be independent of tumor grading or origin (**Fig. 3.9**). The precursor cells of GIST, ICC, were observed to express FAM96A as shown by immunohistochemistry (**Fig 3.9**). Real time PCR analysis of murine cell lines revealed loss of *FAM96A* to occur during GIST development, coincidental with malignant transformation of ICC stem cells (ICC-SC) (T. Ordog, unpublished). Although no experimental evidence exists, one can speculate that LOH of *FAM96A* might be one cancer promoting mutational event in GIST development, and loss of FAM96A obviously resembles a marker for GIST. A tumor xenograft experiment in which re-introduction of FAM96A in ICC-SC undergoing malignant transformation could potentially prevent GIST

development would be interesting to further confirm the tumor suppressor role of FAM96A in GIST. Another potential approach would imply deletion of *FAM96A* in ICC, and the investigation whether cells devoid of the tumor suppressor consequently undergo malignant transformation.

Re-introduction of FAM96A into the established, imatinib-sensitive GIST882 cells that completely lack FAM96A protein expression as measured by immunoblotting (**Fig.3.10**), severely impaired tumor growth and the engraftment potential of these cells (**Fig. 3.12**). In the subcutaneous tumor xenograft experiment performed in NOD/SCID mice, only 5 of the 9 mice injected with GIST882 cells, in which FAM96A expression was re-established, developed tumors, as compared to empty vector-transduced controls. Accordingly, an almost abolished engraftment potential of RKO cells was observed upon FAM96A overexpression. Thus, cell death of tumor-initiating cells might result in decreased engraftment capacity and reduced oncogenic potential in both xenograft experiments.

Furthermore, when GIST882 cells were treated with the tyrosine kinase inhibitor imatinib for 24 hours, simultaneous FAM96A re-expression enhanced cell killing, although no differences compared to control cells could be observed in later passages *post transduction* upon longer imatinib incubation (**Fig. 3.11 B**).

Cell death of the imatinib-resistant GIST48 cell line was increased upon introduction of FAM96A, and additionally, significant pro-apoptotic effects were observed in *FAM96A*-transfected cells when apoptosis was induced by staurosporine compared to control vector-transfected cells (**Fig. 3.11 C**). The imatinib resistance of GIST48, acquired due to a secondary *c-kit* mutation, could not be overcome by overexpression of FAM96A (**Fig. 3.11 D**).

Although FAM96A re-expression was maintained in later passages of the GIST cell lines 48 and 882, pro-apoptotic effects of FAM96A were lost, hinting towards unknown inhibitory or compensatory mechanisms within the cancer cells. This represents one major drawback of FAM96A re-establishment therapy.

However, the results obtained from cell killing experiments upon FAM96A upregulation and depletion, and the three independent subcutaneous xenograft experiments imply that FAM96A exhibits a tumor-suppressive function. In support of this conclusion, reduction of FAM96A expression was observed for a variety of tumor entities in multi-tumor tissue arrays (**Fig.3.13**) and was drastic in the case of renal and transitional cell carcinoma (RCC and TCC) compared to normal tissue material (**Fig. 3.14**). This data derived from primary human renal cancer tissue samples is in accordance with the experimental data obtained from stable upregulation of FAM96A in the murine renal cancer cell line Renca-lacZ, when

overexpression of the protein diminished oncogenic potential (**Figs. 3.3** and **3.4**). An extensive analysis of FAM96A protein expression levels in primary tumor samples from human renal and bladder cancers compared to normal tissue is a focus of current investigations. RCC are strongly chemo- and radiotherapy-resistant, despite the fact that the apoptosome complex remains intact in these cells (Gerhard et al., 2003). Signal transduction of intrinsic apoptosis has therefore been assumed to be disturbed at distinct sites in RCC.

Reduction of oncogenicity upon FAM96A upregulation is not exclusively restricted to GIST, and a role for FAM96A as a novel universal tumor suppressor is suggested. Mechanistically, haploinsufficiency or, in some entities, obligate haploinsufficiency as observed for *PTEN* cannot be excluded (Berger et al., 2011). Obligate haploinsufficiency is present when cancer cells are strictly dependent on residual protein activity or expression of a tumor suppressor, and would succumb to senescence or cell death in the instance of TSG deletion (Berger et al., 2011). It would be of future interest if, besides from genomic deletions, other loss-of function mutations occur within the *FAM96A* gene, and if so, in which tumor entities and at which incidence. Restoration of the levels of the tumor-suppressor protein Par-4 prevents neoplastic transformation. This tumor suppressor protein is inactivated by oncogenic Ras (Garcia-Cao et al., 2005; Qiu et al., 1999). FAM96A function could also be inhibited by anti-apoptotic oncogenes that are constitutively active at early stages of tumor development. Pathway and oncogene expression analyses in different tumor entities will shed light on this possibility. As another level of regulation of *FAM96A* gene expression in cancer, it would be interesting to analyze potential epigenetic influences that lead to silencing of the *FAM96A* promoter in tumors. The promoter of the pro-apoptotic, tumor cell specific suppressor Par-4 has been reported to be hypermethylated as an oncogenic event observed in a number of cancers (Hebbar et al., 2012).

Furthermore, miRNAs regulating *FAM96A* expression could have important regulatory functions on the gene and should be investigated. Here, polymorphic variations in miRNA binding sites in cancer resulting from SNPs within the 3´UTRs or within the promoter region of FAM96A affecting transcription factor interaction could severely affect the regulatory network in tumor cells and with that the levels of protein expression of the TSG. Analysis of the miRNA/TSG interaction can indicate therapy response and is therefore important for patient prognosis (Berger et al., 2011).

4.1.4 FAM96A as a potential therapeutic target for anticancer therapy

FAM96A is lost or decreased in gastrointestinal stromal tumors, and its expression has been observed to be diminished in other cancer entities. Therefore, FAM96A loss can serve as a marker for tumorigenesis. Due to its positive influences on restoration and enhancement of apoptotic signaling, FAM96A represents a potential target for cancer therapy. As reconstitution of FAM96A protein expression strongly reduces the oncogenic potential, reintroduction of the protein into cancer cells would be a therapeutic option. In the case of FAM96A, gene therapy describes the most promising and efficient anti-cancer approach. Initially, gene therapy was designed for treatment of inherited diseases, however, expanded to the field of cancer research, and currently over 3249 clinical trials for gene therapy, of which 1291 are related to cancer, are ongoing worldwide ((Li et al., 2005) www.clinicaltrials.gov). Recombinant adenovirus-associated vectors (rAAV) represent a safe and efficient delivery system for gene therapy (Buning et al., 2008; Zentilin and Giacca, 2008). rAAV-mediated gene therapy approaches for cancer treatment include cytokines, antiangiogenesis genes, apoptosis inducers, suicide gene activation or oncogene downregulation (Li et al., 2005). In murine tumor xenograft experiments, tumor growth was strongly impaired following AAV2-mediated introduction of TRAIL (Mohr et al., 2004). Intratumoral AAV/p53 injection significantly reduced tumor growth *in vivo* in xenograft experiments. Increased expression of telomerase in tumor cells has also been targeted by AAV-vectors conferring siRNA-mediated knockdown of the enzyme (Li et al., 2005). Direct intratumoral application of a FAM96A-rAAV for overexpression in combination with radiation or chemotherapy would presumably exhibit tumor-suppressive effects. Due to its small size, the protein represents a suitable rAAV insert, as these vectors display limited coding capacity (4.5 kb). However, as for other TSGs, FAM96A therapy has some drawbacks due to the ubiquitous expression pattern of the protein and the expected potential side effects on nonmalignant cells upon viral infection. This can be overcome by specific identification of targeting peptides expressed by tumor cells (Büning et al., 2008). Here, an AAV peptide library of 7-mer peptides can be screened for selective targeting of GIST for example. ICC or normal tissue would be spared from infection with the GIST specific FAM96A-rAAV.

Small molecule inhibitors and antisense approaches would be considerable if blockage of FAM96A by another protein would affect the function of the tumor suppressor as it is the case for p53 and Mdm2 or MdmX. Thus, the identification of

potential regulators of FAM96A should gain attention in future investigations (Lane et al., 2010).

If recombinant FAM96A expression would yield high protein concentrations, another putative approach would imply the combination of the small protein with a protein transduction domain and intratumoral application of the fusion protein. The application together with a protein transduction domain has been described for Methallothionein fusion proteins before (Lim et al., 2010).

Overall, cancer therapy approaches addressing the re-establishment of tumor suppressor function are not trivial because cancer cells harbor more than one oncogenic mutation and rapidly adapt to therapy by secondary mutations or oncogene upregulation.

4.2 Involvement of FAM96A in cytosolic iron-sulfur assembly?

As FAM96A efficiently binds the cytosolic iron sulfur cluster assembly protein Ciao1 (**Fig. 3.15**), a potential role for FAM96A in CIA and *vice versa*, a role for Ciao1 in regulation of the intrinsic apoptosis pathway, cannot be excluded. The second mammalian DUF59 domain-containing protein, FAM96B, contains one conserved, hyperreactive cysteine residue and participates in the essential biogenesis pathway of iron-sulfur cluster biogenesis (Weerapana et al., 2010). Upon assembly of the late acting CIA complex which consists of FAM96B and Ciao1 together with MMS19, IOP1/NARFL and ANT2, a wide variety of Fe-S client proteins is loaded with Fe-S clusters for the execution of many cellular functions (Gari et al., 2012; Stehling et al., 2012; van Wietmarschen et al., 2012). The contributions of ANT2 and IOP1 within this complex are currently under discussion. Recently, a DUF59 domain-containing protein has been characterized in *Arabidopsis thaliana*: AE7 (asymmetric leaves 1/2 enhancer7). The DUF59 domain of the protein shares 58% identity with human FAM96B. AE7 is responsible for DNA integrity and exhibits a conserved function in CIA in plants (Luo et al., 2012). However, the *FAM96B* knockout phenotype in yeast could not be rescued by introduction of AE7, while the At-CIA1 (*Arabidopsis thaliana*) was able to protect *Cia1* (the yeast Ciao1 homolog) deleted yeast from dying (Luo et al., 2012). DUF59 domain-containing proteins have been described to inhere several different functions across the biological kingdoms. In aerobic bacteria, two DUF59 domain-containing proteins are responsible for metal binding as subunits of the phenylactely-coenzyme A oxygenase complex PaaI (Song et al., 2006). Furthermore, the first structure of a DUF59 domain-containing protein was

resolved from the anaerobic, hyperthermophilic bacterium *Thermotoga maritima*. The protein was suggested to be associated with Fe-S cluster assembly due to conserved cysteine and threonine residues within the proposed active site (Almeida et al., 2005). In *Arabidopsis thaliana*, the highly conserved, plastid localized DUF59 domain protein HCF101 (high chlorophyll fluorescence 101) was initially described to be involved in Fe-S assembly in 2004 (Lezhneva et al., 2004). Five years later, Schwenkert et al. proved the functional contribution of HCF101 to Fe-S cluster assembly in *Arabidopsis*. The protein can bind and transfer Fe-S clusters to apoproteins, exhibiting a scaffolding function (Schwenkert et al., 2010). Fe-S clusters are bound by three cysteine residues in HCF101 of which one is essential for the binding and, consequently, highly conserved. FAM96A contains five cysteine residues, of which one is highly conserved (Cys90) and a C-X(7)-C motif that has been associated with metal and Fe-S cluster binding (Agnihotri et al., 2004; Schwenkert et al., 2010). Similar to its plant ortholog, FAM96A might potentially bind a Fe-S cluster, that is then transferred to apoproteins and thereby exhibit scaffolding functions during Fe-S biogenesis (**Fig. 4.3 A**). Thus, future investigations should address whether FAM96A is capable of transiently binding an Fe-S cluster, an event that can be analyzed by radiolabelling experiments, and especially, which of the 5 cysteine residues would be responsible for the interaction with the Fe-S cluster. A sequential replacement of the cysteines by serine *via* site-directed mutagenesis would be one method to experimentally address this question.

During CIA, FAM96A could act as a scaffold within an early CIA complex together with Ciao1 and IOP1/NARFL. This complex might be responsible for transport of the labile Fe-S cluster to the late CIA complex (**Fig. 4.3. A1**). Regarding the function of the FAM96A homolog, FAM96B, one would rather suggest a scaffolding function for the protein within the late acting CIA complex together with Ciao1 and probably also with MMS19 and ANT2 (**Fig. 4.3. A2**). The interaction of FAM96A with MMS19, ANT2 or IOP1 has not been investigated so far. Upon FAM96B deletion, DNA maintenance is impaired as various proteins involved in the preservation of genomic stability are dependent on Fe-S clusters (Gari et al., 2012; Stehling et al., 2012). Depletion of FAM96A would probably lead to an impaired loading of yet unknown target apoproteins and should be investigated in future experiments. The presence of a CIA-complex containing FAM96A, Ciao1 and potential novel target apoproteins can be analyzed by mass spectrometry-based immunoprecipitation proteomics (ten Have et al., 2011).

On the other hand, due to its conserved cysteine residues, FAM96A could also be an apoprotein that is loaded with a Fe-S cluster during its interaction with Ciao1 and

which executes its functions upon integration of its prosthetic Fe-S group (**Fig. 4.3 B**). That assumption appears less likely, referring to the described functions of DUF59 domain-containing proteins so far. A summary of the potential involvement of FAM96A in mammalian CIA is presented in Figure 4.3.

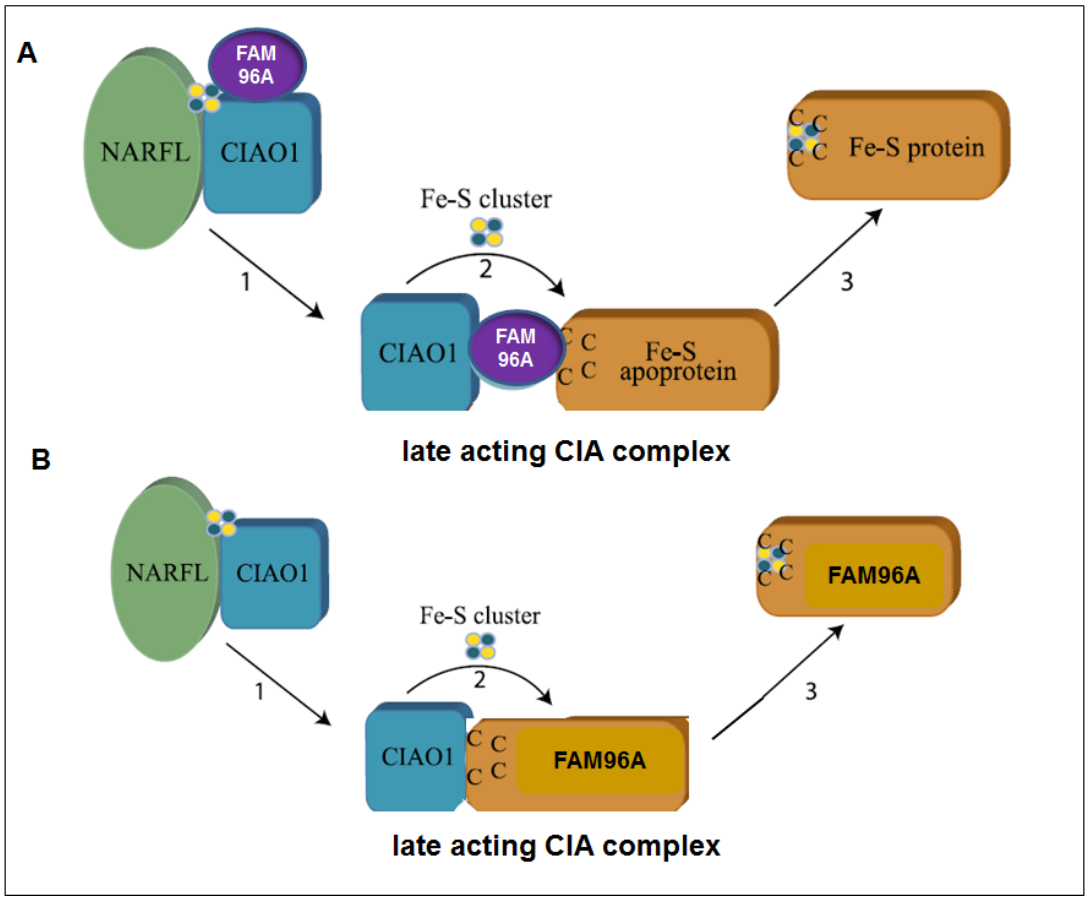

Figure 4.3: Model for FAM96A function in CIA
As a binding partner of Ciao1, FAM96A can contribute to cytosolic iron sulfur cluster assembly as a scaffold protein (A). It might either interact with Ciao1 and NARFL/IOP1 to facilitate the transport of Fe-S-clusters (A 1) to the late acting CIA complex or it can interact, like its homolog FAM96B, with proteins of this complex and thereby enable the loading of apoproteins (A 2). After loading, Fe-S proteins carry out their vital functions (A 3). Due to its conserved cysteine residues, FAM96A could exhibit apoprotein function and might be loaded with its prosthetic group by the CIA complex (B). Adapted from van Wiethmarschen et al., 2012.

FAM96A might exhibit distinct functions in its different structural conformations. Chen et al. speculate that the two separate forms of the proposed dimer (major and minor dimer) fulfill different functions (Chen et al., 2012) *in vivo*. For example, one conformation might interact with APAF-1 or the apoptosome, another one with Ciao1 as an integral part of a CIA complex. A conserved, ancient vital function of FAM96A independent of its regulatory function on PCD has been suggested earlier (Pick, 2006). The potential participation of FAM96A in the ancient process of Fe-S cluster

biogenesis supports this hypothesis. Like Cytochrome c, which exhibits a conserved vital function in energy metabolism, FAM96A might have been integrated in the evolutionarily younger process of programmed cell death.

4.3 A potential contribution of FAM96A and Ciao1 to intrinsic apoptosis and to the transcriptional activation of WT1

A potential common contribution of FAM96A and Ciao1 to the regulation of the mitochondrial pathway of apoptosis was investigated. In overexpression and knockdown analyses, Ciao1 exhibited to some extend anti-apoptotic potential (**Fig. 3.16** and **Fig. 3.18**). Upon co-overexpression of Ciao1 and FAM96A, the decreased pro-apoptotic effects of FAM96A might potentially result from tethering by Ciao1 due to higher affinity of FAM96A for the CIA component. Assuming such a scenario, FAM96A would not be available to interact with APAF-1 and to facilitate apoptosome formation during intrinsic apoptosis. This should have been counteracted by simultaneous downregulation of Ciao1 and overexpression of FAM96A. However, when quantifying cell death, such a tendency could not be confirmed in the *Ciao1* knockdown experiments (**Fig. 3.18**). Reduced Ciao1 protein levels increased susceptibility of treated cells, independent of FAM96A expression. Therefore, it appears as if FAM96A and Ciao1 fulfill distinct functions in apoptosis regulation. It can be speculated that the observed anti-apoptotic nature of Ciao1 results from enhanced Fe-S loading of target apoproteins upon overexpression, and impaired CIA as a consequence of Ciao1 depletion, and the protein therefore has no direct influence on mitochondrial apoptosis.

Ciao1 can bind to and regulate the transcriptional activity of WT1 (Johnstone et al., 1998). It has originally been described as a transcriptional repressor, but recent data obtained in the group of Prof. M. Zörnig from luciferase assays report its activating role on *WT1* (Jung, 2012). FAM96A function was analyzed in the context of Ciao1-dependent regulation of WT1, investigating a potential antagonistic function for FAM96A. However, this weak antagonistic role of FAM96A on WT1 can be considered as inferior to Ciao1 function on WT1 and might result from formation of a putative trimeric complex on the WT1 target gene promoters (Jung, 2012). An interference of the Ciao1-WT1 interaction *via* simultaneous overexpression of FAM96A could not be observed in two independent competitive co-immunoprecipitation analyses from cellular lysates (**Fig. 3.19**). Furthermore, diminished *WT1* mRNA levels resulting from Ciao1 overexpression that were further

reduced by co-expression of FAM96A were only observed for the +KTS isoform of WT1 (**Fig. 3.20**). This isoform is involved in RNA processing and does not display transcription factor activity. The influence of FAM96A in this context was not significant, while the effect of Ciao1 on both isoforms of WT1, -KTS and +KTS was drastic (**Fig. 3.20**). One possible explanation for these conflicting results from luciferase reporter assays and *WT1* mRNA quantification might arise from the fact that the WT1 protein is able to negatively autoregulate its own promoter (Malik et al., 1994; Rupprecht et al., 1994). Unknown co-factors for negative autoregulation have been proposed, and Ciao1 could exhibit such a co-repressing function, conversely resulting in an increase in transcriptional activity of WT1 as the transcription factor is no longer subjected to autosuppression. In that way, Ciao1 would act as a fine-tuning screw for transcriptional activity of WT1 due to inhibition of promoter suppression. The acquisition of further experimental evidence for this assumption should be in the focus of future experiments and here, electrophoretic mobility shift assays (EMSA), chromatin immunoprecipitations (CHiP) and luciferase assays would clarify the occurrence of a ternary WT1/Ciao1/FAM96A complex located on target gene promoters. Furthermore, a Ciao1-regulated activation of the *WT1* promoter could be investigated.

4.4 Analysis of a conditional *FAM96A* knockout mouse model

Knockout mouse models serve to analyze the physiological function of a gene, and conditional knockout mice can specifically serve to investigate pathological, developmental and a variety of other questions for a certain gene as they enable tissue specific gene deletion at will.

4.4.1 Phenotyping of *FAM96A/lacZ* reporter mice

To study the physiological function of FAM96A, a conditional knockout mouse model was established. Mice on a C57Bl/6 background, heterozygous for the expression of the *FAM96A* targeting cassette, were provided by EUCOMM, and matings with *FLPeR* deleter mice prior to *CMV-Cre* mice, or with *CMV-Cre* mice only were performed. Site-specific recombination mediated by the two recombinases FLP and Cre served to generate *FAM96A* Exon 3 knockout mice. Due to a newly generated Stopcodon by an Exon 4 frameshift within the mRNA transcript following FLP and Cre recombination, the RNA is predicted not to be recognized by nonsense-

mediated decay (NMD), and a C-terminally truncated and modified protein of 11.4 kDa is suggested to be generated. The knockout mouse strain was established but not analyzed during my PhD thesis.

Following Cre-mediated recombination, the knockout alleles express a transgenic lacZ reporter cassette upstream of the deleted Exon 3 that serves as a reporter for endogenous *FAM96A* promoter activity. Due to a splice acceptor and a polyadenlyation signal, the remaining mRNA derived from the first two Exons of *FAM96A* is trapped, and a predicted putative novel protein of 22.7 kDa is generated (Skarnes et al., 2011; Testa et al., 2004). A knockout of Exons 3, 4 and 5 is generated at the RNA processing level. Additionally, the produced protein might be subjected to proteasomal degradation due to improper folding. Furthermore, a functional inactivation of the protein resulting from synthesis of the large new C-terminus cannot be excluded and needs further investigations. Heterozygous *FAM96A/lacZ* knockout mice were inbred, and homozygous *FAM96A*$^{-/-}$ animals were preliminarily analyzed for the consequences of the C-terminal Exon 3, 4 and 5 deletion. *FAM96A*$^{-/-}$ mice are born and vital, and they exhibit no differences in body weight compared to heterozygous and wt animals. Observations of *BAK* knockout mice also revealed no phenotype at all, and *BAX*$^{-/-}$ mice display only minor apoptotic defects, and show normal development. The double knockout (DKO) of these two functionally redundant genes *BAX* and *BAK*, however, exhibits severe developmental defects. Thymic selection is disrupted, lymphoid homeostasis is destroyed and 90% of DKO animals die perinatal (Ranger et al., 2001). Smac/DIABLO deficient mice are healthy, fertile and lack histological abnormalities (Okada et al., 2002). The existence of a functionally redundant substitutor *in vivo* or the participation of Smac in apoptosis only under specific circumstances or tissues was suggested as a potential explanation for the lack of phenotype of these mice. In analogy, functional redundancy of the two mammalian DUF59-containing proteins FAM96A and FAM96B might explain the viability of the *FAM96A*$^{-/-}$ mice, and *FAM96A/B* DKO mice might display more obvious phenotypes. A detailed phenotyping of *FAM96A*$^{-/-}$ mice might reveal defects in DNA-damage repair and chromosomal maintenance or other essential metabolic pathways, referring to the potential involvement of FAM96A in Fe-S biogenesis.

Tissues from 6 week old female wt, *FAM96A*$^{-/-}$*/lacZ*, *FAM96A*$^{+/-}$*/lacZ* and a heterozygous *FBP1*$^{+/-}$*/lacZ* mouse as a positive control were compared for their lacZ reporter gene expression by tissue staining with X-Gal, the substrate for β-galactosidase. High activity of the *FAM96A* promoter was observed in lymphatic organs such as spleen and thymus (**Fig. 3. 21**). Data acquired during this thesis by

IHC report FAM96A to be highly expressed in macrophages of lung and spleen, and mRNA expression data on *FAM96A* expression in primary mouse macrophages by Chen et al. support this observation (Chen et al., 2012). Due to these findings, a potential immunomodulatory function of FAM96A in regulation of the immune system should be investigated in more detail.

Furthermore, lacZ was observed to be highly expressed within the gastrointestinal tract of the *FAM96A*$^{-/-}$ mice (**Fig 3.21,** ileum). This finding suggests a significant FAM96A expression within the murine gastrointestinal tract and is in line with the immunohistochemical analysis of FAM96A protein expression in human ICC (**Fig. 3.9**). The strong promoter activity might indicate requirement for FAM96A expression and thereby an increased susceptibility towards development of tumors associated with the GI tract, most probably gastrointestinal stromal tumors when FAM96A is lost. Long term observations and phenotyping of the knockout mice is necessary to monitor their potential spontaneous development of tumors, as it is observed in many other TSG knockout mouse models. 75% of p53$^{-/-}$ animals develop tumors (mainly T cell leukemia) at around 6 months of age (Hakem and Mak, 2001). *Par-4* null animals do not suffer from embryonic lethality, but display age-associated pathologies, a significantly decreased survival, and increased susceptibility to chemically and hormonally induced cancers compared to heterozygous and wt animals (Garcia-Cao et al., 2005). Long-term investigations of spontaneous tumorigenesis in *FAM96A*$^{-/-}$*/lacZ* mice and whether their average lifespan is decreased compared to *FAM96A*$^{+/-}$*/lacZ* and *FAM96A*$^{+/+}$ mice should be one focus of future investigations. Furthermore, mouse embryonic fibroblasts (MEFs) isolated from FAM96A knockout mice are assumed to exhibit increased resistance to apoptotic stimulation. Nucling$^{-/-}$ animals for example are viable and fertile, and their MEFs display severely increased resistance towards apoptosis induction *via* UV irradiation compared to wild type MEFs (Sakai et al., 2004).

The tumor-suppressive role of FAM96A *in vivo* can be further investigated in the future by means of established knockout mouse models. Referring to the observed tumor suppressor function of FAM96A in GIST, *FAM96A* knockout mice can be inbred with homozygous *Kit K641E* animals, a mouse model for GIST (Rubin et al., 2005). Consequently, homozygous knockout progeny might succumb to GIST development more rapidly than heterozygous *FAM96A* animals. Furthermore, tamoxifen-inducible transgenic mouse models such as inducible Cre mice represent a valuable tool for targeted induction of a gene knockout at specific time points during tumorigenesis for example (Feil et al., 2009; Saunders, 2011). Here, the time

point and dependency of FAM96A loss during GIST or development of other tumors such as RCC and TCC could be analyzed *in vivo*.

As a model for the induction of bladder cancer, for which a significant decrease of FAM96A expression has been identified in this study, the carcinogen N-Butyl-N-(4-hydroxybutyl)nitrosamine can be fed to the mice in drinking water (Garcia-Cao et al., 2005). Monitoring of the animals would reveal whether the *FAM96A*$^{-/-}$ mice are predisposed to develop bladder cancer or whether tumorigenesis occurs with a decreased latency as compared to wt and *FAM96A*$^{+/-}$ mice.

5. Literature

Adrain C., Slee E. A., Harte M. T. and Martin S. J., 1999. Regulation of apoptotic protease activating factor-1 oligomerization and apoptosis by the WD-40 repeat region. J Biol Chem 274, 20855-60.

Agnihotri G., Liu Y. N., Paschal B. M. and Liu H. W., 2004. Identification of an unusual [2Fe-2S]-binding motif in the CDP-6-deoxy-D-glycero-l-threo-4-hexulose-3-dehydrase from Yersinia pseudotuberculosis: implication for C-3 deoxygenation in the biosynthesis of 3,6-dideoxyhexoses. Biochemistry 43, 14265-74.

Ali M. H. and Imperiali B., 2005. Protein oligomerization: how and why. Bioorganic & medicinal chemistry 13, 5013-20.

Almeida M. S., Herrmann T., Peti W., Wilson I. A. and Wuthrich K., 2005. NMR structure of the conserved hypothetical protein TM0487 from Thermotoga maritima: implications for 216 homologous DUF59 proteins. Protein Sci 14, 2880-6.

Bai J., Brody J. R., Kadkol S. S. and Pasternack G. R., 2001. Tumor suppression and potentiation by manipulation of pp32 expression. Oncogene 20, 2153-60.

Bao Q., Lu W., Rabinowitz J. D. and Shi Y., 2007. Calcium blocks formation of apoptosome by preventing nucleotide exchange in Apaf-1. Mol Cell 25, 181-92.

Bao Q. and Shi Y., 2007. Apoptosome: a platform for the activation of initiator caspases. Cell Death Differ 14, 56-65.

Bardsley M. R., Horvath V. J., Asuzu D. T., Lorincz A., Redelman D., Hayashi Y., Popko L. N., Young D. L., Lomberk G. A., Urrutia R. A., Farrugia G., Rubin B. P. and Ordog T., 2010. Kitlow stem cells cause resistance to Kit/platelet-derived growth factor alpha inhibitors in murine gastrointestinal stromal tumors. Gastroenterology 139, 942-52.

Baudis M. and Cleary M. L., 2001. Progenetix.net: an online repository for molecular cytogenetic aberration data. Bioinformatics 17, 1228-9.

Bauer S., Duensing A., Demetri G. D. and Fletcher J. A., 2007. KIT oncogenic signaling mechanisms in imatinib-resistant gastrointestinal stromal tumor: PI3-kinase/AKT is a crucial survival pathway. Oncogene 26, 7560-8.

Bauer S., Yu L. K., Demetri G. D. and Fletcher J. A., 2006. Heat shock protein 90 inhibition in imatinib-resistant gastrointestinal stromal tumor. Cancer Res 66, 9153-61.

Benedict M. A., Hu Y., Inohara N. and Nunez G., 2000. Expression and functional analysis of Apaf-1 isoforms. Extra Wd-40 repeat is required for cytochrome c binding and regulated activation of procaspase-9. J Biol Chem 275, 8461-8.

Berger A. H., Knudson A. G. and Pandolfi P. P., 2011. A continuum model for tumour suppression. Nature 476, 163-9.

Beuvink I., Boulay A., Fumagalli S., Zilbermann F., Ruetz S., O'Reilly T., Natt F., Hall J., Lane H. A. and Thomas G., 2005. The mTOR inhibitor RAD001 sensitizes tumor cells to DNA-damaged induced apoptosis through inhibition of p21 translation. Cell 120, 747-59.

Birnboim H. C., 1983. A rapid alkaline extraction method for the isolation of plasmid DNA. Methods in enzymology 100, 243-55.

Borner C., 2003. The Bcl-2 protein family: sensors and checkpoints for life-or-death decisions. Molecular immunology 39, 615-47.

Boussif O., Lezoualc'h F., Zanta M. A., Mergny M. D., Scherman D., Demeneix B. and Behr J. P., 1995. A versatile vector for gene and oligonucleotide transfer

into cells in culture and in vivo: polyethylenimine. Proc Natl Acad Sci U S A 92, 7297-301.

Bradford M. M., 1976. A rapid and sensitive method for the quantitation of microgram quantities of protein utilizing the principle of protein-dye binding, Vol. 72, pp. 248-54.

Broker L. E., Kruyt F. A. and Giaccone G., 2005. Cell death independent of caspases: a review. Clinical cancer research : an official journal of the American Association for Cancer Research 11, 3155-62.

Buckley C. D., Pilling D., Henriquez N. V., Parsonage G., Threlfall K., Scheel-Toellner D., Simmons D. L., Akbar A. N., Lord J. M. and Salmon M., 1999. RGD peptides induce apoptosis by direct caspase-3 activation. Nature 397, 534-9.

Buning H., Perabo L., Coutelle O., Quadt-Humme S. and Hallek M., 2008. Recent developments in adeno-associated virus vector technology. The journal of gene medicine 10, 717-33.

Cain K., Brown D. G., Langlais C. and Cohen G. M., 1999. Caspase activation involves the formation of the aposome, a large (approximately 700 kDa) caspase-activating complex. J Biol Chem 274, 22686-92.

Cain K., Langlais C., Sun X. M., Brown D. G. and Cohen G. M., 2001. Physiological concentrations of K+ inhibit cytochrome c-dependent formation of the apoptosome. J Biol Chem 276, 41985-90.

Cardone M. H., Roy N., Stennicke H. R., Salvesen G. S., Franke T. F., Stanbridge E., Frisch S. and Reed J. C., 1998. Regulation of cell death protease caspase-9 by phosphorylation. Science 282, 1318-21.

Cesaro E., Montano G., Rosati A., Crescitelli R., Izzo P., Turco M. C. and Costanzo P., 2010. WT1 protein is a transcriptional activator of the antiapoptotic bag3 gene. Leukemia : official journal of the Leukemia Society of America, Leukemia Research Fund, U.K 24, 1204-6.

Chandra D., Bratton S. B., Person M. D., Tian Y., Martin A. G., Ayres M., Fearnhead H. O., Gandhi V. and Tang D. G., 2006. Intracellular nucleotides act as critical prosurvival factors by binding to cytochrome C and inhibiting apoptosome. Cell 125, 1333-46.

Chen K. E., Richards A. A., Ariffin J. K., Ross I. L., Sweet M. J., Kellie S., Kobe B. and Martin J. L., 2012. The mammalian DUF59 protein Fam96a forms two distinct types of domain-swapped dimer. Acta crystallographica. Section D, Biological crystallography 68, 637-48.

Chen L. L., Holden J. A., Choi H., Zhu J., Wu E. F., Jones K. A., Ward J. H., Andtbacka R. H., Randall R. L., Scaife C. L., Hunt K. K., Prieto V. G., Raymond A. K., Zhang W., Trent J. C., Benjamin R. S. and Frazier M. L., 2008. Evolution from heterozygous to homozygous KIT mutation in gastrointestinal stromal tumor correlates with the mechanism of mitotic nondisjunction and significant tumor progression. Modern pathology : an official journal of the United States and Canadian Academy of Pathology, Inc 21, 826-36.

Chlenski A., Ketels K. V., Engeriser J. L., Talamonti M. S., Tsao M. S., Koutnikova H., Oyasu R. and Scarpelli D. G., 1999. zo-2 gene alternative promoters in normal and neoplastic human pancreatic duct cells. International journal of cancer. Journal international du cancer 83, 349-58.

Chu Z. L., Pio F., Xie Z., Welsh K., Krajewska M., Krajewski S., Godzik A. and Reed J. C., 2001. A novel enhancer of the Apaf1 apoptosome involved in cytochrome c-dependent caspase activation and apoptosis. J Biol Chem 276, 9239-45.

Corless C. L., Barnett C. M. and Heinrich M. C., 2011. Gastrointestinal stromal tumours: origin and molecular oncology. Nat Rev Cancer 11, 865-78.

D'Amelio M., Tino E. and Cecconi F., 2008. The apoptosome: emerging insights and new potential targets for drug design. Pharmaceutical research 25, 740-51.

Datta S. R., Dudek H., Tao X., Masters S., Fu H., Gotoh Y. and Greenberg M. E., 1997. Akt phosphorylation of BAD couples survival signals to the cell-intrinsic death machinery. Cell 91, 231-41.

Degterev A. and Yuan J., 2008. Expansion and evolution of cell death programmes. Nature reviews. Molecular cell biology 9, 378-90.

Demetri G. D., 2011. Differential properties of current tyrosine kinase inhibitors in gastrointestinal stromal tumors. Seminars in oncology 38 Suppl 1, S10-9.

Dickens L. S., Powley I. R., Hughes M. A. and MacFarlane M., 2012. The 'complexities' of life and death: death receptor signalling platforms. Experimental cell research 318, 1269-77.

du Manoir S., Speicher M. R., Joos S., Schrock E., Popp S., Dohner H., Kovacs G., Robert-Nicoud M., Lichter P. and Cremer T., 1993. Detection of complete and partial chromosome gains and losses by comparative genomic in situ hybridization. Human genetics 90, 590-610.

Evans H. J. and Prosser J., 1992. Tumor-suppressor genes: cardinal factors in inherited predisposition to human cancers. Environmental health perspectives 98, 25-37.

Feil S., Valtcheva N. and Feil R., 2009. Inducible Cre mice. Methods in molecular biology 530, 343-63.

Fischer U., Janicke R. U. and Schulze-Osthoff K., 2003. Many cuts to ruin: a comprehensive update of caspase substrates. Cell Death Differ 10, 76-100.

Fischer U. and Schulze-Osthoff K., 2005. Apoptosis-based therapies and drug targets. Cell Death Differ 12 Suppl 1, 942-61.

Flack M. R., Pyle R. G., Mullen N. M., Lorenzo B., Wu Y. W., Knazek R. A., Nisula B. C. and Reidenberg M. M., 1993. Oral gossypol in the treatment of metastatic adrenal cancer. The Journal of clinical endocrinology and metabolism 76, 1019-24.

Fulda S., Wick W., Weller M. and Debatin K. M., 2002. Smac agonists sensitize for Apo2L/TRAIL- or anticancer drug-induced apoptosis and induce regression of malignant glioma in vivo. Nature medicine 8, 808-15.

Galluzzi L. and Kroemer G., 2008. Necroptosis: a specialized pathway of programmed necrosis. Cell 135, 1161-3.

Galluzzi L., Vitale I., Abrams J. M., Alnemri E. S., Baehrecke E. H., Blagosklonny M. V., Dawson T. M., Dawson V. L., El-Deiry W. S., Fulda S., Gottlieb E., Green D. R., Hengartner M. O., Kepp O., Knight R. A., Kumar S., Lipton S. A., Lu X., Madeo F., Malorni W., Mehlen P., Nunez G., Peter M. E., Piacentini M., Rubinsztein D. C., Shi Y., Simon H. U., Vandenabeele P., White E., Yuan J., Zhivotovsky B., Melino G. and Kroemer G., 2012. Molecular definitions of cell death subroutines: recommendations of the Nomenclature Committee on Cell Death 2012. Cell Death Differ 19, 107-20.

Garcia-Cao I., Duran A., Collado M., Carrascosa M. J., Martin-Caballero J., Flores J. M., Diaz-Meco M. T., Moscat J. and Serrano M., 2005. Tumour-suppression activity of the proapoptotic regulator Par4. EMBO reports 6, 577-83.

Gari K., Leon Ortiz A. M., Borel V., Flynn H., Skehel J. M. and Boulton S. J., 2012. MMS19 links cytoplasmic iron-sulfur cluster assembly to DNA metabolism. Science 337, 243-5.

George S. and Bukowski R. M., 2009. Role of everolimus in the treatment of renal cell carcinoma. Therapeutics and clinical risk management 5, 699-706.

Gerhard M. C., Zantl N., Weirich G., Schliep S., Seiffert B. and Hacker G., 2003. Functional evaluation of the apoptosome in renal cell carcinoma. Br J Cancer 89, 2147-54.

Gonzalez-Mariscal L., Bautista P., Lechuga S. and Quiros M., 2012. ZO-2, a tight junction scaffold protein involved in the regulation of cell proliferation and apoptosis. Annals of the New York Academy of Sciences 1257, 133-41.

Green D. R. and Kroemer G., 2009. Cytoplasmic functions of the tumour suppressor p53. Nature 458, 1127-30.

Gyrd-Hansen M. and Meier P., 2010. IAPs: from caspase inhibitors to modulators of NF-kappaB, inflammation and cancer. Nat Rev Cancer 10, 561-74.

Hakem R. and Mak T. W., 2001. Animal models of tumor-suppressor genes. Annual review of genetics 35, 209-41.

Han Y., San-Marina S., Liu J. and Minden M. D., 2004. Transcriptional activation of c-myc proto-oncogene by WT1 protein. Oncogene 23, 6933-41.

Hanahan D. and Weinberg R. A., 2000. The hallmarks of cancer. Cell 100, 57-70.

Hanahan D. and Weinberg R. A., 2011. Hallmarks of cancer: the next generation. Cell 144, 646-74.

Hastie N. D., 2001. Life, sex, and WT1 isoforms--three amino acids can make all the difference. Cell 106, 391-4.

Hebbar N., Wang C. and Rangnekar V. M., 2012. Mechanisms of apoptosis by the tumor suppressor Par-4. Journal of cellular physiology 227, 3715-21.

Heinrich M. C., Griffith D. J., Druker B. J., Wait C. L., Ott K. A. and Zigler A. J., 2000. Inhibition of c-kit receptor tyrosine kinase activity by STI 571, a selective tyrosine kinase inhibitor. Blood 96, 925-32.

Helling R. B., Goodman H. M. and Boyer H. W., 1974. Analysis of endonuclease R-EcoRI fragments of DNA from lambdoid bacteriophages and other viruses by agarose-gel electrophoresis. J Virol 14, 1235-44.

Hill M. M., Adrain C., Duriez P. J., Creagh E. M. and Martin S. J., 2004. Analysis of the composition, assembly kinetics and activity of native Apaf-1 apoptosomes. Embo J 23, 2134-45.

Hotchkiss R. S., Strasser A., McDunn J. E. and Swanson P. E., 2009. Cell death. N Engl J Med 361, 1570-83.

Huff V., 2011. Wilms' tumours: about tumour suppressor genes, an oncogene and a chameleon gene. Nat Rev Cancer 11, 111-21.

Ito S., Tan L. J., Andoh D., Narita T., Seki M., Hirano Y., Narita K., Kuraoka I., Hiraoka Y. and Tanaka K., 2010. MMXD, a TFIIH-independent XPD-MMS19 protein complex involved in chromosome segregation. Mol Cell 39, 632-40.

Jin M. L., Yang B. Q., Zhang W. and Ren P., 1992. High dose mitomycin C for treatment of advanced gastric cancer. Gan to kagaku ryoho. Cancer & chemotherapy 19, 1193-6.

Johnstone R. W., Tommerup N., Hansen C., Vissing H. and Shi Y., 1999. Structural organization, tissue expression, and chromosomal localization of Ciao 1, a functional modulator of the Wilms' tumor suppressor, WT1. Immunogenetics 49, 900-5.

Johnstone R. W., Wang J., Tommerup N., Vissing H., Roberts T. and Shi Y., 1998. Ciao 1 is a novel WD40 protein that interacts with the tumor suppressor protein WT1. J Biol Chem 273, 10880-7.

Jung J., 2012. Functional analysis of the truncated isoform of the pro-apoptotic protein CABY and the effect of CABY on the transcription factor WT1, Goethe University, Frankfurt am Main.

Kallioniemi O. P., Kallioniemi A., Sudar D., Rutovitz D., Gray J. W., Waldman F. and Pinkel D., 1993. Comparative genomic hybridization: a rapid new method for detecting and mapping DNA amplification in tumors. Seminars in cancer biology 4, 41-6.

Kennedy S. G., Kandel E. S., Cross T. K. and Hay N., 1999. Akt/Protein kinase B inhibits cell death by preventing the release of cytochrome c from mitochondria. Molecular and cellular biology 19, 5800-10.

Kerr J. F., Wyllie A. H. and Currie A. R., 1972. Apoptosis: a basic biological phenomenon with wide-ranging implications in tissue kinetics. Br J Cancer 26, 239-57.

Kessel D. and Reiners J. J., Jr., 2007. Initiation of apoptosis and autophagy by the Bcl-2 antagonist HA14-1. Cancer letters 249, 294-9.

Kim H. E., Jiang X., Du F. and Wang X., 2008. PHAPI, CAS, and Hsp70 promote apoptosome formation by preventing Apaf-1 aggregation and enhancing nucleotide exchange on Apaf-1. Mol Cell 30, 239-47.

Kirkin V., Joos S. and Zornig M., 2004. The role of Bcl-2 family members in tumorigenesis. Biochim Biophys Acta 1644, 229-49.

Kondo S., Shinomura Y., Miyazaki Y., Kiyohara T., Tsutsui S., Kitamura S., Nagasawa Y., Nakahara M., Kanayama S. and Matsuzawa Y., 2000. Mutations of the bak gene in human gastric and colorectal cancers. Cancer Res 60, 4328-30.

Korsmeyer S. J., Wei M. C., Saito M., Weiler S., Oh K. J. and Schlesinger P. H., 2000. Pro-apoptotic cascade activates BID, which oligomerizes BAK or BAX into pores that result in the release of cytochrome c. Cell Death Differ 7, 1166-73.

Lai D., Visser-Grieve S. and Yang X., 2012. Tumour suppressor genes in chemotherapeutic drug response. Bioscience reports 32, 361-74.

Lane D. P., Cheok C. F. and Lain S., 2010. p53-based cancer therapy. Cold Spring Harbor perspectives in biology 2, a001222.

Lauber K., Appel H. A., Schlosser S. F., Gregor M., Schulze-Osthoff K. and Wesselborg S., 2001. The adapter protein apoptotic protease-activating factor-1 (Apaf-1) is proteolytically processed during apoptosis. J Biol Chem 276, 29772-81.

Lavrik I., Golks A. and Krammer P. H., 2005. Death receptor signaling. Journal of cell science 118, 265-7.

Lee S. B., Huang K., Palmer R., Truong V. B., Herzlinger D., Kolquist K. A., Wong J., Paulding C., Yoon S. K., Gerald W., Oliner J. D. and Haber D. A., 1999. The Wilms tumor suppressor WT1 encodes a transcriptional activator of amphiregulin. Cell 98, 663-73.

Lezhneva L., Amann K. and Meurer J., 2004. The universally conserved HCF101 protein is involved in assembly of [4Fe-4S]-cluster-containing complexes in Arabidopsis thaliana chloroplasts. The Plant journal : for cell and molecular biology 37, 174-85.

Li C., Bowles D. E., van Dyke T. and Samulski R. J., 2005. Adeno-associated virus vectors: potential applications for cancer gene therapy. Cancer gene therapy 12, 913-25.

Li D. and Roberts R., 2001. WD-repeat proteins: structure characteristics, biological function, and their involvement in human diseases. Cellular and molecular life sciences : CMLS 58, 2085-97.

Li L. Y., Luo X. and Wang X., 2001. Endonuclease G is an apoptotic DNase when released from mitochondria. Nature 412, 95-9.

Li P., Nijhawan D., Budihardjo I., Srinivasula S. M., Ahmad M., Alnemri E. S. and Wang X., 1997. Cytochrome c and dATP-dependent formation of Apaf-1/caspase-9 complex initiates an apoptotic protease cascade. Cell 91, 479-89.

Liegl B., Kepten I., Le C., Zhu M., Demetri G. D., Heinrich M. C., Fletcher C. D., Corless C. L. and Fletcher J. A., 2008. Heterogeneity of kinase inhibitor resistance mechanisms in GIST. J Pathol 216, 64-74.

Lim K. S., Won Y. W., Park Y. S. and Kim Y. H., 2010. Preparation and functional analysis of recombinant protein transduction domain-metallothionein fusion proteins. Biochimie 92, 964-70.

Lock R., Carol H., Houghton P. J., Morton C. L., Kolb E. A., Gorlick R., Reynolds C. P., Maris J. M., Keir S. T., Wu J. and Smith M. A., 2008. Initial testing (stage 1) of the BH3 mimetic ABT-263 by the pediatric preclinical testing program. Pediatric blood & cancer 50, 1181-9.

Los M., Wesselborg S. and Schulze-Osthoff K., 1999. The role of caspases in development, immunity, and apoptotic signal transduction: lessons from knockout mice. Immunity 10, 629-39.

Lowe S. W. and Lin A. W., 2000. Apoptosis in cancer. Carcinogenesis 21, 485-95.

Luo D., Bernard D. G., Balk J., Hai H. and Cui X., 2012. The DUF59 family gene AE7 acts in the cytosolic iron-sulfur cluster assembly pathway to maintain nuclear genome integrity in Arabidopsis. The Plant cell 24, 4135-48.

Malik K. T., Poirier V., Ivins S. M. and Brown K. W., 1994. Autoregulation of the human WT1 gene promoter. FEBS Lett 349, 75-8.

Malladi S., Challa-Malladi M., Fearnhead H. O. and Bratton S. B., 2009. The Apaf-1*procaspase-9 apoptosome complex functions as a proteolytic-based molecular timer. Embo J 28, 1916-25.

Matei D., Satpathy M., Cao L., Lai Y. C., Nakshatri H. and Donner D. B., 2007. The platelet-derived growth factor receptor alpha is destabilized by geldanamycins in cancer cells. J Biol Chem 282, 445-53.

Miyashita T., Harigai M., Hanada M. and Reed J. C., 1994. Identification of a p53-dependent negative response element in the bcl-2 gene. Cancer Res 54, 3131-5.

Mohr A., Henderson G., Dudus L., Herr I., Kuerschner T., Debatin K. M., Weiher H., Fisher K. J. and Zwacka R. M., 2004. AAV-encoded expression of TRAIL in experimental human colorectal cancer leads to tumor regression. Gene therapy 11, 534-43.

Moore A. W., McInnes L., Kreidberg J., Hastie N. D. and Schedl A., 1999. YAC complementation shows a requirement for Wt1 in the development of epicardium, adrenal gland and throughout nephrogenesis. Development 126, 1845-57.

Morrison D. J., English M. A. and Licht J. D., 2005. WT1 induces apoptosis through transcriptional regulation of the proapoptotic Bcl-2 family member Bak. Cancer Res 65, 8174-82.

Mortenson L. E., Valentine R. C. and Carnahan J. E., 1962. An electron transport factor from Clostridium pasteurianum. Biochemical and biophysical research communications 7, 448-52.

Nakano K. and Vousden K. H., 2001. PUMA, a novel proapoptotic gene, is induced by p53. Mol Cell 7, 683-94.

Nicoletti I., Migliorati G., Pagliacci M. C., Grignani F. and Riccardi C., 1991. A rapid and simple method for measuring thymocyte apoptosis by propidium iodide staining and flow cytometry. Journal of immunological methods 139, 271-9.

Niksic M., Slight J., Sanford J. R., Caceres J. F. and Hastie N. D., 2004. The Wilms' tumour protein (WT1) shuttles between nucleus and cytoplasm and is present in functional polysomes. Human molecular genetics 13, 463-71.

O'Brien S. M., Claxton D. F., Crump M., Faderl S., Kipps T., Keating M. J., Viallet J. and Cheson B. D., 2009. Phase I study of obatoclax mesylate (GX15-070), a small molecule pan-Bcl-2 family antagonist, in patients with advanced chronic lymphocytic leukemia. Blood 113, 299-305.

Ocker M. and Hopfner M., 2012. Apoptosis-modulating drugs for improved cancer therapy. European surgical research. Europaische chirurgische Forschung. Recherches chirurgicales europeennes 48, 111-20.

Oda E., Ohki R., Murasawa H., Nemoto J., Shibue T., Yamashita T., Tokino T., Taniguchi T. and Tanaka N., 2000. Noxa, a BH3-only member of the Bcl-2 family and candidate mediator of p53-induced apoptosis. Science 288, 1053-8.

Ogawa T., Shiga K., Hashimoto S., Kobayashi T., Horii A. and Furukawa T., 2003. APAF-1-ALT, a novel alternative splicing form of APAF-1, potentially causes impeded ability of undergoing DNA damage-induced apoptosis in the LNCaP human prostate cancer cell line. Biochemical and biophysical research communications 306, 537-43.

Okada H., Suh W. K., Jin J., Woo M., Du C., Elia A., Duncan G. S., Wakeham A., Itie A., Lowe S. W., Wang X. and Mak T. W., 2002. Generation and

characterization of Smac/DIABLO-deficient mice. Molecular and cellular biology 22, 3509-17.

Olsson M. and Zhivotovsky B., 2011. Caspases and cancer. Cell Death Differ 18, 1441-9.

Oltersdorf T., Elmore S. W., Shoemaker A. R., Armstrong R. C., Augeri D. J., Belli B. A., Bruncko M., Deckwerth T. L., Dinges J., Hajduk P. J., Joseph M. K., Kitada S., Korsmeyer S. J., Kunzer A. R., Letai A., Li C., Mitten M. J., Nettesheim D. G., Ng S., Nimmer P. M., O'Connor J. M., Oleksijew A., Petros A. M., Reed J. C., Shen W., Tahir S. K., Thompson C. B., Tomaselli K. J., Wang B., Wendt M. D., Zhang H., Fesik S. W. and Rosenberg S. H., 2005. An inhibitor of Bcl-2 family proteins induces regression of solid tumours. Nature 435, 677-81.

Philpott N. J., Turner A. J., Scopes J., Westby M., Marsh J. C., Gordon-Smith E. C., Dalgleish A. G. and Gibson F. M., 1996. The use of 7-amino actinomycin D in identifying apoptosis: simplicity of use and broad spectrum of application compared with other techniques. Blood 87, 2244-51.

Pick R., 2006. Molekulare und funktionelle Analyse des neu identifizierten APAF-1-bindenden Proteins CABY.

Piddubnyak V., Rigou P., Michel L., Rain J. C., Geneste O., Wolkenstein P., Vidaud D., Hickman J. A., Mauviel A. and Poyet J. L., 2007. Positive regulation of apoptosis by HCA66, a new Apaf-1 interacting protein, and its putative role in the physiopathology of NF1 microdeletion syndrome patients. Cell Death Differ 14, 1222-33.

Porta C., Zimatore M., Imarisio I., Natalizi A., Sartore-Bianchi A., Danova M. and Riccardi A., 2004. Gemcitabine and oxaliplatin in the treatment of patients with immunotherapy-resistant advanced renal cell carcinoma: final results of a single-institution Phase II study. Cancer 100, 2132-8.

Portt L., Norman G., Clapp C., Greenwood M. and Greenwood M. T., 2011. Anti-apoptosis and cell survival: a review. Biochim Biophys Acta 1813, 238-59.

Powles T., McFaul S., Stebbing J., Wilson P., Oliver T., Tranter N. and Shamash J., 2008. The efficacy and safety of irinotecan cisplatin and mitomycin chemotherapy in sunitinib pre-treated metastatic clear cell renal cancer. OncoTargets and therapy 1, 35-9.

Proskuryakov S. Y., Konoplyannikov A. G. and Gabai V. L., 2003. Necrosis: a specific form of programmed cell death? Experimental cell research 283, 1-16.

Qi X., Wang L. and Du F., 2010. Novel small molecules relieve prothymosin alpha-mediated inhibition of apoptosome formation by blocking its interaction with Apaf-1. Biochemistry 49, 1923-30.

Qin H., Srinivasula S. M., Wu G., Fernandes-Alnemri T., Alnemri E. S. and Shi Y., 1999. Structural basis of procaspase-9 recruitment by the apoptotic protease-activating factor 1. Nature 399, 549-57.

Qin J., Xie L. P., Zheng X. Y., Wang Y. B., Bai Y., Shen H. F., Li L. C. and Dahiya R., 2007. A component of green tea, (-)-epigallocatechin-3-gallate, promotes apoptosis in T24 human bladder cancer cells via modulation of the PI3K/Akt pathway and Bcl-2 family proteins. Biochemical and biophysical research communications 354, 852-7.

Qiu S. G., Krishnan S., el-Guendy N. and Rangnekar V. M., 1999. Negative regulation of Par-4 by oncogenic Ras is essential for cellular transformation. Oncogene 18, 7115-23.

Rampino N., Yamamoto H., Ionov Y., Li Y., Sawai H., Reed J. C. and Perucho M., 1997. Somatic frameshift mutations in the BAX gene in colon cancers of the microsatellite mutator phenotype. Science 275, 967-9.

Ranger A. M., Malynn B. A. and Korsmeyer S. J., 2001. Mouse models of cell death. Nat Genet 28, 113-8.

Reubold T. F., Wohlgemuth S. and Eschenburg S., 2009. A new model for the transition of APAF-1 from inactive monomer to caspase-activating apoptosome. J Biol Chem 284, 32717-24.

Reubold T. F., Wohlgemuth S. and Eschenburg S., 2011. Crystal structure of full-length Apaf-1: how the death signal is relayed in the mitochondrial pathway of apoptosis. Structure 19, 1074-83.

Reynoso D., Nolden L. K., Yang D., Dumont S. N., Conley A. P., Dumont A. G., Zhou K., Duensing A. and Trent J. C., 2011. Synergistic induction of apoptosis by the Bcl-2 inhibitor ABT-737 and imatinib mesylate in gastrointestinal stromal tumor cells. Molecular oncology 5, 93-104.

Riccardi C. and Nicoletti I., 2006. Analysis of apoptosis by propidium iodide staining and flow cytometry. Nature protocols 1, 1458-61.

Riedl S. J., Li W., Chao Y., Schwarzenbacher R. and Shi Y., 2005. Structure of the apoptotic protease-activating factor 1 bound to ADP. Nature 434, 926-33.

Riedl S. J. and Shi Y., 2004. Molecular mechanisms of caspase regulation during apoptosis. Nature reviews. Molecular cell biology 5, 897-907.

Rouault T. A., 2012. Biogenesis of iron-sulfur clusters in mammalian cells: new insights and relevance to human disease. Disease models & mechanisms 5, 155-64.

Rozen S. and Skaletsky H., 2000. Primer3 on the WWW for general users and for biologist programmers. Methods in molecular biology 132, 365-86.

Rual J. F., Venkatesan K., Hao T., Hirozane-Kishikawa T., Dricot A., Li N., Berriz G. F., Gibbons F. D., Dreze M., Ayivi-Guedehoussou N., Klitgord N., Simon C., Boxem M., Milstein S., Rosenberg J., Goldberg D. S., Zhang L. V., Wong S. L., Franklin G., Li S., Albala J. S., Lim J., Fraughton C., Llamosas E., Cevik S., Bex C., Lamesch P., Sikorski R. S., Vandenhaute J., Zoghbi H. Y., Smolyar A., Bosak S., Sequerra R., Doucette-Stamm L., Cusick M. E., Hill D. E., Roth F. P. and Vidal M., 2005. Towards a proteome-scale map of the human protein-protein interaction network. Nature 437, 1173-8.

Rubin B. P., Antonescu C. R., Scott-Browne J. P., Comstock M. L., Gu Y., Tanas M. R., Ware C. B. and Woodell J., 2005. A knock-in mouse model of gastrointestinal stromal tumor harboring kit K641E. Cancer Res 65, 6631-9.

Rupprecht H. D., Drummond I. A., Madden S. L., Rauscher F. J., 3rd and Sukhatme V. P., 1994. The Wilms' tumor suppressor gene WT1 is negatively autoregulated. J Biol Chem 269, 6198-206.

Sakai T., Liu L., Teng X., Mukai-Sakai R., Shimada H., Kaji R., Mitani T., Matsumoto M., Toida K., Ishimura K., Shishido Y., Mak T. W. and Fukui K., 2004. Nucling recruits Apaf-1/pro-caspase-9 complex for the induction of stress-induced apoptosis. J Biol Chem 279, 41131-40.

Salvesen G. S. and Dixit V. M., 1999. Caspase activation: the induced-proximity model. Proc Natl Acad Sci U S A 96, 10964-7.

Sanchez-Olea R., Ortiz S., Barreto O., Yang Q., Xu C. J., Zhu H. and Yuan J., 2008. Parcs is a dual regulator of cell proliferation and apaf-1 function. J Biol Chem 283, 24400-5.

Sanders K. M., 1996. A case for interstitial cells of Cajal as pacemakers and mediators of neurotransmission in the gastrointestinal tract. Gastroenterology 111, 492-515.

Sanders K. M., Ordog T., Koh S. D., Torihashi S. and Ward S. M., 1999. Development and plasticity of interstitial cells of Cajal. Neurogastroenterology and motility : the official journal of the European Gastrointestinal Motility Society 11, 311-38.

Saunders T. L., 2011. Inducible transgenic mouse models. Methods in molecular biology 693, 103-15.

Scaffidi C., Fulda S., Srinivasan A., Friesen C., Li F., Tomaselli K. J., Debatin K. M., Krammer P. H. and Peter M. E., 1998. Two CD95 (APO-1/Fas) signaling pathways. Embo J 17, 1675-87.

Schafer Z. T. and Kornbluth S., 2006. The apoptosome: physiological, developmental, and pathological modes of regulation. Dev Cell 10, 549-61.

Schwenkert S., Netz D. J., Frazzon J., Pierik A. J., Bill E., Gross J., Lill R. and Meurer J., 2010. Chloroplast HCF101 is a scaffold protein for [4Fe-4S] cluster assembly. Biochem J 425, 207-14.

Shi Y., 2002. Mechanisms of caspase activation and inhibition during apoptosis. Mol Cell 9, 459-70.

Shi Y., 2004. Caspase activation: revisiting the induced proximity model. Cell 117, 855-8.

Sieker L. C., Adman E. and Jensen L. H., 1972. Structure of the Fe-S complex in a bacterial ferredoxin. Nature 235, 40-2.

Skarnes W. C., Rosen B., West A. P., Koutsourakis M., Bushell W., Iyer V., Mujica A. O., Thomas M., Harrow J., Cox T., Jackson D., Severin J., Biggs P., Fu J., Nefedov M., de Jong P. J., Stewart A. F. and Bradley A., 2011. A conditional knockout resource for the genome-wide study of mouse gene function. Nature 474, 337-42.

Skulachev V. P., 1998. Cytochrome c in the apoptotic and antioxidant cascades. FEBS Lett 423, 275-80.

Soengas M. S., Capodieci P., Polsky D., Mora J., Esteller M., Opitz-Araya X., McCombie R., Herman J. G., Gerald W. L., Lazebnik Y. A., Cordon-Cardo C. and Lowe S. W., 2001. Inactivation of the apoptosis effector Apaf-1 in malignant melanoma. Nature 409, 207-11.

Song F., Zhuang Z., Finci L., Dunaway-Mariano D., Kniewel R., Buglino J. A., Solorzano V., Wu J. and Lima C. D., 2006. Structure, function, and mechanism of the phenylacetate pathway hot dog-fold thioesterase PaaI. J Biol Chem 281, 11028-38.

Srinivasan V., Netz D. J., Webert H., Mascarenhas J., Pierik A. J., Michel H. and Lill R., 2007. Structure of the yeast WD40 domain protein Cia1, a component acting late in iron-sulfur protein biogenesis. Structure 15, 1246-57.

Stehling O., Vashisht A. A., Mascarenhas J., Jonsson Z. O., Sharma T., Netz D. J., Pierik A. J., Wohlschlegel J. A. and Lill R., 2012. MMS19 assembles iron-sulfur proteins required for DNA metabolism and genomic integrity. Science 337, 195-9.

Stein A. and Arnold D., 2012. Oxaliplatin: a review of approved uses. Expert opinion on pharmacotherapy 13, 125-37.

Stein A., Glockzin G., Wienke A., Arnold D., Edelmann T., Hildebrandt B., Hollerbach S., Illerhaus G., Konigsrainer A., Richter M., Schlitt H. J. and Schmoll H. J., 2012. Treatment with bevacizumab and FOLFOXIRI in patients with advanced colorectal cancer: presentation of two novel trials (CHARTA and PERIMAX) and review of the literature. BMC cancer 12, 356.

Sumimoto H. and Kawakami Y., 2007. Lentiviral vector-mediated RNAi and its use for cancer research. Future oncology 3, 655-64.

ten Have S., Boulon S., Ahmad Y. and Lamond A. I., 2011. Mass spectrometry-based immuno-precipitation proteomics - the user's guide. Proteomics 11, 1153-9.

Testa G., Schaft J., van der Hoeven F., Glaser S., Anastassiadis K., Zhang Y., Hermann T., Stremmel W. and Stewart A. F., 2004. A reliable lacZ expression reporter cassette for multipurpose, knockout-first alleles. Genesis 38, 151-8.

Thornborrow E. C., Patel S., Mastropietro A. E., Schwartzfarb E. M. and Manfredi J. J., 2002. A conserved intronic response element mediates direct p53-dependent transcriptional activation of both the human and murine bax genes. Oncogene 21, 990-9.

Tong W. H., Jameson G. N., Huynh B. H. and Rouault T. A., 2003. Subcellular compartmentalization of human Nfu, an iron-sulfur cluster scaffold protein,

and its ability to assemble a [4Fe-4S] cluster. Proc Natl Acad Sci U S A 100, 9762-7.

Tong W. H. and Rouault T. A., 2006. Functions of mitochondrial ISCU and cytosolic ISCU in mammalian iron-sulfur cluster biogenesis and iron homeostasis. Cell metabolism 3, 199-210.

Tran J., Rak J., Sheehan C., Saibil S. D., LaCasse E., Korneluk R. G. and Kerbel R. S., 1999. Marked induction of the IAP family antiapoptotic proteins survivin and XIAP by VEGF in vascular endothelial cells. Biochemical and biophysical research communications 264, 781-8.

Twiddy D., Cohen G. M., Macfarlane M. and Cain K., 2006. Caspase-7 is directly activated by the approximately 700-kDa apoptosome complex and is released as a stable XIAP-caspase-7 approximately 200-kDa complex. J Biol Chem 281, 3876-88.

van Wietmarschen N., Moradian A., Morin G. B., Lansdorp P. M. and Uringa E. J., 2012. The mammalian proteins MMS19, MIP18, and ANT2 are involved in cytoplasmic iron-sulfur cluster protein assembly. J Biol Chem.

Vogelstein B. and Kinzler K. W., 2004. Cancer genes and the pathways they control. Nature medicine 10, 789-99.

Vogt K., 1842. Untersuchungen über die Entwicklungsgeschichte der Geburtshelferkrœte (Alytes obstetricans).

Wachtershauser G., 1988. Before enzymes and templates: theory of surface metabolism. Microbiological reviews 52, 452-84.

Wajant H., 2003. Death receptors. Essays in biochemistry 39, 53-71.

Weber K., Bartsch U., Stocking C. and Fehse B., 2008. A multicolor panel of novel lentiviral "gene ontology" (LeGO) vectors for functional gene analysis. Molecular therapy : the journal of the American Society of Gene Therapy 16, 698-706.

Weerapana E., Wang C., Simon G. M., Richter F., Khare S., Dillon M. B., Bachovchin D. A., Mowen K., Baker D. and Cravatt B. F., 2010. Quantitative reactivity profiling predicts functional cysteines in proteomes. Nature 468, 790-5.

Wei M. C., Lindsten T., Mootha V. K., Weiler S., Gross A., Ashiya M., Thompson C. B. and Korsmeyer S. J., 2000. tBID, a membrane-targeted death ligand, oligomerizes BAK to release cytochrome c. Genes & development 14, 2060-71.

Yang L., Han Y., Suarez Saiz F. and Minden M. D., 2007. A tumor suppressor and oncogene: the WT1 story. Leukemia : official journal of the Leukemia Society of America, Leukemia Research Fund, U.K 21, 868-76.

Yang W., Itoh F., Ohya H., Kishimoto F., Tanaka A., Nakano N., Itoh S. and Kato M., 2011. Interference of E2-2-mediated effect in endothelial cells by FAM96B through its limited expression of E2-2. Cancer science 102, 1808-14.

Yu J., Wang Z., Kinzler K. W., Vogelstein B. and Zhang L., 2003. PUMA mediates the apoptotic response to p53 in colorectal cancer cells. Proc Natl Acad Sci U S A 100, 1931-6.

Yu X., Acehan D., Menetret J. F., Booth C. R., Ludtke S. J., Riedl S. J., Shi Y., Wang X. and Akey C. W., 2005. A structure of the human apoptosome at 12.8 A resolution provides insights into this cell death platform. Structure (Camb) 13, 1725-35.

Yuan S., Yu X., Asara J. M., Heuser J. E., Ludtke S. J. and Akey C. W., 2011. The holo-apoptosome: activation of procaspase-9 and interactions with caspase-3. Structure 19, 1084-96.

Yuan S., Yu X., Topf M., Ludtke S. J., Wang X. and Akey C. W., 2010. Structure of an apoptosome-procaspase-9 CARD complex. Structure 18, 571-83.

Zentilin L. and Giacca M., 2008. Adeno-associated virus vectors: versatile tools for in vivo gene transfer. Contributions to nephrology 159, 63-77.

Zhang G., Gurtu V., Kain S. R. and Yan G., 1997. Early detection of apoptosis using a fluorescent conjugate of annexin V. Biotechniques 23, 525-31.

Zhang H. Z., Kasibhatla S., Wang Y., Herich J., Guastella J., Tseng B., Drewe J. and Cai S. X., 2004. Discovery, characterization and SAR of gambogic acid as a potent apoptosis inducer by a HTS assay. Bioorganic & medicinal chemistry 12, 309-17.

Zornig M., Hueber A., Baum W. and Evan G., 2001. Apoptosis regulators and their role in tumorigenesis. Biochim Biophys Acta 1551, F1-37.

Zou H., Henzel W. J., Liu X., Lutschg A. and Wang X., 1997. Apaf-1, a human protein homologous to C. elegans CED-4, participates in cytochrome c-dependent activation of caspase-3. Cell 90, 405-13.

6. Appendix

6.1 Abbreviations

7-AAD	7-Aminoactinomycin D
17-AAG	17-*N*-Allylamino-17-demethoxygeldanamycin
°C	degree Celsius
aa	amino acids
AGM	aorta-gonad-mesonephros region
Akt	v-akt murine thymoma viral oncogene homolog 1
APAF-1	Apoptotic protease activating factor-1
APS	ammoniumperoxodisulphate
ATCC	American type culture collection
ATP	adenosine-5´triphosphate
Bak	Bcl2-antagonist/killer 1
Bax	Bcl2-associated X protein
BCL-2	B-cell CLL/lymphoma associated 2
BCL_{xL}	Bcl2-like 1
bp	base pairs
BSA	bovine serum albumine
C. elegans	*Caenorhabditis elegans*
CARD	Caspase activation and recruitment domain
Caspase	*asp*artate-specific *c*ystein *p*rote*ase*s
Casp-	Caspase
Ciao1	cytosolic iron sulphur cluster assembly protein 1
CD	cluster of differentiation
Cdk	Cyclin-dependent kinase
cDNA	complementary DNA
CED-4	Cell death abnormality-4
ChIP	chromatin immunoprecipitation
Chk	checkpoint kinase
CIP	calf alkaline phosphatase
dATP	2´-deoxy adenosine-5triphosphate
DD	death domain
DED	death effector domain
DIABLO	direct IAP-binding protein with a low pI
DISC	death-inducing signaling complex
DMEM	Dulbecco´s modified Eagle´s medium
DMSO	dimethyl sulphoxide
DNA	deoxyribonucleic acid
DPBS	Dulbecco´s phosphate buffered saline
DR	Death receptor
DTT	dithiothreitol
E. coli	*Escherichia coli*
ECL	enhanced chemiluminescence
EDTA	ethylenediaminetetraacetic acid
e.g.	exempli gratia
EGF	epidermal growth factor
EMSA	electrophoretic mobility shift assay

EtOH	ethanol
Etc	et cetera
EtBr	ethidium bromide
FACS	fluorescence-activated cell sorting
FADD	Fas associated protein with a death domain
FBP	FUSE binding protein
FBS	fetal bovine serum
FL	fluorescence
FSC	forward scatter
g	gravity
GTE	glucose-Tris-EDTA
GI	gastrointestinal
GIST	Gastrointestinal stromal tumor
h	hour(s)
HEPES	2-(4-(2-Hydroxyethyl)-1-piperazinyl)-ethanolsulfonsäure
HPRT	Hypoxanthine phosphoribosyltransferase 1
HRP	horseradish peroxidase
HSP	heat shock protein
HTRA2	high temperature requirement protein A2
IAP	Inhibitor of apoptosis
ICC	Interstitial cells of Cajal
Ig	immunoglobuline
IHC	immunohistochemistry
IP	immunoprecipitation
ISCU	iron sulfur cluster scaffold homolog
kb	kilobase
kDa	kilo-Dalton
l	liter
LB	Luria-Bertani medium
LOH	Loss of heterozygosity
µg	microgramm
µl	microliter
µM	micromolar
µm	micrometer
M	molar
MAP kinase	mitogen-activated protein kinase
MCS	multiple cloning site
MEFs	Mouse embryonic fibroblasts
min	minute(s)
mJ	millijoule
ml	milliliter
mM	millimolar
mRNA	messenger ribonucleic acid
mTor	mechanistic target of rapamycin
myc	v-myc myelocytomatosis viral oncogene homolog (avian)
NaOAc	sodium acetate
nm	nanometer
NF1	neurofibromin 1
NOD	Nucleotide binding and oligomerization domain
Noxa	phorbol-12-myristate-13-acetate-induced protein 1
OD	optical density
P/S	penicillin/ streptomycin
PAGE	polyacrylamide gel electrophoresis
PBS	phosphate buffered saline
PCD	programmed cell death
PCR	polymerase chain reaction

PDGF	platelet-derived growth factor
PDGFR	platelet-derived growth factor receptor
PEI	polyethyleneimine
PI	propidium iodide
PI3K	phosphoinositide-3-kinase
pH	pondus Hydrogenii
PMSF	phenyl-methyl-sulfonylfluoride
qPCR	quantitative real time PCR
Rb	Retinoblastoma protein
RGD	Arginine-Glycine-Aspartic acid
RNA	ribonucleic acid
RCC	renal cell carcinoma
RNase	ribonuclease
rpm	revolutions per minute
RPMI	Roswell Park Memorial Institute medium
RT-PCR	reverse transcriptase-PCR
RTK	receptor tyrosine kinase
SC	stem cell
SD	standard deviation
SDS	sodium dodecyl sulphate
sec	second(s)
SEM	standard error of the mean
shRNA	short hairpin RNA
SMAC	second mitochondria-derived activator of caspases
SSC	side scatter
ssDNA	single-stranded DNA
SDH	succinate dehydrogenase
TAE	Tris-acetate-EDTA buffer
TBE	Tris-borate-EDTA buffer
tBid	truncated Bid
TCC	transitional cell carcinoma
TE	Tris-EDTA buffer
TEMED	N, N, N´, N, -tetramethylethylendiamine
TNF-α	Tumor necrosis factor alpha
TRAIL	TNF-related apoptosis-inducing ligand
TRAILR	TNF-related apoptosis-inducing ligand receptor
Tris	tris(hydroxymethyl)aminomethane
TSG	tumor suppressor gene
UV	ultraviolet
V	volt
WHD	winged helix domain
X-Gal	bromo-chloro-indoyl-galactopyranosidase
XPD	xeroderma pigmentosum group D
YTH	yeast two hybrid

6.2 Danksagung

Diese Arbeit wurde am Georg-Speyer-Haus in Frankfurt am Main unter Betreuung von Herrn Prof. Dr. Martin Zörnig angefertigt. Bei ihm möchte ich mich hiermit herzlich für die Bereitstellung des interessanten Projektes, die freundschaftliche Zusammenarbeit und die stetige Möglichkeit eigene Ideen zu verwirklichen bedanken.

Bei Frau Prof. Dr. Beatrix Süß und Herrn Prof. Dr. Bodo Laube bedanke ich mich recht herzlich für die Betreuung dieser Arbeit seitens des Fachbereichs Biologie der TU Darmstadt.

Ein weiterer Dank gilt meinen Kooperationspartnern Dr. Abbas Agaimy, Prof. Dr. Volker Dötsch, Prof. Dr. Matthias Hammerschmidt, Prof. Dr. Ralf Rieker, Prof. Dr. Tamas Ordog, Prof. Dr. Kurt Zatloukal und zu guter Letzt Jan Heering für die konstruktive fachliche Zusammenarbeit im Rahmen dieses Projektes.

Ich danke den Verantwortlichen und Organisatoren des Graduiertenkollegs 1172 für die fachliche Weiterbildung und den Einblick in die beruflichen Optionen nach der Promotion.

Meinen aktuellen und ehemaligen Kollegen: Uta, Moritz, Katha, Susanne, Inga, Venkatesh, Marek, Frederic, Sabrina, Steffi W.,G. und H., Katharina, Rasa, Patrik, Giel, Dagmar, Bernd, Julia, Nanni und Jenny danke ich für die schöne Zeit im Labor, das außerordentlich gute Arbeitsklima, ihre Unterstützung und Hilfe. Bleibt so wie ihr seid, simply nonexpendable! Jenny danke ich für ihre motivierte Mithilfe am FAM96A-Projekt im Rahmen ihrer Diplomarbeit.

Bei allen Mitarbeitern des Georg-Speyer-Hauses möchte ich mich für die angenehme Arbeitsatmosphäre und die interessante und lehrreiche Zeit bedanken.

Last but not least möchte ich mich ganz herzlich bei meiner Familie und meinen Freunden, allen voran meinen Eltern und meinem Bruder, für ihre liebevolle Unterstützung bedanken.

6.3 Curriculum Vitae

Name	Bettina Schwamb
Date/Place of birth	08/03/1983 Worms, Germany
E-Mail	bettina.schwamb@web.de
Address	Georg-Speyer-Haus, Paul Ehrlich-Str. 42-44, 60596 Frankfurt am Main
01/04/2009-today	PhD student Research Group of Prof. M. Zörnig, Georg-Speyer-Haus, Frankfurt am Main, Germany; *"*Functional analysis of the APAF-1 binding protein FAM96A"
08/2009-03/2012	Associate member of GK1172 Goethe University, Frankfurt am Main, Germany; Participation in the interdisciplinary program *"*Biologicals*"*
03/2010-03/2012	Speaker of FIRST (Frankfurt International Research Graduate School for Translational Medicine)
05/2008- 03/2009	Junior scientist University Hospital Hamburg-Eppendorf, Department of Medical Microbiology, Hamburg, Germany; *"*Interaction studies on Cdc42-GAP *"*
05/2007-02/2008	Diploma degree student Department of Medical Microbiology, University of Mainz, Germany; „Investigations on cytokine responses of *C. parvum*-infected immunocompromised mice"
10/2002-02/2008	Diploma studies in Biology
10/2002-09/2004	Basic study period; intermediate diploma degree (University of Mainz , Germany)

09/2004-07/2005	Academic year (3rd year student); Microbiology, Parasitology, Virology course (University of Glasgow, Scotland)
07/2005-02/2008	Advanced study period (University of Mainz, Germany)
04/2007	Diploma examinations: Immunology, Microbiology, Zoology
02/2006-04/2006	Working student at Sanofi Aventis Department of Metabolism, Frankfurt Hoechst, Germany
11/2005 and 11/2006-12/2006	Research assistant Department of Microbiology (Group of Prof. G. Unden);
02/2008-05/2008	Medical Microbiology, University of Mainz, Germany (Group of Prof. F. Petry)
1993-2002	Secondary school, general qualification for university entrance, Gymnasium zu St. Katharinen Oppenheim, Germany
Mother tongue	German (native)
Other languages	English (fluent), French (good)

Grants

09/2004-06/2005	ERASMUS scholarship, University of Mainz, Germany
01/07/07-31/12/07	Diploma student scholarship, University of Mainz, Germany
05/2008-03/2009	PhD student grant, Research Training Group 1459: "Sorting and interactions between proteins of subcellular compartments"
Vocational training	ÄKTA FPLC training course (GE Healthcare, Munich) Mouse experimental training (UKE, Hamburg)

Publications:

"Dynamics of gut mucosal and systemic Th1/Th2 cytokine responses in interferon-gamma and interleukin-12p40 knock out mice during primary and challenge *Cryptosporidium parvum* infection"; Tessema TS, **Schwamb B**, Lochner M, Förster I, Jakobi V, Petry F; Immunobiology 2009

"Complexome profiling identifies TMEM126B as a component of the mitochondrial complex I assembly (MCIA) complex"; Heide H, Bleier L, Steger M, Ackermann J, Dröse S, **Schwamb B**, Zörnig M, Reichert AS, Koch I, Wittig I, Brandt U; Cell Metabolism 2012

"A functional yeast survival screen of tumor- derived cDNA libraries to identify novel anti-apoptotic mammalian oncoproteins"; Eißmann M, **Schwamb B**, Moser J, Köhl U, Rieker R, Agaimy A, Herpel E, Gutschner T, Kögel D, Riberio V, Böhm S, Diederichs S and Zörnig M; 2013 (*in revision*)

"FAM96A is a Novel Pro-Apoptotic Tumor Suppressor in Gastrointestinal Stromal Tumors", **Schwamb B**, Pick R, Mateus Fernández S, Völp K, Heering J, Dötsch V, Hammerschmidt M, Nowak M, Bösser S, Dälken B, Jung J, Penzel R, Beinoraviciute-Kellner R, Zörnig I, Rabenhorst U, Zatloukal K, Truss M, Joos S, Rieker R, Agaimy A, Söder S, Herpel E, Bardsley M, Hayashi Y, Asuzu D, Syed S, Ordog T and Zörnig M; 2013 (*in preparation*)

Talks and Poster presentations

"Influence of IL-18 on the systemic and local immune response to *C. parvum* infection in IFN$\gamma^{-/-}$ and IL-12$^{-/-}$ mice"; B. Schwamb, T. S. Tessema and F. Petry, DGP conference 2008, Hamburg; Germany; 05/03/2008

"CABY, a novel pro-apoptotic APAF-1 binding protein" Embo Molecular Medicine Workshop, Cell death and disease: -"Death in the alps 3.0"-; B. Schwamb and M. Zörnig; Obergurgl, Austria; 10/03/11-14/3/11

"CABY in tumorigenicity of gastrointestinal stromal tumors" LOEWE Oncogenic signalling; Frankfurt, Germany; 09/02/12

"*Loss of the pro-apoptotic protein FAM96A is involved in tumorigenicity of gastrointestinal stromal tumors***"** The 8th European Workshop on Cell Death; EWCD, Death à la carte; Le-Monêtier-les Bains, France; 03/06/12-08/06/12